NAVAL POSTGRADUATE SCHOOL

MONTEREY, CALIFORNIA

THESIS

LONG-RANGE FORECASTING IN SUPPORT OF OPERATIONS IN THE HORN OF AFRICA

by

Benjamin D. Lemke

September 2010

Thesis Advisor:	Tom Murphree
Co-Advisor:	David Meyer

Approved for public release; distribution is unlimited

THIS PAGE INTENTIONALLY LEFT BLANK

REPORT DOCUMENTATION PAGE			Form Approved OMB No. 0704-0188
Public reporting burden for this collection of information is estimated to average 1 hour per response, including the time for reviewing instruction, searching existing data sources, gathering and maintaining the data needed, and completing and reviewing the collection of information. Send comments regarding this burden estimate or any other aspect of this collection of information, including suggestions for reducing this burden, to Washington headquarters Services, Directorate for Information Operations and Reports, 1215 Jefferson Davis Highway, Suite 1204, Arlington, VA 22202-4302, and to the Office of Management and Budget, Paperwork Reduction Project (0704-0188) Washington DC 20503.			
1. AGENCY USE ONLY *(Leave blank)*	**2. REPORT DATE** September 2010	**3. REPORT TYPE AND DATES COVERED** Master's Thesis	
4. TITLE AND SUBTITLE Long-range Forecasting in Support of Operations in the Horn of Africa		**5. FUNDING NUMBERS**	
6. AUTHOR(S) Benjamin D. Lemke			
7. PERFORMING ORGANIZATION NAME(S) AND ADDRESS(ES) Naval Postgraduate School Monterey, CA 93943-5000		**8. PERFORMING ORGANIZATION REPORT NUMBER**	
9. SPONSORING /MONITORING AGENCY NAME(S) AND ADDRESS(ES) N/A		**10. SPONSORING/MONITORING AGENCY REPORT NUMBER**	
11. SUPPLEMENTARY NOTES The views expressed in this thesis are those of the author and do not reflect the official policy or position of the Department of Defense or the U.S. Government. IRB Protocol number _____.			
12a. DISTRIBUTION / AVAILABILITY STATEMENT Approved for public release, distribution is unlimited.		**12b. DISTRIBUTION CODE**	

13. ABSTRACT (maximum 200 words)

Over the past several decades, the Horn of Africa (HOA) has experienced recurring climate variations, including droughts and floods that have devastated the region's livelihoods and prompted increased investment in strategies to minimize the negative effects of climate variations. These preventative strategies include the enactment of early warning systems, such as the Famine Early Warning System Network, and military commands such as U.S. Africa Command. If these organizations are to be successful, they must account for the many climate factors that affect Africa, including seasonal climate variations and climate change. Thus, skillful long-range forecasts, especially of precipitation, have become increasingly valuable in planning the operations of these organizations.

In this study, we focused on assessing the potential for predicting HOA precipitation rate (PR) during the October–November rain season at lead times of several seasons. We correlated HOA PR and remote climate variables, and discovered a strong potential for skillful long-range forecasts of HOA PR using sea surface temperatures (SST) near New Zealand, the Philippines, and Namibia as predictors. Our forecast methods included deterministic (tercile matching, linear regression, optimal climate normals) and probabilistic (composite analysis) methods. Our verification metrics showed a definite improvement in forecast skill over existing long-range forecasts based on long-term means, and indicated that our forecasting methods have the potential to improve the planning of military and non-military operations in the HOA.

14. SUBJECT TERMS Horn of Africa, HOA, Precipitation Rate, Early Warning Systems, Long-Range Forecasting, Climate, Climate Analysis, Climate Prediction, Reanalysis, Smart Climatology, AFRICOM, Statistical Forecast, Meteorology, Conditional Climatology, Optimal Climate Normals			**15. NUMBER OF PAGES** 155
			16. PRICE CODE
17. SECURITY CLASSIFICATION OF REPORT Unclassified	**18. SECURITY CLASSIFICATION OF THIS PAGE** Unclassified	**19. SECURITY CLASSIFICATION OF ABSTRACT** Unclassified	**20. LIMITATION OF ABSTRACT** UU

NSN 7540-01-280-5500 Standard Form 298 (Rev. 8-98)
Prescribed by ANSI Std. Z39.18

THIS PAGE INTENTIONALLY LEFT BLANK

Approved for public release, distribution is unlimited

LONG-RANGE FORECASTING IN SUPPORT OF OPERATIONS IN THE HORN OF AFRICA

Benjamin D. Lemke
Captain, United States Air Force
B.S., Saint Cloud State University, 1999

Submitted in partial fulfillment of the
requirements for the degree of

MASTER OF SCIENCE IN METEOROLOGY

from the

NAVAL POSTGRADUATE SCHOOL
September 2010

Author: Benjamin D. Lemke

Approved by: Tom Murphree
Advisor

David Meyer
Co-Advisor

Phillip Durkee
Chairman, Department of Meteorology

THIS PAGE INTENTIONALLY LEFT BLANK

ABSTRACT

Over the past several decades, the Horn of Africa (HOA) has experienced recurring climate variations, including droughts and floods that have devastated the region's livelihoods and prompted increased investment in strategies to minimize the negative effects of climate variations. These preventative strategies include the enactment of early warning systems, such as the Famine Early Warning System Network, and military commands such as U.S. Africa Command. If these organizations are to be successful, they must account for the many climate factors that affect Africa, including seasonal climate variations and climate change. Thus, skillful long-range forecasts, especially of precipitation, have become increasingly valuable in planning the operations of these organizations.

In this study, we focused on assessing the potential for predicting HOA precipitation rate (PR) during the October–November rain season at lead times of several seasons. We correlated HOA PR and remote climate variables, and discovered a strong potential for skillful long-range forecasts of HOA PR using sea surface temperatures (SST) near New Zealand, the Philippines, and Namibia as predictors. Our forecast methods included deterministic (tercile matching, linear regression, optimal climate normals) and probabilistic (composite analysis) methods. Our verification metrics showed a definite improvement in forecast skill over existing long-range forecasts based on long-term means, and indicated that our forecasting methods have the potential to improve the planning of military and non-military operations in the HOA.

THIS PAGE INTENTIONALLY LEFT BLANK

TABLE OF CONTENTS

I. INTRODUCTION 1
A. BACKGROUND 1
B. IMPACTS OF CLIMATE ON THE SOCIAL, ECONOMIC, AND POLITICAL CONDITIONS IN THE HOA 1
C. U.S. AND INTERNATIONAL POLICY TOWARD HOA 3
D. CLIMATE VARIATIONS AND TELECONNECTIONS IN THE HOA 4
E. NON-DOD OPERATIONS IN THE HOA AND LONG-RANGE FORECASTING 8
F. NON-DOD OPERATIONS IN THE HOA AND LONG-RANGE FORECASTING 15
G. MOTIVATIONS FOR AND OUTLINE OF THIS STUDY 20
1. Scientific Motivations 20
2. Operational Motivations 20
3. Research Questions 21
4. Study Region 21
5. Period 24
6. Thesis Organization 25

II. DATA AND METHODS 27
A. DATASETS AND SOURCES 27
1. NCEP/NCAR Atmospheric Reanalysis Data 27
2. Multivariate ENSO Index (MEI) 28
3. Nino 3.4 Index (Nino3.4) 28
4. Indian Ocean Dipole Mode Index (DMI) 29
B. ANALYSIS AND FORECASTING METHODS 29
1. Predictand Selection 29
2. Composite Anomalies, Correlations, and Teleconnections 31
3. Predictor Selection 33
4. Predictor and Predictand Time Series 33
5. Long-Range Forecasting Methods 33
a. Method 1 – Tercile Matching 35
b. Method 2 – Averaged Linear Regression 36
c. Method 3 – Non-Averaged Linear Regression 38
d. Method 4 – Composite Analysis Forecast 38
e. Optimal Climate Normals (OCN) Approach 42
6. Hindcast and Forecast Verification Methods 43
C. SUMMARY OF FORECAST METHODS 48

III. RESULTS 49
A. CLIMATE ANALYSES 49
1. Composites Conditioned on Extreme PR in the HOA 49
2. Correlations 57

3. Predictor Selection 60
B. LONG-RANGE HINDCASTS: ALL YEARS APPROACH 63
1. Tercile Matching Method with NZ SST Predictor 63
2. Composite Analysis Forecasting Method with NZ SST Predictor 67
3. Verification of Hindcasts Based on All Years Approach 70
C. LONG-RANGE HINDCASTS: OPTIMAL CLIMATE NORMALS APPROACH 70
1. Basic OCN Approach 71
2. Advanced OCN Approach 74
3. Verification of Hindcasts Based on Advanced OCN Approach 75
D. LONG-RANGE HINDCAST CASE STUDIES 77
1. 2009 Test Case 78
2. 1997, 1998, and 2006 Test Cases 82
E. HINDCAST VERIFICATION SUMMARY 86
F. FORECAST FOR OCTOBER–NOVEMBER 2010 94
G. CLIMATE DYNAMICS BASIS FOR LONG-RANGE FORECASTS 95
1. NZ SST and HOA Precipitation Teleconnections 96
2. MR SST and HOA Precipitation Teleconnections 105
a. Teleconnections at 4–6 Month Lead Time 105
b. Teleconnections at 0–3 Month Lead Time 107

IV. SUMMARY, CONCLUSION AND RECOMMENDATIONS 115
A. ANALYSIS OF FORECASTING METHODS AND RESULTS 115
B. RECOMMENDATIONS 116

LIST OF REFERENCES 119

INITIAL DISTRIBUTION LIST 125

LIST OF FIGURES

Figure 1. Schematic illustration of anomalies in the Indian and Pacific basin Walker circulations, and in low-level atmospheric pressures and sea-surface temperatures, during EN and positive IOD phase events. These anomalous conditions tend to contribute to above normal precipitation in the HOA. These anomalies tend to be most pronounced during August–February, and thus tend to have their greatest impact on the HOA short rains period in October–December. Figure from Hunt (2009). 7

Figure 2. Outline of process used to generate some of the climate forecasts used by FEWS NET. Observations (left box) are used to identify statistical relationships between climate system variables (middle box; e.g., conditions in the Indian Ocean) and food related variables (e.g., precipitation in southern Africa). These relationships are used to build predictive statistical models that generate forecasts for the food security related variables (right box). Figure from Funk (2009). 9

Figure 3. Outline of contingency planning and response process used by FEWS NET. Climate forecasts are used as inputs to the development of potential food insecurity scenarios that are then used to develop contingency plans and food security outlooks (e.g., Figure 4). Figure from Funk (2009). 9

Figure 4. Example of a food security outlook product generated by FEWS NET. This outlook is for conditions in eastern central Africa and the HOA in April–June 2010. Climate forecasts are an essential element in the generation of such outlooks. These outlooks are used by agricultural, emergency management, and other planners to mitigate the food insecurity events and their effects. Figure from U.S. Aid, FEWSNET, May 2010; available online at http://www.fews.net/Pages/region.aspx?gb=r2&l=en; accessed May 2010. 10

Figure 5. Example of a seasonal precipitation outlook from ICPAC. This outlook shows the predicted probability of above normal (AN), near normal (NN), and below normal (BN) precipitation in the greater Horn of Africa during March–May 2010. The yellow, green, and gray shading represents areas expected to experience similar AN, NN, and BN precipitation conditions. Yellow: relatively high probability of NN or BN precipitation. Green: relatively high probability of NN or AN conditions. Gray: equal chances of AN, NN, and BN. The vertical boxes with three numbers show the probabilities for each category, with AN at the top of the box, NN in the middle, and BN at the bottom. Note that in each colored region, the three probabilities sum to 100%. Example: in zone III the

probabilities are 35% AN; 40% NN; and 25% BN. Figure from ICPAC; available online at **www.icpac.net/Forecasts**; accessed March 2010. 12

Figure 6. Examples of seasonal precipitation forecasts from the Kenya Meteorological Department for March–May 2010. March–May in central east Africa is normally a period of relatively high precipitation that is often referred to as the long rains season. Top panel: forecast of areas of above and below normal precipitation. Bottom left panel: forecast of onset dates for long rains season. Bottom right panel: forecast of cessation dates for long rains season. Figure from Kenya Meteorological Department; available online at **www.meteo.go.ke/**; accessed March 2010. 14

Figure 7. Examples of U.S. Africa Command (AFRICOM) activities that contribute to U.S. government efforts in Africa. Accurate long-range climate forecasts have the potential to improve planning by AFRICOM and its African government partners and non-governmental organization (NGO) partners. Figure from U.S. Africa Command (2010)..... 16

Figure 8. The African region (outlined in yellow) for which the 14th Weather Squadron (14 WS) produces its LRFs for the HOA. The 14 WS produces for this region narrative-only long-range forecasts (lead times of one to six months) of surface air temperature, precipitation, and cloud ceilings. These LRFs are based on composite analysis methods employed by the 14 WS, and on LRFs produced by civilian operational climate centers (e.g., CPC, IRI, UKMO). The locations marked with red dots are ones from which in situ observations are collected and for which terminal aerodrome forecasts (TAFs) are issued. Figure from personal communication with 14 WS. 18

Figure 9. The broad Horn of Africa (HOA) region. The continental scale view (left panel) shows the HOA region (red outlined box) in relation to all of Africa. The HOA focused view (right panel) shows the general HOA region for our study. The darker brown shading indicates the countries that are often considered part of the broad HOA region. Figure from World Health Organization (WHO); available online at: **www.who.int/.../hoafrica/en/index.html**; accessed May 2010..... 22

Figure 10. Long-term mean (LTM) composite of surface precipitation rate (PR; mm/day) during October–November (Oct–Nov) for 1970–2009. Oct–Nov tends to be a period of relatively high precipitation for the general HOA region (see Figures 9 and 11). HOA precipitation in this period is: (1) lower than in the western and central tropical African and tropical Indian Ocean regions; and (2) higher in these months that in the tropical and subtropical regions to the north and south of the HOA. Image created using ESRL (2010). 23

Figure 11. Monthly precipitation rate (PR; mm/day; black bars) and standard deviation of the precipitation rate (SD; mm/day; white bars) in the east African region (5^oS-5^oN, 35^o-46^oE) from in situ observations. Two rainy seasons occur in east Africa, including the HOA as defined in this study: (1) the March to May long rains period; and (2) the October to December short rains period. The PR during Oct–Nov tends to be relatively high and has a relatively high SD. Thus, the Oct–Nov PR is an especially important, but difficult, variable to be able to predict at long lead times. The Oct–Nov PR in the HOA was the primary target, or predictand, for the LRFs we developed and tested in this study. Figure from Behera et al. 2005. . 24

Figure 12. CAF method equations for forecasting the probability of AN, NN, and BN PR (the predictand categories; the terms on the left hand sides of the equations) given: (a); the conditional probabilities of the PR predictand categories given the occurrence of the specified SST predictor categories (the first terms on the right hand sides of the equations); and (b) the probability of SST predictor categories occurring (the second terms on the right hand sides). See main text for more information. The forecast lead time is not specified in these equations. Adapted from MetEd (2010). 39

Figure 13. Equations used in our modified CAF process to calculate long-range forecasts of PR based on observed AN SST predictor conditions at the forecast lead time. The lead time is unspecified in these equations. Compare to the standard equations in Figure 12. .. 41

Figure 14. Time series of Oct–Nov HOA PR predictand (top panel) and New Zealand SST predictor (bottom panel) for 1970–2009. of the bold black and red horizontal lines denote the boundaries between the AN, NN, and BN categories for the predictand and predictor, respectively. For example, PR values are categorized as AN when ≥ 3.5 mm/day; NN when < 3.5 mm/day but ≥ 3.1 mm/day, and BN when < than 3.1 mm/day. 46

Figure 15. Flow chart showing main datasets and methods used to conduct climate analyses and long-range forecasts in this study..... 48

Figure 16. The Oct–Nov HOA PR predictand region for our study (black box) overlaid on the LTM Oct–Nov PR (color shading; mm/day; cf. Figure 10). PR image created using ESRL (2010). 49

Figure 17. Time series of HOA PR (predictand, purple line, mm/day), and El Nino–La Nina (ENLN) and Indian Ocean Dipole (IOD) indices (MEI, red line, and DMI, green line, respectively) for Oct–Nov 1970–2009. Note the similarities in the interannual variability of the predictand and the two indices. Indications of teleconnections between HOA PR, ENLN, and IOD are highlighted during: (a) a strong LN and negative IOD period in Oct–Nov 1974–75; and (b) a strong EN and positive IOD period in Oct–Nov 1997. Relationships such as these

suggest the usefulness of evaluating ENLN and IOD indicators as potential predictors for HOA PR. 51
Figure 18. Conditional composite anomalies of Oct–Nov precipitation rate (PR; mm/day) for the five most extreme AN (wet) and BN (dry) events of HOA PR during Oct–Nov for 1970–2009. The left (right) panels show regional (global) scale views. See Chapter II, Section B.2 for the five most extreme AN and BN PR event years. The red box outlines our HOA predictand region. Note the generally opposite patterns in the wet and dry composites, and the correspondence to PR patterns associated with ENLN and the IOD. PR anomaly patterns such as these suggest possible predictors and linkages associated with the climate variations in the HOA. Images created using ESRL (2010). 52
Figure 19. Conditional composite anomalies of sea surface temperature (^{o}C) for five most extreme wet (left panel) and dry (right panel) HOA PR events during Oct–Nov 1970–2009. Note in the wet (dry) composite the positive (negative) SSTAs in the WIO and central-eastern tropical Pacific and the negative (positive) SSTAs in the tropical EIO and western tropical Pacific, consistent with positive (negative) IOD and EN (LN) conditions. Images created using ESRL (2010)..... 53
Figure 20. Conditional composite anomalies of 200 hPa GPH (gpm) for five most extreme wet (left panel) and dry (right panel) HOA PR events during Oct–Nov 1970–2009. Note in the wet (dry) composite the positive (negative) GPHAs over Africa and the central-eastern tropical Pacific (central and southern Africa and central-eastern tropical Pacific), consistent with positive (negative) IOD and EN (LN) conditions. These features are indicative of Rossby-Kelvin wave responses to anomalous convection over the WIO, MC and central-eastern tropical Pacific. Images created using ESRL (2010). 54
Figure 21. Conditional composite anomalies of 850 hPa zonal wind (m/s) for the five most extreme wet (left panel) and dry (right panel) HOA PR events during Oct–Nov 1970–2009. The red arrows represent the sense of the wind flow anomalies. Note in the wet (dry) composite the anomalous low-level convergence (divergence) over the HOA and divergence (convergence) over the MC, consistent with above normal PR in the HOA and with positive (negative) IOD and EN (LN) conditions. Images created using ESRL (2010)..... 56
Figure 22. Conditional composite anomalies of OLR (W/m^2) for five most extreme wet (left panel) and dry (right panel) HOA PR events during Oct–Nov 1970–2009. OLR is a good proxy for convection and precipitation in the tropics, with positive (negative) OLRAs indicating negative (positive) convection anomalies. Note in the wet (dry) composite the negative (positive) OLRAs in the HOA,

WIO, and central-eastern tropical Pacific, and the positive (negative) OLRAs in the tropical eastern IO and western tropical Pacific, consistent with wet (dry) conditions in the HOA, and positive (negative) IOD and EN (LN) conditions. Images created using ESRL (2010). 57

Figure 23. Correlations of HOA PR in Oct–Nov with global SST for 1970–2009 with SST leading by: (a) one month (Sep–Oct), (b) two months (Aug–Sep), (c) three months (Jul–Aug), and (d) four months (Jun–Jul). The blue box represents the Oct–Nov HOA PR predictand region. The red box indicates a region north of New Zealand of persistently strong and significant negative correlation between SST and the predictand. Note the similarities between the correlation patterns in this figure and the SSTA patterns in Figure 18. Images created using ESRL (2010)..... 59

Figure 24. Magnitude of correlations between Oct–Nov HOA PR predictand and four potential predictors of this predictand, with the predictors leading by zero to six months. The four predictors are: NZ SST, MEI, Nino3.4, and DMI. The colored text boxes on the right of the figure describe the climate variations associated with the last three of these potential predictors. Correlations ≥ 0.304 indicate significance at the 95% level (dashed line)..... 61

Figure 25. Time series of HOA Oct–Nov PR (mm/day) predictand in Oct–Nov (black line) and NZ SST (^{o}C) predictor in (a) Oct–Nov (red line), (b) Jul–Aug (purple line), and (c) Apr–May (blue line) during 1970–2009. Note the persistence in the SSTs indicated by the similarities in the SST time series. Note also the indications of negative correlations between the predictand and NZ SSTs. 62

Figure 26. Correlations of HOA PR in Oct–Nov with global SST in Sep–Oct based on data from 1970–2009.. These and related correlations (Figures 23–24) led us to select SST north of New Zealand (red box) as the initial predictor for use in forecasting HOA PR in Oct–Nov (our predictand; blue box) at leads of one to six months. Image created using ESRL (2010). 63

Figure 27. Average verification metrics by forecast lead time for hindcasts of HOA PR in Oct–Nov 1970–2009 using Method 1 (tercile matching) and the NZ SST predictor. Averaging is done over all forecast categories (AN, NN, and BN PR). Verification metrics consist of percent correct (% Corr), false alarm rate (FA Rate), probability of detection (POD), and Heidke Skill Score (HSS). Refer to Chapter II, Section B.6 for more information on the metrics listed in this table. Note the general decline in skill as lead time increases, but that HSS remains positive at all lead times. 66

Figure 28. Results from composite analysis forecasts of Oct–Nov HOA PR using the NZ SST predictor at a lead time of six months (i.e., using NZ SST in Apr–May). (a) Historical frequency distribution of HOA

PR probabilities given any SST condition at six months lead. Statistically significant results are outlined in black. (b) Corresponding probabilistic long-range hindcast of HOA PR in Oct–Nov based on AN NZ SST in Apr–May. (c) Corresponding probabilistic long-range hindcast of HOA PR in Oct–Nov based on BN NZ SST in Apr–May..... 68

Figure 29. Time series by forecast lead time of: (1) correlations between HOA PR predictand and NZ SST predictor; and (2) HSS values for tercile matching method hindcasts at lead times of zero to six months, and using tercile categories based on the most recent 10, 15, and 40 years. (a) 1995–2009 correlations (green line); (b) 2000–2009 correlations (red line); (c) 1995–2009 hindcast HSS values (orange and light blue lines); and (d) 2000–2009 hindcast HSS values (purple and turquoise lines). The bin periods represent the period used to form the predictor and predictand AN, NN, and BN categories. Note that the correlations shift from negative to positive, and the HSS values decrease, as lead time increases. 73

Figure 30. Correlations of HOA PR in Oct–Nov with global SST for 1995–2009 with SST leading by: (left panel) zero months (Oct–Nov) and (right panel) four months (Jun–Jul). The yellow outlined boxes represent the multi-region SST predictor regions identified as having the highest correlations to the HOA PR predictand at specific lead times when using the advanced OCN approach. We used the SST predictor east of the Philippines (left panel) was used for forecasting at leads of zero to three months. We used the SST predictor west of Namibia (right panel) for forecasting at leads of four to six months. Images created using ESRL (2010). 74

Figure 31. Composite mean SST (^{o}C) in Apr–May 2009 averaged over: (top right) NZ predictor region and (bottom left) MR predictor region. The black (red) box represents the NZ (MR) SST predictor regions used for analyzing the SSTs at lead times of six months. The area averaged SST for Apr–May 2009 was 23.875 (22.958) ^{o}C in the NZ (MR) predictor regions. Images created using ESRL (2010). 78

Figure 32. Composite mean (left panel) and anomaly (right panel) PR (mm/day) in Oct–Nov 2009. The black outlined box represents the HOA PR predictand region. Note that AN, NN, and BN PR anomalies occurred within the predictand region (right panel); however the actual area-averaged PR was 2.836 mm/day, or NN. Images created using ESRL (2010)..... 80

Figure 33. Composite anomalies of PR (mm/day) during Oct–Nov for three different years: (left panel) 1997, (middle panel) 1998, and (right panel) 2006. The red outlined boxes represent the HOA PR predictand region. The HOA experienced extreme AN or BN PR in each of these years: AN in 1997 and 2006, and BN in 1998). These years were chosen to test the four forecast methods using

the non-OCN and OCN-based predictor sets. Images created using ESRL (2010). 83
Figure 34. Total verification metrics for hindcasts of HOA PR in Oct–Nov averaged over all forecast categories (AN, BN, NN) and all lead times of zero to six months. Columns 1–4 (5–8) represent verification metrics using the NZ (Multi-Region) SST predictor for 1970–2009 (1995–2009) with each of the forecast methods listed at the bottom right of the figure (e.g., tercile matching, linear regression and CAF). For example, column 5 represents the verification metrics for Method 1 (tercile matching) using the Multi-Region SST predictor. Verification metrics consist of percent correct (% Corr), false alarm rate (FA Rate), probability of detection (POD), and Heidke Skill Score (HSS). Refer to Chapter II, Section B.6 for more information on these metrics. The bold black line highlights the HSSs. 88
Figure 35. Time series of actual HOA PR (black line) and hindcasted PR values using Method 2 (averaged linear regression) and the NZ SST predictor for Oct–Nov 1970–2009 at lead times of zero to six months. The hindcast PR values are dark red (green) at the longest (shortest) lead times. Note: (a) the periods of relatively good model performance before 1984 and after 1993 (see Chapter III, Section A.3; Figure 24); and (b) the lower variability in the hindcasted PR than the observed PR, especially at longer leads. All PR values in mm/day..... 89
Figure 36. Time series of actual HOA PR (black line) and hindcasted PR values using Method 3 (non-averaged linear regression) and the NZ SST predictor for Oct–Nov 1970–2009 at lead times of zero to six months. The hindcast PR values are dark red (green) at the longest (shortest) lead times. Note: (a) the periods of relatively good model performance before 1984 and after 1993 (see Chapter III, Section A.3; Figure 24); and (b) the lower variability in the hindcasted PR than the observed PR, especially at longer leads. All PR values in mm/day..... 90
Figure 37. Time series of actual HOA PR (black line) and hindcasted PR values using Method 2 (averaged linear regression) and the MR SST predictors for Oct–Nov 1995–2009 at lead times of zero to six months. The hindcast PR values are dark red (green) at the longest (shortest) lead times. Note: (a) the overall very good model performance, especially at shorter leads; and (b) the relatively realistic variability, especially at shorter leads. All PR values in mm/day..... 91
Figure 38. Time series of actual HOA PR (black line) and hindcasted PR values using Method 3 (non-averaged linear regression) and the MR SST predictors for Oct–Nov 1995–2009 at lead times of zero to six months. The hindcast PR values are dark red (green) at the

longest (shortest) lead times. Note: (a) the overall very good model performance, especially at shorter leads; and (b) the relatively realistic variability, especially at shorter leads variability in the hindcasted PR than the observed PR, especially at longer leads. All PR values in mm/day..... 92
Figure 39. Correlations between the actual Oct–Nov HOA PR and the hindcasted HOA PR values shown in Figures 35–38 by lead time. Forecast method and predictor indicated by colored lines and symbols (see key)..... 93
Figure 40. Conditional composite anomalies of sea surface temperature (^{o}C) for the five most extreme BN NZ SST events during Oct–Nov 1970–2009. Recall that BN NZ SST is associated with EN and positive IOD events (Figure 17), and with AN HOA PR during Oct–Nov. Red box indicates NZ SST region. Red oval indicates area of pronounced negative SSTAs in the tropical Atlantic. Image created using ESRL (2010). 97
Figure 41. Conditional composite anomalies of sea surface temperature (^{o}C) for the five most extreme EN events (left panel) and LN events (right panel) during Oct–Nov 1970–2009. EN and LN events identified by use of MEI. Image created using ESRL (2010). 98
Figure 42. (Left panel) 3-D schematic of the anomalous Hadley-Walker Circulation (HWC) over the Pacific Ocean corresponding to LN events and enhanced convection over the MC. (Right panel) Conditional composite anomalies of 850 hPa vector winds (m/s) for the five most extreme AN NZ SST events during Oct–Nov 1970–2009. Recall that AN NZ SST is associated with LN and negative IOD events (Figure 17), and with BN HOA PR during Oct–Nov. Bold black line indicates SPCZ. H (L) indicates location of anomalous high (low) low-level pressure system. Red arrows schematically show the anomalous low-level flow. Image on left adapted from Murphree (2009a). Image on right created using ESRL (2010)..... 99
Figure 43. Conditional composite anomalies of 200 hPa GPH (gpm) for the five most extreme BN NZ SST events during Oct–Nov 1970–2009. Recall that BN NZ SST is associated with EN and positive IOD events (Figure 17), and with AN HOA PR during Oct–Nov. The red arrows schematically show anomalous wave trains that emanate from the maritime continent sector, extend into the extratropcial northern and southern hemispheres, and then into the tropics near Africa. The arrow directions indicate schematically the direction of energy propagation in the anomalous wave trains. The *Wet* label in the upper left indicates that these anomalies are associated with above normal precipitation in the HOA. Image created using ESRL (2010). 100

Figure 44. Conditional composite anomalies of 200 hPa GPH (gpm) for the five most extreme AN NZ SST events during Oct–Nov 1970–2009. Recall that AN NZ SST is associated with LN and negative IOD events (Figure 17), and with BN HOA PR during Oct–Nov. The red arrows schematically show anomalous wave trains that emanate from the maritime continent sector, extend into the extratropical northern and southern hemispheres, and then into the tropics near Africa. The arrow directions indicate schematically the direction of energy propagation in the anomalous wave trains. The *Dry* label in the upper left indicates that these anomalies are associated with below normal precipitation in the HOA. Image created using ESRL (2010). 101
Figure 45. Conditional composite anomalies of 850 hPa GPH (gpm) for the five most extreme BN NZ SST events during Oct–Nov 1970–2009. Recall that BN NZ SST is associated with EN and positive IOD events (Figure 17), and with AN HOA PR during Oct–Nov. H (L) indicates location of anomalous high (low) low level geopotential heights. The red arrows show schematically the anomalous wind directions. Note the anomalous convergence into the HOA region. Image created using ESRL (2010). 103
Figure 46. Conditional composite anomalies of precipitation rate (PR; mm/day) for the five most extreme BN NZ SST events during Oct–Nov 1970–2009. Recall that BN NZ SST is associated with EN and positive IOD events (Figure 17), and with AN HOA PR during Oct–Nov. The red box indicates our HOA PR predictand region. Image created using ESRL (2010). 104
Figure 47. Conditional composite anomalies of 850 hPa GPH (gpm) for the five most extreme BN Namibia SST events during Apr–May 1970–2009. Recall that BN Namibia SST is associated with AN HOA PR during Oct–Nov. The H indicates an anomalous high-pressure region. The direction of the corresponding wind anomalies is shown schematically by the red arrow. The cooler SSTs region is explained in the main text discussion of Figure 40. Image created using ESRL (2010). 106
Figure 48. Conditional composite anomalies of SST (^{o}C) for the five most extreme BN Namibia SST events during Apr–May 1970–2009. Recall that BN Namibia SST is associated with AN HOA PR during Oct–Nov. The negative SSTA region west of Namibia corresponds to the Namibia SST predictor region identified as having the highest correlations, at leads of four to six months, to the HOA PR predictand for 1995–2009 (see Chapter III, Section C.2). The H indicates an anomalous lower tropospheric high-pressure region and the black arrow indicates the corresponding wind anomaly (see Figure 47). Image created using ESRL (2010). 107

Figure 49. Correlations of HOA PR in Oct–Nov with global SST for 1970–2009 (left panel) and 1995–2009 (right panel), with SSTs leading by zero months (Oct–Nov). The yellow outlined boxes represent NZ predictor region (left panel) and the Philippine SST predictor region (right panel). Note the similar patterns for the two periods, but with stronger correlations for 1995–2009. Images created using ESRL (2010). 108
Figure 50. Composite anomalies of SST (^{o}C) for Oct–Nov of 1995–2009. Note the positive SSTAs, especially in the northern hemisphere and in the western North and South Pacific. Image created using ESRL (2010). 109
Figure 51. Schematic diagram of lower tropospheric and sea surface conditions that occur in October–November when: (a) precipitation is greater than normal in the HOA (i.e., during AN HOA PR events); *and* (b) when SSTs north of New Zealand are cooler than normal (i.e., during BN NZ SST events) and. Map background from Google Maps (**www.maps.google.com**). 110
Figure 52. Schematic diagram of lower tropospheric and sea surface conditions that occur in October–November when: (a) precipitation is less than normal in the HOA (i.e., during BN HOA PR events); *and* (b) when SSTs north of New Zealand are warmer than normal (i.e., during AN NZ SST events) and. Map background from Google Maps (**www.maps.google.com**). 111
Figure 53. Schematic diagram of lower tropospheric and sea surface conditions that occur in October–November when precipitation is greater than normal in the HOA (i.e., during AN HOA PR events). Map background from Google Maps (**www.maps.google.com**). 112

LIST OF TABLES

Table 1. Climate system variables that we analyzed to identify: (a) potential predictors of HOA PR; and (b) the physical processes that lead to climate variations in HOR PR. All variables were assessed on a global scale, except for soil moisture. 32

Table 2. Example of contingency table assignments for the verification of forecasts of AN PR when using a categorical SST predictor, for the case in which AN SST leads to a forecast of BN PR. 44

Table 3. Schematic contingency table of hit and miss assignments based on a negative correlation between a SST predictor and a PR predictand. 45

Table 4. Verification results from hindcasts generated using Method 1 (tercile matching). The hindcasts predicted Oct–Nov HOA PR during 1970–2009 based on the NZ SST predictor, with the predictor leading by zero to six months. Columns A, B, C, and D represent the number of hits, false alarms, misses, and correct rejections, respectively, for predictions of AN, BN, and NN PR. Verification metrics consist of percent correct (% Corr), false alarm rate (FA Rate), probability of detection (POD), and Heidke skill score (HSS). See Chapter II, Section B.6 for more information on our verification methods. 65

Table 5. Average verification metrics for hindcasts of HOA PR in Oct–Nov 1970–2009 using each of the four forecast methods and the NZ SST Predictor. Averaging done over all forecast categories (AN, BN, NN) and all lead times of zero to six months. Note the HSS values are all positive, indicating forecast skill. See Chapter II, Section B.6 for more information on the metrics listed in this table. ... 70

Table 6. TVerification results from hindcasts generated using Method 1 (tercile matching). The hindcasts predicted Oct–Nov HOA PR during 1995–2009 based on the multi-region SST predictors (advanced OCN approach; Figure 39), with the predictor leading by zero to six months. Columns A, B, C, and D represent the number of hits, false alarms, misses, and correct rejections, respectively, for predictions of AN, BN, and NN PR. Verification metrics consist of percent correct (% Corr), false alarm rate (FA Rate), probability of detection (POD), and Heidke skill score (HSS). Compare these advanced OCN verification metrics results to those obtained from non-OCN approaches (Table 4). 76

Table 7. Average verification metrics for hindcasts of HOA PR in Oct–Nov 1995–2009 using each of the four forecast methods and the multi-region SST predictors (advanced OCN approach; Figure 30). Averaging done over all forecast categories (AN, BN, NN) and all lead times of zero to six months. Compare these advanced OCN

verification metrics results to those obtained from non-OCN approaches (Table 5). 77
Table 8. Results from hindcasts of HOA PR (mm/day) for Oct–Nov 2009 for each forecast method using each of the four forecast methods, and the NZ SST (non-OCN) and MR SST (OCN) predictors, at lead times of zero to six months. The forecast methods (1–4) are listed at the left. Lead times (top row) decrease from left to right. The SST predictor used (NZ or MR) is listed in the second row from the top. The forecasted PR values are the numerical quantities shown within the columns for each lead time and each predictor. The forecasted tercile categories are shown just below each forecasted PR. The actual Oct–Nov HOA PR value and categories are located at the bottom left (left (right) column shows observed tercile category based on non-OCN (OCN) process). Method 1: tercile matching; Method 2: averaged linear regression; Method 3: non-averaged linear regression; and Method 4: CAF. 82
Table 9. Results from hindcasts of HOA PR (mm/day) for Oct–Nov of three different years using each of the four forecast methods, and the NZ SST (non-OCN) and multi-region (OCN) SST predictors, at lead times of zero to six months The years are: (top table) 1997, (middle table) 1998, and (bottom table) 2006. The forecast methods (1–4) are listed at the left. Lead times (top row) decrease from left to right. The SST predictor used (NZ or MR) is listed in the second row from the top. The forecasted PR values are the numerical quantities shown within the columns for each lead time and each predictor. The forecasted tercile categories are shown just below each forecasted PR. The actual Oct–Nov HOA PR value and categories are located at the bottom left (left (right) column shows observed tercile category based on non-OCN (OCN) process). Method 1: tercile matching; Method 2: averaged linear regression; Method 3: non-averaged linear regression; and Method 4: CAF. Note that all forecast method perform well at lead times of zero to four months, but have lower skill at the longer lead times, possibly indicating the effects of the spring predictability barrier (Chapter III, Section B.2; van den Dool 2007). The OCN approach leads to some improvement in performance, especially at the longer leads. ... 84
Table 10. Eight long-range forecasts of HOA PR categories for Oct–Nov 2010 that we issued on 01 June 2010 at a six month lead time. The LRF methods and predictors for each LRF are shown in the table. The predictor values were the reanalyzed Apr–May SSTs from the NZ and MR predictor regions. Note that all the LRFs predict NN PR in the HOA for Oct–Nov 2010, except for one (Method 4, CAF, using the NZ SST predictor). Hindcasts generated using these LRF methods and SST predictors have their lowest skill at the longest

lead (six months). Thus, these LRFs should be used with caution and updated LRFs at shorter leads should be closely monitored. 94
Table 11. The years in which the five most extreme AN and BN conditions occurred during Oct–Nov 1970–2009 for each of our three predictors. 95
Table 12. The years in which the five most extreme EN and LN conditions occurred during Oct–Nov 1970–2009, as indicated by the MEI. 96

THIS PAGE INTENTIONALLY LEFT BLANK

LIST OF ACRONYMS AND ABBREVIATIONS

% Corr	Percent correct
14 WS	14th Weather Squadron
AF MAJCOM	Air Force major command
AFRICOM	U.S. Africa Command
AFW	Air Force Weather
AFWA	Air Force Weather Agency
AN	Above normal
AO	Arctic Oscillation
Apr-May	April-May
Aug-Sep	August-September
BN	Below normal
BOM	Bureau of Meteorology
C	Celsius
CAF	Composite analysis forecast
CPC	Climate Prediction Center
CR	Correct rejections
DMC	Drought Monitoring Centre
DMI	Dipole Mode Index
DoD	Department of Defense
ECMWF	European Centre for Medium-range Weather Forecasts
EIO	Eastern Indian Ocean
EN	El Nino
ENLN	El Nino – La Nina
ENSO	El Nino Southern Oscillation
ESRL	Earth Systems Research Laboratory
EWS	Early warning system
FA	False alarm
FAR	False alarm rate

FEWS NET	Famine early warning system network
GPH	Geopotential height
gpm	Geopotential meter
HOA	Horn of Africa
hPa	Hecto-pascal
HSS	Heidke skill score
HWC	Hadley-Walker circulation
ICPAC	IGAD Climate Prediction and Application Centre
IDP	Internally displaced person
IGAD	Intergovernmental Authority on Development
IO	Indian Ocean
IOD	Indian Ocean Dipole
IOZM	Indian Ocean Zonal Mode
IRI	International Research Institute for Climate and Society
ITCZ	Intertropical Convergence Zone
JAMSTEC	Japan Agency for Marine-Earth Science and Technology
Jun-Jul	June-July
Jul-Aug	July-August
KMD	Kenya Meteorological Department
LN	La Nina
LRF	Long range forecast
LTM	Long term mean
m	meter
m^2	square meter
MC	Maritime continent
MEI	Multivariate ENSO Index
MJO	Madden-Julian Oscillation
mm	millimeter
MR	Multi-region
m/s	meter per second

NAO	North Atlantic Oscillation
NCAR	National Center for Atmospheric Research
NCEP	National Centers for Environmental Prediction
NGO	Non-governmental organization
NN	Near normal
NOAA	National Oceanic and Atmospheric Administration
NZ	New Zealand
OCN	Optimal climate normals
Oct-Nov	October-November
OLR	Outgoing longwave radiation
OLRA	Outgoing longwave radiation anomaly
PC	Percent correct
POD	Probability of detection
PR	Precipitation rate
R1	NCEP/NCAR reanalysis
SASH	South Atlantic subtropical high
Sept-Oct	September-October
SLP	Sea level pressure
SLPA	Sea level pressure anomaly
SOI	Southern Oscillation Index
SPCZ	South Pacific Convergence Zone
SST	Sea surface temperature
SSTA	Sea surface temperature anomaly
TAF	Terminal aerodrome forecast
UCL	University College London
UKMO	United Kingdom Meteorological Office
UN	United Nations
U.S.	United States
USAF	U.S. Air Force
USAID	United States Agency for International Development

USDA	U.S. Department of Agriculture
WIO	Western Indian Ocean
WMO	World Meteorological Organization
W/m^2	Watts per square meter

ACKNOWLEDGMENTS

This thesis would not have been possible without the honest contributions of several individuals. My sincerest gratitude and appreciation goes out to my advisors, Dr. Tom Murphree and Mr. David Meyer for their wisdom, patience, and guidance throughout this research process.

I would also like to thank my fellow classmates (Matt, Rose, Ryan, Eric, Jay, Megan, Lucky and my fellow USN friends), for their friendship and support throughout this process. Moreover, thanks to the folks at 14th Weather Squadron for their contributions.

THIS PAGE INTENTIONALLY LEFT BLANK

I. INTRODUCTION

A. BACKGROUND

Much of Africa has experienced extreme climate variations in the last several decades that have had devastating impacts on the environment and societies (Time 2009). The effects of climate change associated with global warming have been projected to be especially severe in Africa due in part to on-going poverty and the lack of strong governance to prepare for and mitigate climate change effects (IPCC 2004). Skillful long-range forecasts (LRFs; forecasts at lead times of two weeks or longer) of climate variations and climate change, and their impacts on specific regions, are critical in managing climate related risks, such as the risks of famine, and economic and political instability. These LRFs can contribute to the development of early warning systems (EWS), such as the Famine Early Warning System Network (FEWS NET; Funk 2009), that help military and non-military planners manage the impacts of climate variations and climate change.

In this study, we have investigated the potential for improving LRFs of precipitation in the Horn of Africa (HOA). Our over-arching goal is to develop long-range forecasting methods that contribute to the development of a more holistic approach to dealing with military and non-military challenges in the HOA, and to contribute to the welfare of the people of this region—for example, to help support early warnings and decisions that save lives and minimize conflicts.

B. IMPACTS OF CLIMATE ON THE SOCIAL, ECONOMIC, AND POLITICAL CONDITIONS IN THE HOA

The HOA, as defined in this study, comprises six countries (Djibouti, Eritrea, Somalia, Ethiopia, Kenya, and Sudan) and covers approximately six million square kilometers (ICRC 2004). There are an estimated 260 million pastoralists and agro-pastoralists in sub-Saharan Africa, which means 60 to 100

percent of the livelihood of most of the regions' population, and most of the region's gross domestic product comes from agriculture (ICRC 2004). Thus, arable land and water (e.g., from rainfall) are extremely important. The population is estimated to grow on the order of 100% from 2000 to 2050, leading to increasing stress on natural resources and social management structures, and increased economic, social, and political tension (ICRC 2004). Competition over natural resources is one of the most common causes of conflict in the HOA (ICRC 2004).

Extreme climate events, such as droughts and floods, initiate many societal emergencies in the HOA; for example, drought triggers many of these emergency events in Ethiopia (ICRC 2004). The effects of these climate related emergencies are wide ranging and have multiple direct and indirect cascading effects that span the social, economic, political and cultural sectors. Pre-existing conditions tend to make the HOA especially vulnerable to the effects of droughts and floods. These pre-existing conditions include weak governance, lack of early warning and basic social services, poverty, and ongoing recovery from previous extreme climate events (UNEP 2009). Extreme climate events often reinforce or exacerbate the pre-existing conditions (UNEP 2009). Some of the harsh negative effects that are the direct or indirect results of droughts and floods are (e.g., ICRC 2004; UNEP 2009; Time 2009; Ogallo 2010):

(1) Shortages of food and water

(2) Environmental degradation

(3) Large losses to hydroelectric power generation

(4) Agriculture, wildlife and livestock devastation

(5) Famine and starvation

(6) Increased health risks and incidences of diseases

(7) Internally displaced persons (IDPs), refugees, and forced migration

(8) Large economic losses, trade bans, and border restrictions

(9) Economic and political mismanagement; strongman governments

(10) Border conflicts and extremism

This list of effects is not all-inclusive and does not capture the interplay between effects that can greatly amplify the environmental, social, economic, and political impacts of climate variations. The hazards of extreme climate events are highlighted by several recent cases. The prolonged droughts in the Darfur region of Sudan during recent decades that have greatly contributed to conflicts over control of scarce resources, such as fertile land and water, that have led in turn to over 300,000 deaths and two million DPs since 2003 (UNEP 2009). During 1992–1993, famine related to drought helped create political instability that let the U.S. to send troops into Somalia; the resulting conflicts led to the deaths of 1,000 Somalis and 18 Americans (Baker 2010). In the past decade, approximately 23 million people in seven East African countries have been fed by aid agencies after a decade of poor rains have led to food and water shortages (CNN 2009; Time 2009). In 2006, the UN said it expected climate change related to global warming to have the greatest societal impacts in Africa, where nearly 90 million Africans are especially vulnerable to the impacts of extreme weather and climate events, such as droughts and floods (Time 2009).

C. U.S. AND INTERNATIONAL POLICY TOWARD HOA

The U.S., UN, aid agencies, and other nations and organizations have begun to account for climate factors in their attempts to manage environmental, societal, economic, and political problems in the HOA and other regions (e.g., UNEP 2009). The long-standing band-aid and reactive responses climate related problems are being replaced by early warning systems (EWSs) designed to integrate environmental analyses and forecasts into societal, economic, and political planning, and conflict prevention and peace building efforts. The UN has strongly recommended increased development of EWSs and early action in countries that are vulnerable to conflicts over natural resources and environmental issues (UNEP 2009). U.S. policy toward such countries is

evolving from primarily a crisis intervention approach to an approach based on identifying and responding to the factors that cause the crises (e.g., Baker 2010; U.S Africa Command 2010).

The U.S. recognizes the importance of early action in the HOA because the region is prone to extremist groups and predatory elites that can thrive largely with impunity, and that often exacerbate the suffering of the populations under their control (Baker 2010). The Army Field Manual 3-07 (USAFM 2008), states the greatest threat to U.S. national security will *not* come from emerging ambitious states but from nations unable or unwilling to meet the basic needs and aspirations of their people (Baker 2010). The Failed States Index of 2009 listed five out of the six HOA countries in alert status; Somalia and Sudan being number one and three, respectively (FSI 2009). Extreme climate events can escalate conflicts and generate others, especially in failed or failing states (UNEP 2009). Thus, investments in EWSs for conflict prevention and peacebuilding, in addition to humanitarian assistance, are especially important in nations that are in, or vulnerable to, failed state status. Better long-range forecasts of environmental conditions (e.g., of precipitation in the HOA) are vital to the operation of EWSs and other aspects of a holistic approach to dealing with climate related societal, economic, and political problems.

D. CLIMATE VARIATIONS AND TELECONNECTIONS IN THE HOA

Before attempting to develop methods for long-range forecasting of climate variations in the HOA, it is important to understand what the major variations are and what regional and global scale dynamical processes help create these variations. Numerous prior studies have identified intraseasonal to interdecadal variations that tend to occur in the HOA and nearby regions (e.g., Nicholson and Entekhabi 1987; Farmer 1988; Ogallo 1988; Hutchinson 1992; Hastenrath et al. 1993, 2004; Mutai et al. 1998; Kabanda and Jury 1999; Mutai

and Ward 2000; Poccard et al. 2000; Camberlin et al. 2001; Black et al. 2002; Clark et al. 2002; Behera et al. 2005; LaJoie 2006; Vorhees 2006; Montgomery 2007).

The focus of many of these studies has been on interannual climate variations in precipitation, in large part because these variations can be very pronounced and have serious impacts on the environment and the human population. These precipitation variations are generally expressed as extremes in the precipitation that occurs during the two main rainy seasons in east African and the HOA region—the long rains during Mar–May and the short rains during Oct–Dec (e.g., Mutai and Ward 2000). The precipitation variations tend to be associated with teleconnections between HOA precipitation and sea surface temperature (SST) in other regions of the tropics and subtropics (e.g., Ogallo 1988; Hutchinson 1992). Some of the most notable teleconnections are those associated with the SST changes that occur in the tropical Pacific and Indian basins during El Nino—La Nina (ENLN) and Indian Ocean Dipole (IOD; also known as Indian Ocean Zonal Mode (IOZM); Saji et al. 1999) events. Numerous studies have linked variations in Oct–Nov precipitation in the HOA with ENLN, IOD, and, to a lesser extent, with SST variations in the Atlantic Ocean (e.g., Nicholson and Entekhabi 1987; Farmer 1988; Poccard et al. 2000; Camberlin et al. 2001; Black et al. 2002; Clark et al. 2002; Behera et al. 2005; LaJoie 2006; Vorhees 2006).

Much of the impact of remote SSTs on HOA precipitation occurs via fluctuations of the circulation over the tropical and subtropical Indian Ocean (IO). As SSTs decrease (increase) near the maritime continent during EN (LN) events, the zonally oriented Walker Circulation over the IO tends to weaken (strengthen), which results in: (a) less (more) subsidence over east Africa and the HOA; (b) more (less) subsidence over the maritime continent; (c) weaker (stronger) low level westerlies over the tropical IO; (d) warmer (cooler) SSTs off east Africa and the HOA; (e) cooler (warmer) SSTs in the eastern tropical IO; (f) more (less) favorable conditions for precipitation over east Africa, the HOA, and the western

topical IO; and (g) less (more) favorable conditions for precipitation over the maritime continent and the eastern tropical IO (e.g., Ogallo 1988; Mutai and Ward 2000; Black et al. 2002; Clark and Cole 2002; LaJoie 2006; Vorhees 2006). A similar set of variations tends to occur during the positive (negative) phases of the IOD (Saji et al. 1999; Behera et al. 2005; Vorhees 2006; Twigg 2008). The IOD and ENLN are well correlated, with the positive (negative) IOD phase tending to occur during EN (LN) events (Twigg 2008) ENLN and IOD events tend to reach their maximum amplitudes during September–January. Thus, they tend to have relatively large impacts on the short rains during Oct-Dec ((cf. Hastenrath et al. 1993; LaJoie 2006; Vorhees 2006). Figure 1 provides a schematic illustration of the typical relationships between HOA precipitation and EN and positive IOD events.

The typical relationships between HOA precipitation variations and ENLN and IOD events can break down if ENLN and IOD do not follow their usual relationships (e.g., EN with positive IOD; LN with negative IOD), or if they peak at different times than is typical, or if they occur simultaneously with other climate variations (e.g., Madden-Julian Oscillation; MJO) (cf. LaJoie 2006; Vorhees 2006).

Public awareness to these climate variations is increasing as mainstream media highlight the associated environmental, societal, and economic impacts of the variations. Figure 1 is an example of how the news media is informing the general public about ENLN, IOD, and their global scale impacts.

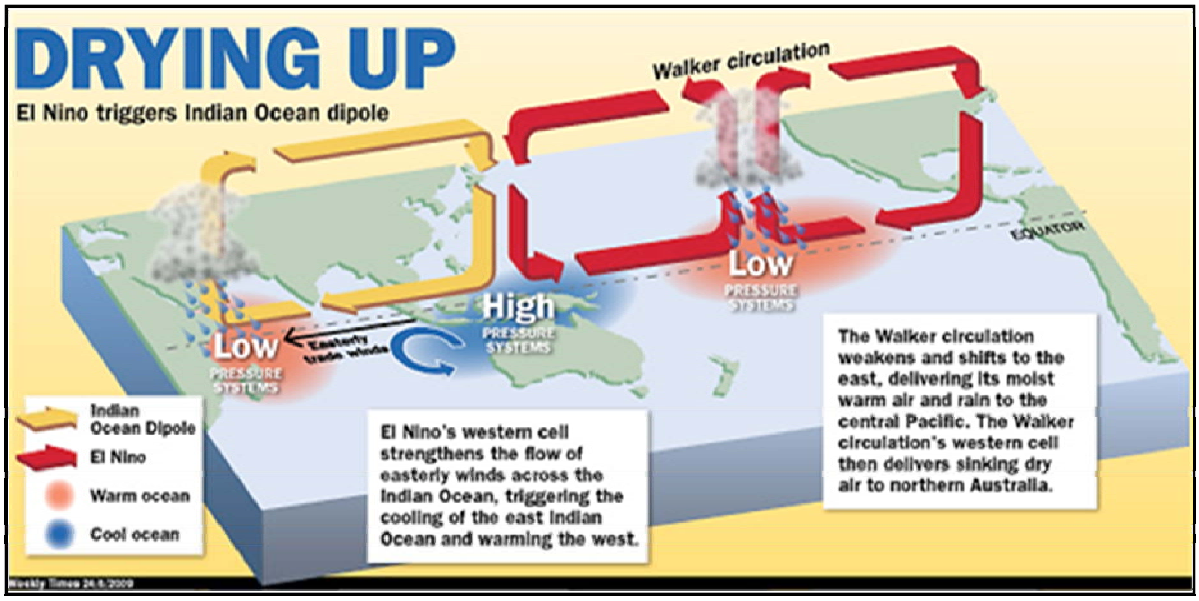

Figure 1. Schematic illustration of anomalies in the Indian and Pacific basin Walker circulations, and in low-level atmospheric pressures and sea-surface temperatures, during EN and positive IOD phase events. These anomalous conditions tend to contribute to above normal precipitation in the HOA. These anomalies tend to be most pronounced during August–February, and thus tend to have their greatest impact on the HOA short rains period in October–December. Figure from Hunt (2009).

Teleconnections between the east Africa and HOA short rains and conditions in the Atlantic Ocean are also important, but have not been as extensively studied as teleconnections between the Pacific and IO basins. Nicholson and Entekhabi (1987) found that below (above) normal SSTs in the equatorial Atlantic off the coast of West Africa tended to be associated with below (above) normal precipitation in the east Africa short rains period. However, Mutai and Ward (2000) found that above (below) normal SSTs in the equatorial and tropical Atlantic off the coast of Africa were associated with above (below) normal east African short rains.

E. NON-DOD OPERATIONS IN THE HOA AND LONG-RANGE FORECASTING

The regional and international community has instituted EWSs and other preventative systems for much of Africa and the HOA in particular. EWSs are vital to the HOA because the early identification of populations at risk can enable the timely focused actions needed to avert widespread hunger, destitution, famine, and violent conflict. Several EWSs use the results from climate monitoring and long-range forecasting to develop early warnings of food and agricultural insecurity, drought, flooding, and famine (Verdin et al. 2005).

The Famine Early Warning System Network (FEWS NET), an activity of the U.S. Agency for International Development (USAID), is a multi-disciplinary project that collects, analyzes, and distributes national and regional information to decision makers about potential or current climate, famine, or socio-economic hazards (FEWS NET 2010). This allows decision makers to authorize timely measures to prevent food insecurity and other societal problems related to climate factors (e.g., drough, flooding, high temperatures). The U.S. National Aeronautics and Space Administration (NASA), the U.S. Geological Survey (USGS), U.S. Department of Agriculture (USDA), and NOAA provide satellite based analyses of recent HOA temperature, precipitation, and land surface vegetation, plus other scientific and technical support, to FEWS NET (FEWS NET 2010). These analyses and related long-range forecasts of climate conditions (e.g., surface air temperature, precipitation) are used to develop food insecurity outlooks at lead times of several months or less. In particular, the environmental analyses and forecasts are combined with in-country analyses of prices, grain stores, political conditions, and agriculture inputs to provide assessments of present and potential food shortages (Funk 2009). Figure 2 outlines the process used to generate the climate forecasts. Figure 3 outlines the process used to develop a food security outlook product based on climate analyses and forecasts, and on inputs from experts on climate, agriculture,

health, economics, disaster management, and many other fields. Figure 4 provides an example of a food security outlook product from FEWS NET. This type of outlook is intended for use by public and private organizations in planning mitigation response activities.

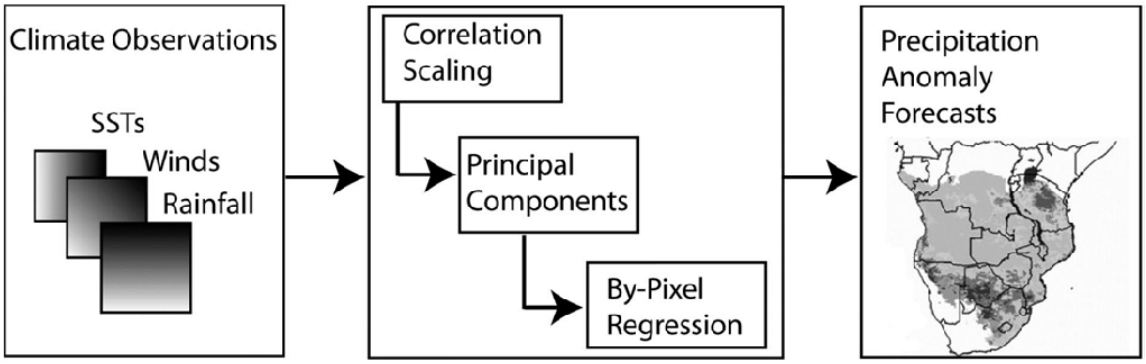

Figure 2. Outline of process used to generate some of the climate forecasts used by FEWS NET. Observations (left box) are used to identify statistical relationships between climate system variables (middle box; e.g., conditions in the Indian Ocean) and food related variables (e.g., precipitation in southern Africa). These relationships are used to build predictive statistical models that generate forecasts for the food security related variables (right box). Figure from Funk (2009).

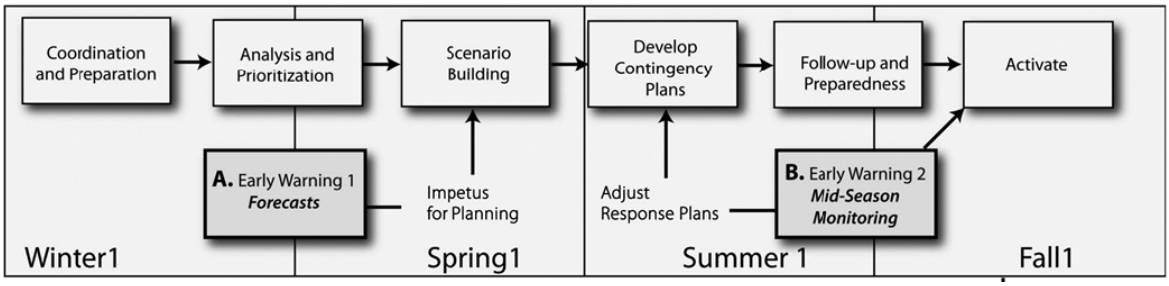

Figure 3. Outline of contingency planning and response process used by FEWS NET. Climate forecasts are used as inputs to the development of potential food insecurity scenarios that are then used to develop contingency plans and food security outlooks (e.g., Figure 4). Figure from Funk (2009).

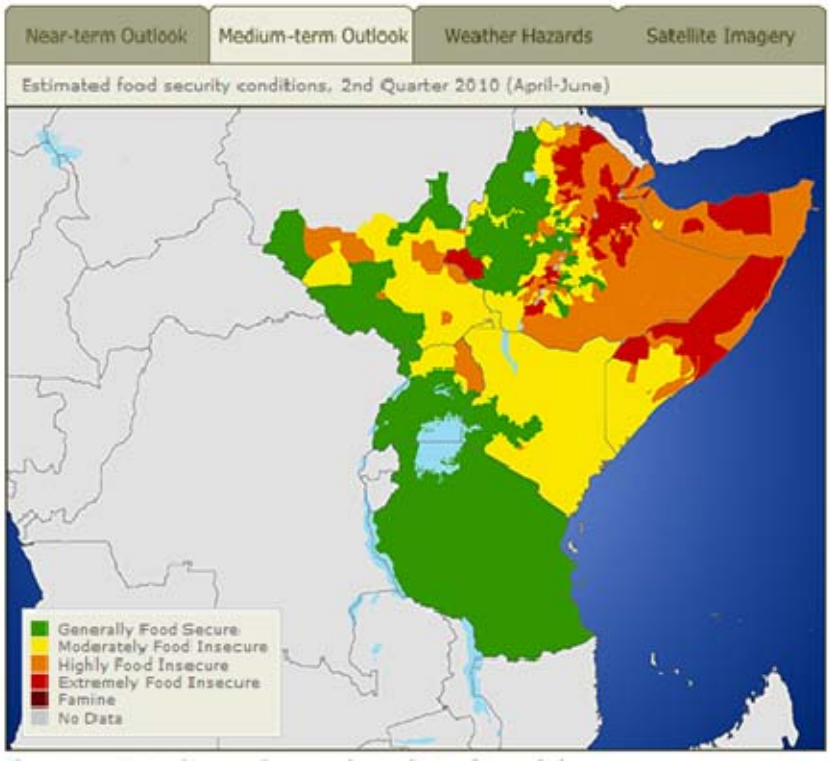

Figure 4. Example of a food security outlook product generated by FEWS NET. This outlook is for conditions in eastern central Africa and the HOA in April–June 2010. Climate forecasts are an essential element in the generation of such outlooks. These outlooks are used by agricultural, emergency management, and other planners to mitigate the food insecurity events and their effects. Figure from U.S. Aid, FEWSNET, May 2010; available online at http://www.fews.net/Pages/region.aspx?gb=r2&l=en; accessed May 2010.

Other organizations that incorporate climate forecasts into their EWSs include the Intergovernmental Authority on Development (IGAD) Climate Prediction and Applications Center (ICPAC; IGAD 2010). The Drought Monitoring Center (DMC) in Nairobi, Kenya, a specialized institution of the ICPAC, is responsible for climate monitoring, prediction, early warning, and applications for the reduction of climate-related risks in the greater HOA (WMO 2010a, b). ICPAC provides regular climate advisories, including 10-day, monthly, and seasonal climate bulletins as well as early warning information on evolving climate extremes and associated impacts. Prior to each rainy season a greater

HOA climate outlook forum is held that brings together international, regional, and national experts in climate, health, agriculture, economics, and disaster management. This forum examines prevailing and expected climate variations that affect weather and climate in the HOA. Using atmosphere-ocean dynamical models, statistical models, and expert interpretation, a consensus regional seasonal forecast is produced in the form of probability distributions of above normal (AN; upper tercile), near normal (NN; middle tercile), and below normal (BN; lower tercile) precipitation for the greater HOA. The contributors to the regional consensus climate outlook include the ICPAC regional meteorological offices, International Research Institute for Climate and Society (IRI), FEWS NET, United Kingdom Meteorological Office (UKMO), World Meteorological Organization (WMO), National Centers for Environmental Prediction (NCEP) / Climate Prediction Center (CPC), and the European Centre for Medium-range Weather Forecasts (ECMWF) (ICPAC 2010). Figure 5 is an example of the ICPAC precipitation outlook for the greater HOA for Mar–May 2010.

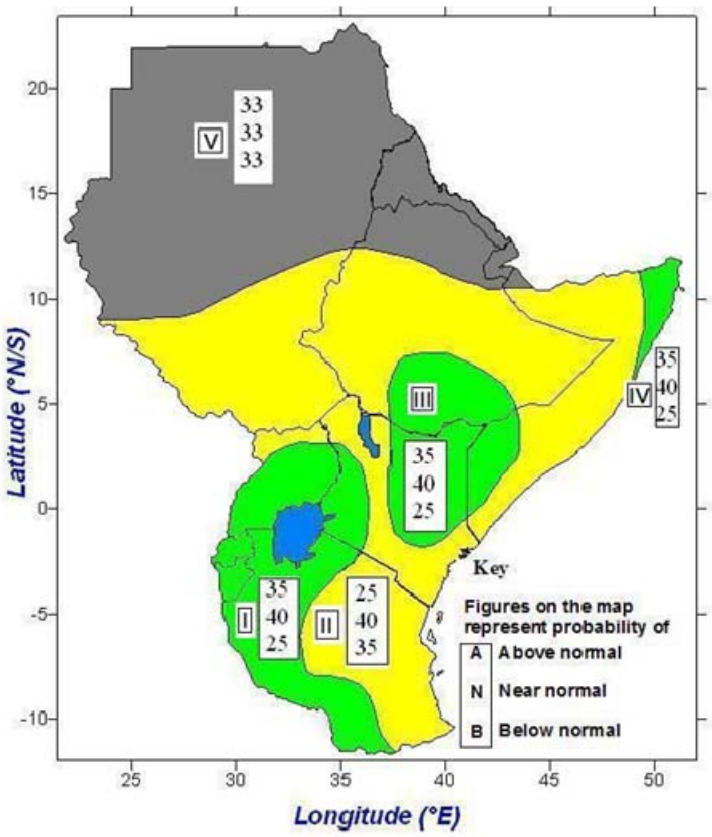

Figure 5. Example of a seasonal precipitation outlook from ICPAC. This outlook shows the predicted probability of above normal (AN), near normal (NN), and below normal (BN) precipitation in the greater Horn of Africa during March–May 2010. The yellow, green, and gray shading represents areas expected to experience similar AN, NN, and BN precipitation conditions. Yellow: relatively high probability of NN or BN precipitation. Green: relatively high probability of NN or AN conditions. Gray: equal chances of AN, NN, and BN. The vertical boxes with three numbers show the probabilities for each category, with AN at the top of the box, NN in the middle, and BN at the bottom. Note that in each colored region, the three probabilities sum to 100%. Example: in zone III the probabilities are 35% AN; 40% NN; and 25% BN. Figure from ICPAC; available online at **www.icpac.net/Forecasts**; accessed March 2010.

The Kenya Meteorological Department (KMD) produces seasonal precipitation forecasts for Kenya of precipitation probabilities, and of the dates of the onset and cessation of precipitation. These forecasts are based mainly on empirical statistical models for which the expected evolution of global SST anomalies and the Southern Oscillation Index (SOI) are the main predictors (KMD 2009). Figure 6 shows examples of KMD seasonal forecasts for Kenyan precipitation for March–May 2010.

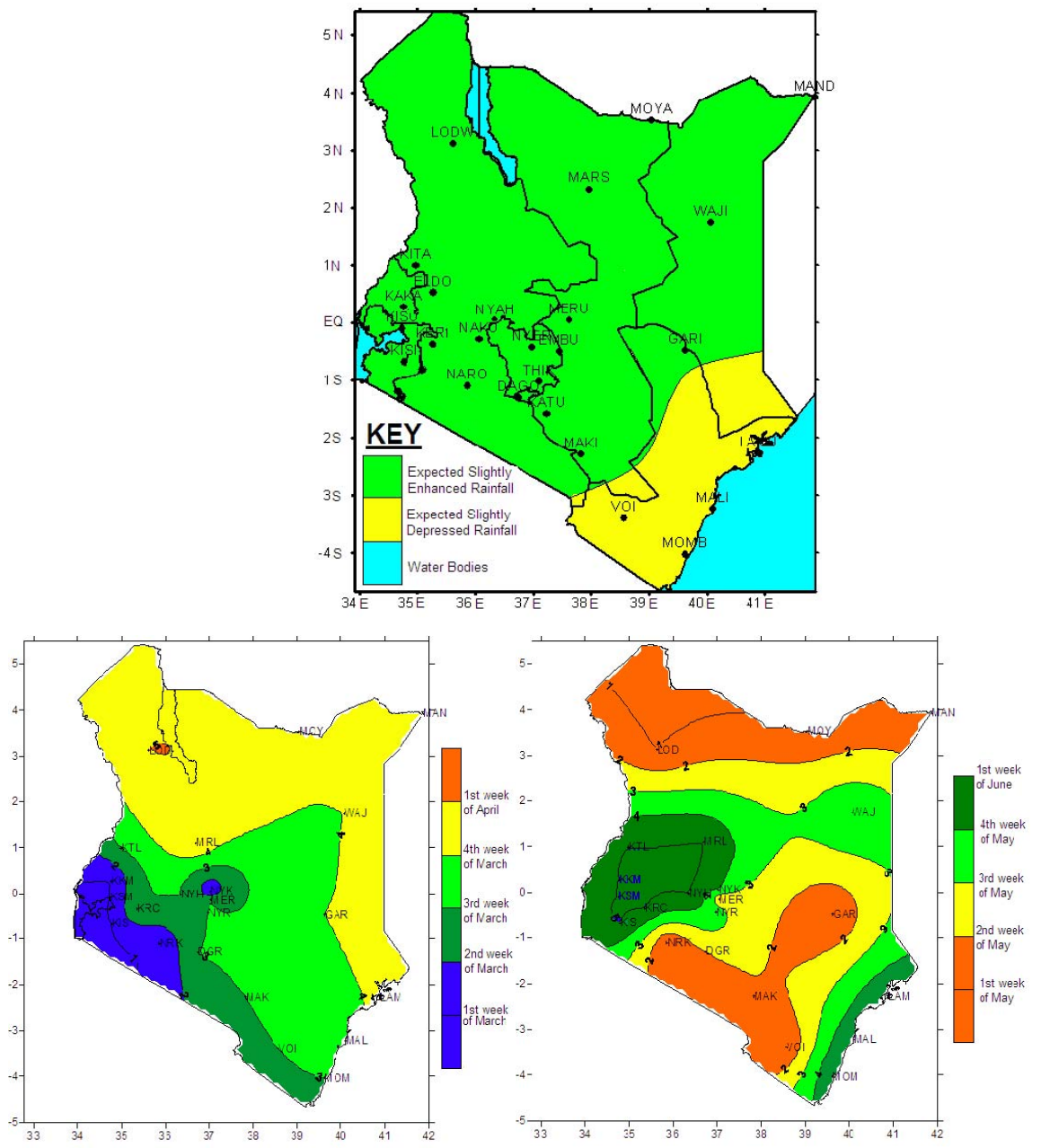

Figure 6. Examples of seasonal precipitation forecasts from the Kenya Meteorological Department for March–May 2010. March–May in central east Africa is normally a period of relatively high precipitation that is often referred to as the long rains season. Top panel: forecast of areas of above and below normal precipitation. Bottom left panel: forecast of onset dates for long rains season. Bottom right panel: forecast of cessation dates for long rains season. Figure from Kenya Meteorological Department; available online at **www.meteo.go.ke/**; accessed March 2010.

F. NON-DOD OPERATIONS IN THE HOA AND LONG-RANGE FORECASTING

DoD has recently been restructured in order to address African peace and stability issues, including the creation of U.S. Africa Command, or AFRICOM. AFRICOM is directly responsible to the U.S. Secretary of Defense and is the only U.S. combatant commands devoted solely to Africa. Part of the AFRICOM mission is to enable DoD and other elements of the U.S. government to work in concert and with partners to achieve a more stable environment in which political and economic growth can take place (U.S. Africa Command 2010). Unlike traditional combatant commands, AFRICOM's focus is on war *prevention* rather than on war-fighting, including working with over 53 African nations and organizations to build regional stability and crises response capacity in support of U.S. government efforts in Africa. Among President Obama's main priorities for Africa are: (a) helping to develop strong and sustainable democratic governments; (b) strengthening public health; and (c) promoting peace and security (U.S. Africa Command 2010). Some of the AFRICOM activities include health services, humanitarian aid and support, and training of the African military and security forces—all in an effort to support the African people in peacefully building a foundation on which to grow economically and politically. Figure 7 illustrates some of these activities, all of which benefit to some degree from accurate long-range forecasts of precipitation and other climate system variables.

Figure 7. Examples of U.S. Africa Command (AFRICOM) activities that contribute to U.S. government efforts in Africa. Accurate long-range climate forecasts have the potential to improve planning by AFRICOM and its African government partners and non-governmental organization (NGO) partners. Figure from U.S. Africa Command (2010).

If AFRICOM is to be successful, it must account for the many climate factors that affect Africa, including climate variations and climate change. To do so, it will have to collaborate with operational weather and climate organizations that have the capacity to provide climate analyses and long-range predictions of climate factors that affect operations in Africa (Montgomery 2008). Presently, AFRICOM relies mainly and indirectly on civilian climate organizations (e.g., NOAA, UKMO). However, the US Air Force (USAF) 14th Weather Squadron (14 WS) has recently started producing long-range forecasts (LRFs) for the HOA that

support military operations in the region. The 14 WS is also investigating the possibility of producing similar forecasts for the pan-sub-Saharan African region (e.g., the Sahel).

The 14th Weather Squadron (14 WS), formerly known as the Air Force Combat Climatology Center, located in Asheville, NC is the primary operational climate support center for the USAF and much of the rest of DoD (14th Weather Squadron 2010). Its mission is to receive, store, and quality control worldwide weather data to create climatological products to strengthen the combat capability of U.S. warfighters. Customers include all the military services, the combatant commands (e.g., AFRICOM), the USAF MAJCOMS, U.S. intelligence agencies, the White House, and many more. Military planners intending to exploit the environment for operations worldwide, including the HOA region, use the information and services provided by the 14 WS. The information in this section on the 14 WS LRFs is based on personal communication with the 14 WS personnel and examination of sample LRFs from the 14 WS.

In January 2010, the 14 WS started producing narrative-only LRFs (lead times of one to six months) of HOA surface air temperature, precipitation, and cloud ceilings. The forecasts include discussions of: (a) the state of El Nino – La Nina (ENLN); (b) expected departures from normal conditions; (c) forecast summary conditions; and (d) annual climatologies for each country within the HOA. Figure 8 shows the region for which the 14 WS produces its HOA LRFs.

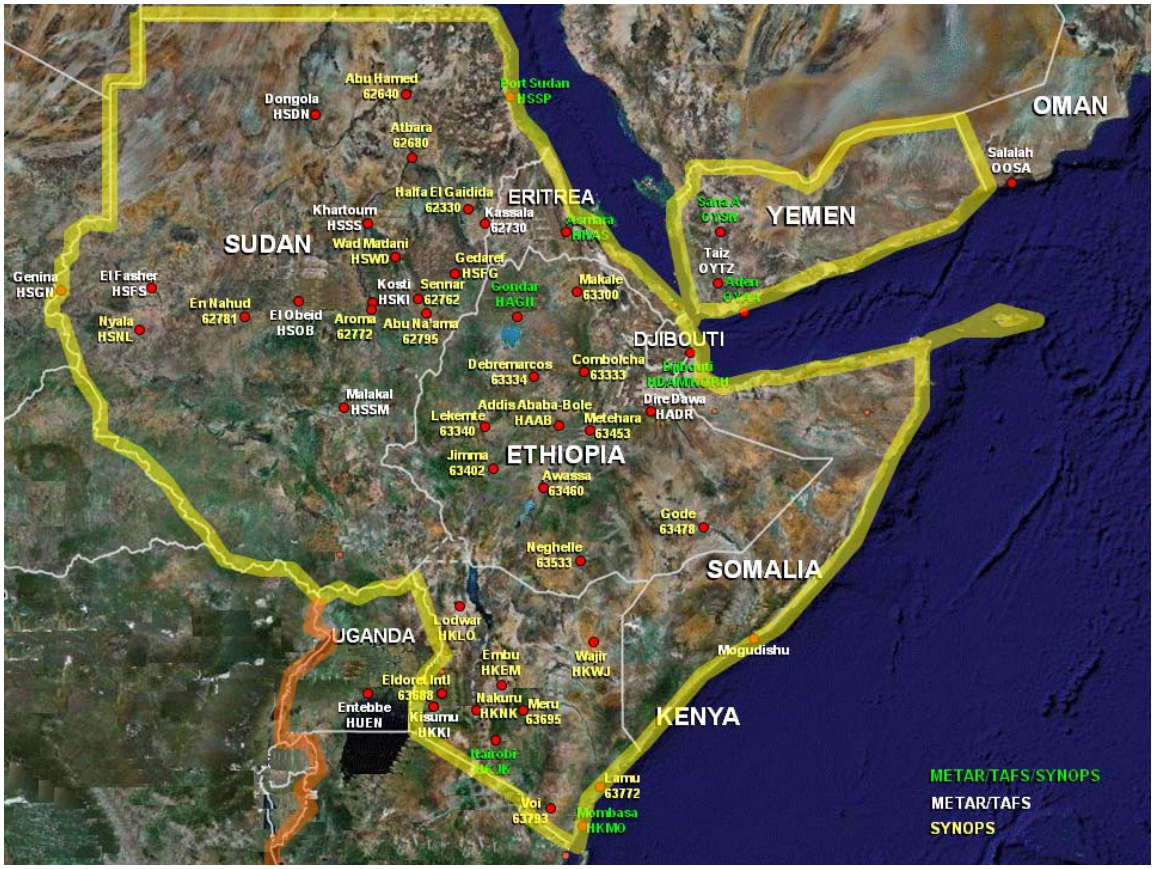

Figure 8. The African region (outlined in yellow) for which the 14th Weather Squadron (14 WS) produces its LRFs for the HOA. The 14 WS produces for this region narrative-only long-range forecasts (lead times of one to six months) of surface air temperature, precipitation, and cloud ceilings. These LRFs are based on composite analysis methods employed by the 14 WS, and on LRFs produced by civilian operational climate centers (e.g., CPC, IRI, UKMO). The locations marked with red dots are ones from which in situ observations are collected and for which terminal aerodrome forecasts (TAFs) are issued. Figure from personal communication with 14 WS.

To produce these LRFs, the 14 WS generates composite analysis forecasts (CAFs; discussed in Chapter II) that are then synthesized with a suite of climate analysis and forecast products from CPC, IRI, UKMO, Australian Bureau of Meteorology (BOM), Beijing Climate Center, Hydrometeorological Center of Russia, University College London (UCL) Dept of Space and Climate Physics, USDA, and Air Force Weather Agency (AFWA) dust transport products.

The 14 WS uses the composite analysis forecast (CAF) process to develop LRFs based on using Nino 3.4 sea surface temperature (SST) anomalies (SSTAs) as a predictor. University of Delaware (or NCEP reanalysis) precipitation data is used to develop the HOA precipitation predictand data set. The resulting CAF LRFs predict the probability of AN, NN, and BN conditions for the HOA for a given month. Monthly and seasonal prediction products from outside sources (e.g., CPC, IRI, UKMO, BOM) are evaluated and synthesized with the 14 WS CAF LRF to produce the final narrative-only LRFs of surface air temperature, precipitation, and cloud ceilings. The narrative also discusses the potential for droughts, floods, and dust storms, and expected snow pack conditions. The LRF is updated monthly or on a specific needs basis valid for 1–180 days from issuance.

The 14 WS uses NCEP reanalysis composites to verify their forecasts. The composites are subjectively analyzed and categorized into AN, NN, or BN terciles for several sub-regions of the HOA and compared to the forecasts made 90, 60, and 30 days prior. For example, a 90-day forecast made in January valid for April is compared to the April reanalysis composite. The subjective tercile categorizations from both the forecast and observed data are manually fed into a program that computes the Heidke skill and Brier skill scores, the primary verification metrics for the LRFs.

Long-range forecasts, narratives and other products and services from the 14 WS can be found at https://notus2.afccc.af.mil/SCIS/. The user will need a password or U.S. government common access card to view the suite of products.

To the best of our knowledge, no other military service provides LRFs for the HOA at the time of this research.

G. MOTIVATIONS FOR AND OUTLINE OF THIS STUDY

1. Scientific Motivations

We had several scientific and operational motivations for conducting this research. Scientifically, very few climate studies focus on the HOA as defined in this study; instead, focusing further south in central East Africa (especially Kenya, Tanzania, Uganda, Zimbabwe; e.g., Funk 2009). Vorhees (2006) and LaJoie (2006) conducted analyses of the patterns, processes, and teleconnections associated with precipitation and temperature anomalies in the HOA and nearby regions. They identified physical linkages between precipitation variability and global scale climate variations, especially ENLN, the IOZM, and the MJO. They both noted the potential for LRFs of HOA surface air temperature and precipitation, but did not conduct any forecasting research. Relatively little research has been done on long range prediction for the HOA, and most of these studies have focused on seasonally averaged forecasts at lead times of three months or less. Many of the LRF studies for the HOA and East Africa have used SOI, ENLN, IOZM and other forecasted and well-known climate indices as predictors. Heidt (2009) developed deterministic and probabilistic LRFs for the western North Pacific that were based on SST predictors that were specifically selected for the predictand variables, times, and locations. Our study builds on the climate analysis results of Vorhees (2006) and LaJoie (2006), plus the forecasting methodology used by Heidt (2009), to identify and apply predictors that are specific for LRFs of HOA precipitation. We also develop and test methods for skillful forecasting at leads of up to six months.

2. Operational Motivations

With the recent advent of long-range forecast support for the HOA by Air Force Weather (AFW), the 14 WS has requested the assistance of NPS in improving their long-range forecasting for the HOA, using quantitative, objective methods with demonstrated skill. At present, the 14 WS LRFs for the HOA are

narrative-only, lengthy, generalized, have lower skill than desired, and are not well suited for use in warfighter planning. Part of our objective in this study was to develop and test methods for the 14 WS to produce more reliable and actionable LRFs. We also intended to improve the climate forecasts used by governmental and non-governmental planners and governmental organizations in preparing for future environmental, agricultural, societal, and economic impacts, and in mitigating social and political instability in the HOA. The vast majority of the people living in the HOA depend heavily on precipitation for their livelihoods, so better LRFs of precipitation, especially during the relatively unpredictable short rain period, would be very beneficial to them.

3. Research Questions

This study explored the viability of using advanced climate datasets and methods to skillfully forecast atmospheric conditions at long lead times, in order to provide DoD and non-DoD organizations with cost-effective information to significantly enhance their planning processes. We focused primarily on investigating the following questions:

(1) What atmospheric variables in the HOA are both operationally significant and predictable at long lead times?

(2) What climate system variables are the most viable predictors of climate variations in the HOA, and can these variables be used to skillfully predict atmospheric conditions in the HOA at long lead times?

(3) What are the best LRF methods to use at all lead times in the HOA?

(4) What are the best formats for presenting LRFs to planners preparing for operations in the HOA?

4. Study Region

Our general study region was the broad HOA Sudan, Ethiopia, Eritrea, Djibouti, Somalia, and Kenya and the adjacent waters (Figure 9).

Figure 9. The broad Horn of Africa (HOA) region. The continental scale view (left panel) shows the HOA region (red outlined box) in relation to all of Africa. The HOA focused view (right panel) shows the general HOA region for our study. The darker brown shading indicates the countries that are often considered part of the broad HOA region. Figure from World Health Organization (WHO); available online at: **www.who.int/.../hoafrica/en/index.html**; accessed May 2010.

We chose to focus on this region for several reasons. This region is an important area of operations for DoD and non-DoD organizations, especially due to political instability, and terrorist and piracy activities, in the region. There are extensive interactions of governmental and non-governmental organizations in the region (e.g., between Ethiopia, Somalia, and Kenya). There are a number of broad socio-economic similarities for the countries in this region (e.g., similar agricultural practices, economies, religions). There are also many environmental similarities (e.g., similar geography, weather, climate, land surface vegetation). In particular, the region tends to experience similar seasonal cycles and variations in climate (e.g., monsoonal cycles, rainy seasons, intraseasonal to interannual variations in temperature and precipitation; Figure 11).

For most of the HOA, precipitation tends to be focused in two high precipitation periods: the March-May long rains period and the October–December short rains period (Figures 10, 11). These rainy periods occur as the intertropical convergence zone (ITCZ) passes overhead as it shifts northward (southward) over eastern Africa during the northern spring and summer (fall and winter). Figure 10 shows the precipitation patterns associated with the southward shift of the ITCZ during the northern fall.

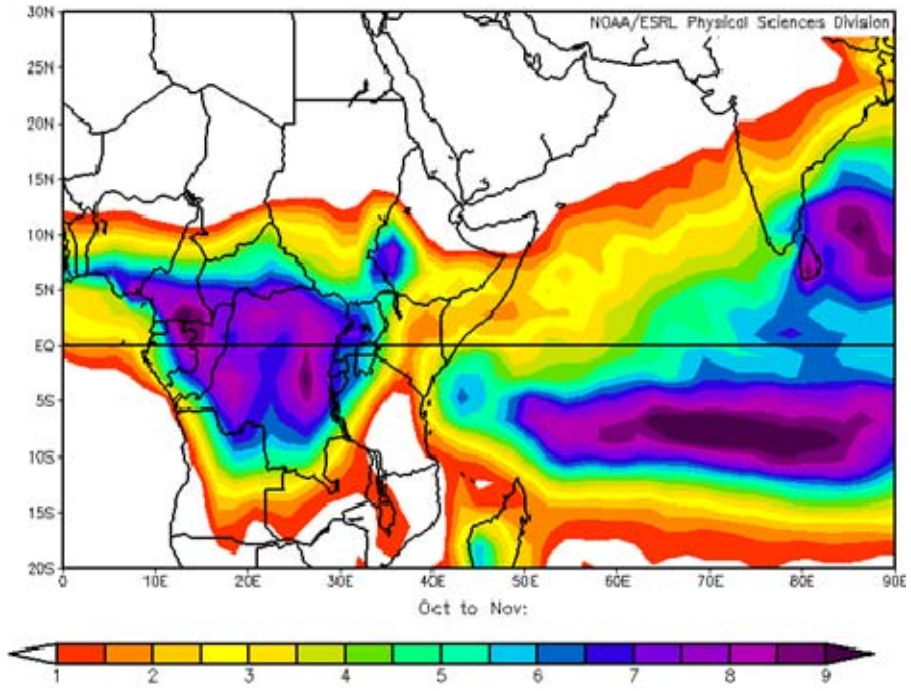

Figure 10. Long-term mean (LTM) composite of surface precipitation rate (PR; mm/day) during October–November (Oct–Nov) for 1970–2009. Oct–Nov tends to be a period of relatively high precipitation for the general HOA region (see Figures 9 and 11). HOA precipitation in this period is: (1) lower than in the western and central tropical African and tropical Indian Ocean regions; and (2) higher in these months that in the tropical and subtropical regions to the north and south of the HOA. Image created using ESRL (2010).

5. Period

The focus period for this study was October–November of the 40-year period 1970–2009. This period was chosen based on the availability and quality of NCEP reanalysis and other datasets. These datasets are available for earlier years, but we chose to maximize the positive impacts of satellite data on the reanalysis data by excluding years prior to 1970. The 1970–2009 period is long enough to provide relatively good depictions of intraseasonal to interannual climate variations, such as the Madden-Julian Oscillation (MJO), ENLN, and the Indian Ocean Zonal Mode (IOZM) (e.g., Vorhees 2006), as well as some representation of decadal variations. We focused on October–November because this short rains period provides much of the annual precipitation for the HOA and is the most rainy period for the HOA (e.g., Hastenrath et al. 1993; Ogallo 1988; Behera et al. 2005), as shown in Figure 11.

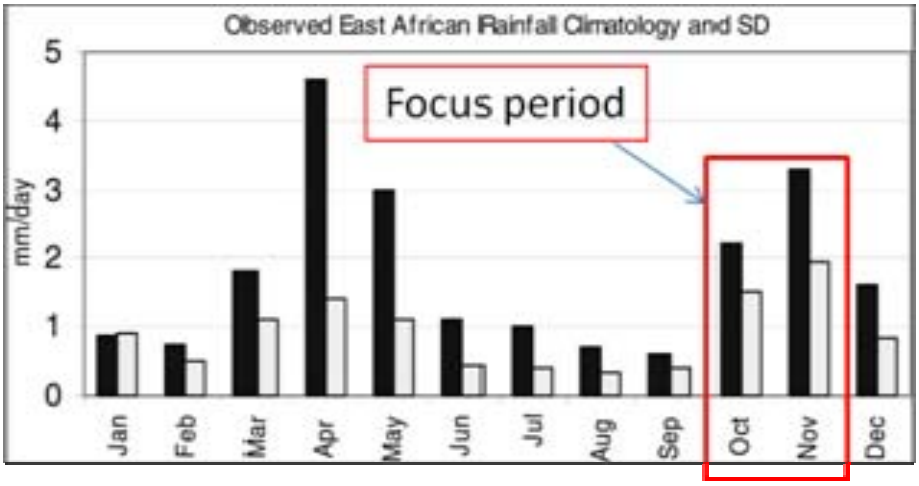

Figure 11. Monthly precipitation rate (PR; mm/day; black bars) and standard deviation of the precipitation rate (SD; mm/day; white bars) in the east African region (5°S-5°N, 35°-46°E) from in situ observations. Two rainy seasons occur in east Africa, including the HOA as defined in this study: (1) the March to May long rains period; and (2) the October to December short rains period. The PR during Oct–Nov tends to be relatively high and has a relatively high SD. Thus, the Oct–Nov PR is an especially important, but difficult, variable to be able to predict at long lead times. The Oct–Nov PR in the HOA was the primary target, or predictand, for the LRFs we developed and tested in this study. Figure from Behera et al. 2005.

6. Thesis Organization

Chapter II provides an overview of the datasets, and analysis and LRF methods, used in this study. Chapter III outlines the results of each LRF method when applied to various periods and predictors, and concludes with a LRF of precipitation rate (PR) in the HOA during October–November 2010. Chapter IV provides a summary of our results and conclusions, and offers suggestions for future research.

THIS PAGE INTENTIONALLY LEFT BLANK

II. DATA AND METHODS

A. DATASETS AND SOURCES

1. NCEP/NCAR Atmospheric Reanalysis Data

The main climate dataset we used in this study is the NCEP/NCAR reanalysis dataset (R1: Kalnay et al. 1996; Kistler et al. 2001). This dataset provides a global retrospective analysis (i.e., a reanalysis) of atmospheric and surface climate system variables from 1948 to present. Observational data from in situ, airborne, and satellite sensors are quality controlled and assimilated with a data assimilation system that is kept unchanged over the reanalysis period. We used reanalysis data at the standard temporal resolution of six hours and horizontal resolution of 2.5°, and at standard tropospheric and stratospheric levels. Our primary variables of interest were air temperature, sea surface temperatures (SST), geopotential heights (GPH), winds, and precipitation rate (PR).

The strengths of the R1 dataset are its uniform global coverage; accessibility; and ability to capture low frequency climate variations. However, the 2.5°spatial resolution limits our ability to represent mesoscale features, such as those associated with the HOA's complex topography.

Our study period of 1970 to 2009 was chosen for the reasons given in Chapter I, Section D.2, and because prior studies have shown the R1 dataset is problematic and may be unreliable for tropical Africa prior to 1970 (Pocard et al. 2000; Camberlin et al. 2001).

NCEP released a major new coupled atmosphere-ocean-land-ice reanalysis dataset, the Climate Forecast System Reanalysis (CFSR), in January 2010 that includes major improvements to the data assimilation and underlying dynamical model. CFSR spans the period January 1979–present. Some of the

improvements over prior reanalyses are a) coupling to the ocean during the generation of the six-hour guess field, b) an interactive sea-ice model, c) assimilation of satellite radiances for the entire period and d) higher spatial (0.5^o x 0.5^o in the atmosphere) and temporal (hourly) resolution (Saha et al. 2010). CFSR became available too late in our study to allow us to use it. However, CFSR should be considered for use in similar future studies.

2. Multivariate ENSO Index (MEI)

We analyzed the MEI as a possible predictor given the significant links between the HOA and ENLN (e.g., Black et al. 2002; Behera et al. 2005; LaJoie 2006; Vorhees 2006). The MEI combines six atmospheric and oceanic variables into one index to characterize and monitor current and past states of ENLN in the tropical Pacific (Wolter and Timlin 1993; Wolter and Timlin 1998). Because the MEI integrates multiple variables into a single bi-monthly index, the MEI is a more integrated and stable index of ENLN and a potentially more useful predictor than other ENLN indices that only monitor one variable (e.g., SST from the Nino 3.4 index or sea level pressure (SLP from the Southern Oscillation Index (SOI)). A positive (negative) value of MEI represents an EN (LN).

3. Nino 3.4 Index (Nino3.4)

We also investigated as a potential predictor of HOA PR another widely used index of ENLN (Trenberth 1996), the Nino 3.4 index (Nino3.4) based on area-averaged SST anomalies (SSTAs) in the region 5°N – 5°S, 120° – 170°W. This index is defined as the three-month average of the SST anomalies, with index values greater than or equal to +0.5 °C (less than or equal to -0.5 °C) indicating EN (LN) conditions.. We investigated the use of the Nino3.4 as a predictor of HOA PR because 1) the 14 WS uses this index as its primary predictor for the HOA, and 2) long-range probabilistic forecasts of this index are available from CPC and the International Research Institute for Climate and Society (IRI).

4. Indian Ocean Dipole Mode Index (DMI)

We also investigated as a potential predictor of HOA PR an index of the Indian Ocean Dipole Mode, or Indian Ocean Zonal Mode (Saji et al. 1999). For this, we used the Dipole Mode index (DMI) based on SSTAs in the Indian Ocean. The DMI is based on the SSTA difference between the western equatorial Indian Ocean (50°E-70°E and 10°S-10°N) and the southeastern equatorial Indian Ocean (90°E-110°E and 10°S-0°N). A positive (negative) DMI represents a positive (negative) phase IOD (Saji et al. 1999) and is associated with above (below) normal PR in the HOA during October–November (e.g., Behera et al. 2005; Vorhees 2006). The DMI is also forecasted, with long-range forecasts available from the Bureau of Meteorology (BOM) in Australia and the Japanese Agency for Marine-Earth Science and Technology (JAMSTEC), from which all DMI data for this study were obtained.

B. ANALYSIS AND FORECASTING METHODS

Much of the analysis and forecast methodology for this study is similar to that used by Heidt (2009) in her study of LRFs of ocean conditions in the western North Pacific.

1. Predictand Selection

The predictand, or forecast target, for our study was area-averaged precipitation rate (PR) in October–November for a selected region within the HOA at lead times of zero to six months. The major reasons for selecting this predictand are given in Chapter I, Section D. A primary motivation for using area-averaged predictands is that they are simpler and larger forecast targets than point forecast targets, which tends to: (a) make the development of the forecast method simpler; (b) increase predictability at long lead times (e.g., leads of several months or seasons); and (c) simplify forecast verification (cf. van den Dool 2007). The disadvantage of using a spatially large predictand is that the forecast applies uniformly to the whole predictand region and does not identify

variability within the region. However, this disadvantage can be mitigated by selecting a predictand region that tends to be spatially coherent (e.g., a region for which the temporal variations of the predictand variable tend to be spatially uniform). Also, this disadvantage may not be as important to end users of the forecasts as they are to the forecasters. This tends to be the case for operational planners who, at long lead times, only need LRFs for a general region. The need for such threshold forecasts is common for DoD planners, who often only need to develop spatially broad plans at long leads, with the spatial details being planned at shorter leads. Finally, if LRFs of more specific forecast regions do not have skill, then spatially broad LRFs may be the only viable option.

The major factors involved in our selection of the specific predictand region within the HOA were:

(1) The spatial patterns of environmental variability in and near the region

(2) Significant correlations between PR in the region and potential predictors at lags of 0-6 months

(3) The operational importance of the region

(4) The need for long-range forecast support in the region

(5) The overlap with the HOA region defined by the 14 WS

To select the specific region within the HOA, we began by comparing the LTM October–November (Oct–Nov) PR composite (Figure 10) with the PR anomaly for October–November of each year during 1970–2009 (not shown). These comparisons allowed us to identify a region within which: (a) the LTM PR and the PR anomalies were relatively homogeneous, especially for the strongest positive and negative PR anomalies. We first conducted these comparisons for the broad HOA region bounded by 5S-20N, 30-55E, which encompasses all of Ethiopia, Eritrea, Djibouti, Yemen, Somalia, and Kenya. This region also includes most of the HOA region defined by the 14 WS (Figure 8). Based on these initial comparisons, we subdivided this broad HOA region into 20 sub-

regions for which we constructed PR time series that we then correlated with each other and with potential predictors (e.g., MEI, Nino3.4, DMI, global SST). From this process, we identified the sub-regions for which: (a) the PR and PR anomaly patterns were large, uniform, and spatially coherent; and (b) the PR correlations with potential predictors were large and statistically significant.

Based on this process, we selected as our predictand region, the rectangular area bounded by 5S-10N, 30-55E. This predictand includes almost all of what is generally considered to be the HOA, but also includes some adjacent land and ocean areas. We did not include the northern portion of the broad HOA region (e.g., northern Ethiopia, Eritrea, Djibouti, and most of Sudan) in our predictand region because it was too dissimilar from the HOA region further to the south, primarily in terms of the signs, magnitudes, and spatial and temporal patterns of the PR anomalies.

2. Composite Anomalies, Correlations, and Teleconnections

We used the predictand region PR times series for Oct–Nov of 1970–2009 to identify: (a) the above normal (AN), near normal (NN), and below normal (BN) terciles (i.e., the upper, middle, and lower terciles); and (b) the top five AN and top five BN events. For the 40 years of our 1970–2009 study period, each tercile represents approximately 13 years (one-third of the 40 years). The resulting tercile categories for HOA PR were: AN PR is ≥ 3.5 mm/day; NN PR is < 3.5 mm/day but ≥ 3.1 mm/day; and BN PR is < 3.1 mm/day. The resulting top five AN (BN) Oct–Nov HOA PR years were 1972, 1977, 1994, 1997, 2006 (1971, 1974, 1998, 2005, 2007).

We then developed composites of global and regional anomalous PR, SST, GPH, and other climate variables (Table 1) for the top five AN and top five BN events. We also composited according to the top five AN and top five BN events for the three climate variation indices (MEI, Nino3.4, and DMI) and for the potential predictors. We used these composites to assess the patterns and processes during extreme event years. In particular, we used the extreme event

composites to identify potential predictors and the dynamical processes that influence Oct–Nov precipitation in the predictand region. We focused in composites based on just the top five AN and BN events, because composites based on more than five events tend to include weaker events and tend to obscure important climate patterns, processes, and mechanisms of interest (LaJoie 2006). All the anomalies in our study were calculated using a base period of 1968–1996 (cf. ESRL 2010).

Table 1. Climate system variables that we analyzed to identify: (a) potential predictors of HOA PR; and (b) the physical processes that lead to climate variations in HOR PR. All variables were assessed on a global scale, except for soil moisture.

Variable	Abbreviation	Units
Sea surface temperature	SST	degrees Celsius (°C)
Air temperature at 10 m	T air/air temperature	degrees Celsius (°C)
200 hPa geopotential heights	200 hPa GPH	geopotential meters (GPM)
850 hPa geopotential heights	850 hPa GPH	geopotential meters (GPM)
200 hPa vector winds	-	meters/second (m/s)
850 hPa vector winds	-	meters/second (m/s)
Specific humidity	SH	grams/centimeter3 (g/cm3)
500 hPa vertical velocity	Omega	Pascals/second (Pa/s)
Precipitation rate	PR	millimeters/day (mm/day)
Outgoing longwave radiation	OLR	watts/ meter2 (w/m2)
Volumetric Soil Moisture (0-10cm)	soil moisture	fraction

We calculated bi-monthly (e.g., Oct–Nov) correlations at lag times of zero to six months between the predictand PR time series and the climate system variables shown in Table 1. We also calculated similar correlations between the three climate variation indices and global PR. These correlations were analyzed to identify the spatial patterns and teleconnections associated with climate variations in HOA PR. For correlations based on the full study period of 1970–2009, correlations greater than +/- 0.304 were considered statistically significant at the 95% confidence interval based on the standard normal distribution of a two tailed *t* test (Wilks 2006). When the dataset was reduced to 10 years and 15 years for our optimum climate normal analyses, correlations greater than +/- 0.48

and +/- 0.57, respectively, were considered statistically significant at the 95% confidence interval. The correlations were conducted using Excel and the ESRL web sites (ESRL 2010).

3. Predictor Selection

In our study, we defined potential predictors as variables with significant long lead correlations and dynamically plausible teleconnections with the predictand. All the predictors we analyzed represented area averaged values (e.g., the average of SST in a 5 x 5 degree region). Multiple potential predictor variables were investigated (see Table 1), primarily via correlations with the predictand. SST at several locations was found to have the consistently highest significant correlations with the predictand at 0-6 month lead times. The method for selecting the predictor region was the same as that used for selecting the predictand region (see Chapter II, Section B.1). After selecting the predictors, we conducted composite analyses of the top five AN and top five BN predictor events to identify the patterns and dynamical processes associated with extreme predictor events and their relationships to extreme predictand events.

4. Predictor and Predictand Time Series

After choosing the predictors, we compared the predictor and predictand time series at all lead times. This allowed us to: (a) do visual quality control checks of the predictor-predictand correlations; (b) identify interannual to decadal variations in the relationships between the predictors and predictand; (c) identify periods and lead times for which the correlations were relatively strong and weak; and (d) identify case studies for additional composite, correlation, and dynamical analyses, and hindcast testing.

5. Long-Range Forecasting Methods

We developed and assessed several LRF methods for this study in order to improve upon: (a) the LTM forecast methods commonly used by DoD

forecasters, and (b) the LRF methods presently being used by 14 WS and other non-DoD organizations. A number of prior studies have shown that climate analyses and forecasts that account for deviations from LTMs have several potential benefits to DoD planners by providing more accurate and reliable assessments and forecasts than those based on LTMs alone (LaJoie 2006; Vorhees 2006; Hanson 2007; Moss 2007; Turek 2007; Crook 2009; Heidt 2009; Ramsaur 2009). In addition, LRFs based on customized predictors selected for a specific forecast target often have more skill than those based on general predictors, such as ENLN indices (e.g., Crook 2009; Heidt 2009).

The deterministic and probabilistic LRF methods we used in this study include tercile matching, averaged linear regression, non-averaged linear regression, composite analysis, and optimal climate normals. We applied these forecast methods to several predictor-predictands pairs and to several hindcast and forecast time periods. The main results from each of these methods were categorical forecasts; that is, forecasts of the predictand tercile category—AN, NN, or BN HOA PR.

A primary motivation for using such categorical forecast targets is that they are simpler and larger forecast targets than discrete value forecast targets, which tends to: (a) make the development of the forecast method simpler; (b) increase predictability at long lead times (e.g., leads of several months or seasons); and (c) simplify forecast verification (cf. van den Dool 2007). The disadvantage of using a categorical predictand is that the forecast gives only a range of predictand values and does not specify where within that range the actual predictand variable will occur. However, this disadvantage can be mitigated by selecting smaller categories than terciles (e.g., quintiles). This disadvantage may not be as important to end users of the forecasts as they are to the forecasters. This tends to be the case for operational planners who only need to know the likelihood that an environmental variable will be above or below a given operational threshold. The need for such threshold forecasts is common

for DoD planners, especially when planning operations at long lead times. Finally, if LRFs of more specific forecast targets do not have skill, then categorical LRFs may be the only viable option.

All of the forecast methods use just one to three predictors, and are thus unlikely to predict (or explain) all of the predictand variations. However, by careful selection of the predictors (and the predictand), these methods have the potential to predict many of the predictand variations, and thereby produce skillful LRFs (cf. Hanson 2007; Moss 2007; van den Dool 2007; Heidt 2009).

To assess the viability of our LRF methods, we used the methods to conducted hindcasts for the period 1970–2009. We then assessed the skill of these multi-decadal hindcasts according to the predictor, lead time, and forecast method.

For all the forecast methods, we used Excel to help analyze the predictor and predictand data, generate the forecasts, and assess the performance of the forecasts. The methods are described in the following subsections.

a. Method 1 – Tercile Matching

For the tercile matching method, we then used the sign of the correlation between the predictor and predictand to determine the expected relationships between the predictor tercile categories and the predictand tercile categories. For example, if the correlation was negative, then the expected relationships would be: If AN (BN, NN) predictor, then expect BN (AN, NN) predictand. The forecast is based on the expected relationship between the known tercile category for the predictor and the unknown tercile category for the predictand. So, for the negative correlation example just given, an AN (NN, BN) predictor value would lead to a forecast of a BN (NN, AN) predictand value. To apply this method, we grouped the predictor and predictand seasonal values into their respective AN, NN, and BN tercile categories. We then determined for each year whether the predictor-predictand pair categories matched the expected

relationship (e.g., AN predictor and BN predictand, for the previous example), were opposite to the expected relationship (e.g., AN predictor and AN predictand, for the previous example), or were otherwise (e.g., AN predictor and NN predictand, for the previous example). For the years in which the pairs matched the expected relationship, the forecast was deemed accurate. For example, if we found a negative correlation between an SST predictor in Apr–May and HOA PR in Oct–Nov, then we used the occurrence of an AN (NN, BN) SST in Apr–May to produce a forecast of BN (NN, AN) HOA PR for the following Oct–Nov.

The advantages of the tercile matching method include its conceptual and computational simplicity. In principle, it can be thought of as a very simple categorical version of linear regression.

b. Method 2 – Averaged Linear Regression

We used two linear regression methods to model the relationships between HOA PR and several predictors, based on the R1 dataset. Linear regression (LR) refers to any approach to modeling the relationship between a predictor variable and two or more predictand variables, such that the model depends linearly on unknown parameters that are estimated from predictor and predictand datasets (cf. Wilks 2006). If the relationship is linear, LR can be a useful method for long-range forecasting giving an exact value. The LR model does not provide a determination that there is a causal relationship between the predictor and predictand. However, the LR model may help corroborate other evidence of a causal relationship.

Liner regression result in the derivation of a regression equation that has the form (cf. Wilks 2006):

Predicted value = slope * predictor + y-intercept

This equation is the LR model and is determined by analysis of the predictor and predictand datasets. The resulting forecasts are discrete,

deterministic forecasts of the predictand that we then assigned to the AN, NN, or BN tercile categories, with the terciles being defined by the predictand time series derived from the R1 dataset.

The 1970–2009 hindcasts for the two LR methods were formulated and tested by using a leave-one-out cross validation approach (Wilks 2006). That is, data for the year to be hindcasted were withheld when developing the regression model that was applied to that year, with the model for that year being based on data from all the other years (cf. Jury 1996; Wilks 2006). New AN, NN, and BN terciles were determined from the remaining years, which were used to determine the tercile of the new hindcasted value. For example, to formulate the 1970 PR hindcast, we excluded the SST and PR values for 1970 from the R1 dataset, leaving the 1971–2009 SST and PR values to form new AN, NN, BN terciles, and the slope and y-intercept. For the 1971 PR hindcast, we excluded the 1971 SST and PR from the R1 dataset, leaving 1970 and 1972–2009 to form the new terciles, slope and y-intercept, and so on through 2009.

For the average linear regression method, all of the slope and y-intercepts were averaged together to come up with a single slope and y-intercept regression equation model in which the predictor value for the excluded year was inserted into the equation to get a hindcasted PR for the excluded year. The hindcasted value was then assigned to one of the new tercile bins and compared to the actual PR for that year. The average LR method yields one regression model for the entire dataset. The LR models that use non-averaged slope and y-intercept values were very similar from year to year, and very similar to the average LR model, as might be expected when only one out of a total of 40 years is being omitted per hindcast year. These similarities indicated that the average LR model was a simple but reasonable alternative to the non-averaged LR model. These similarities also indicated that the non-averaged LR models were not overfit (i.e., were not overly reliant on predictor-predictand relationships that were unique to a few years and unrepresentative of most years). This result

helped validate the use of non-averaged LR models. We developed averaged regression equations for lead times of zero to six months.

c. Method 3 – Non-Averaged Linear Regression

The development of the non-averaged LR models is described in Section 5.b, but without the averaging of each year's slope and y-intercept values to produce a single average LR model. So, in Method 3 we did not average the 40 regression equations into one. For example, to hindcast the 1970 PR, we used the leave-one-out cross validation approach described in Section 5b, excluding 1970 from the dataset and produced a slope and y-intercept from the remaining 1971–2009 data. This gave us our regression equation from that dataset and became our LR model to hindcast the 1970 PR, and so on through 2009. The difference between the predictions from the averaged and non-averaged regression equations were small, although sometimes large enough, to change the predicted PR to a different tercile (e.g. BN to NN, or NN to AN). We developed regression equations for all hindcast years 1970–2009 and at lead times of zero to six months. The non-averaged LR model based on the years 1970–2009 was our preferred LR model for producing LRFs for 2010. Likewise, a non-averaged LR model for the years 1970–2010 would be our preferred LR model for LRFs of 2011.

d. Method 4 – Composite Analysis Forecast

We used the composite analysis forecast (CAF; MetEd 2010) process to generate probabilistic, categorical, long-range forecasts based on the historical occurrence, or conditional probability, of a certain predictand category occurring given the occurrence of a specified predictor category (e.g., the probability of AN PR in Oct–Nov given the occurrence of BN SST conditions near New Zealand in Apr–May). In the CAF method, the statistical significance of the predictor-predictand relationship needs to be determined, with a 90 percent confidence level being the standard for application of the method. The statistical significance: (a) is a standard measure of the confidence in the rejection of the

null hypothesis that there is no relationship the predictor and predictand; and (b) provides insight into whether the use of conditional composite probabilities based on the predictor-predictand relationships is valid in the development of forecasts (MetEd 2010). If there are no statistically significant results for any given lead time and predictor condition, then the CAF method would not be used.

A forecast based on the CAF method involves three equations to compute the probability of a predictand state (AN, NN, or BN). Figure 12 shows the three equations used to forecast the probability of HOA PR in the AN, NN, and BN categories (the left hand side terms in the equations) based on the relationship between the PR predictand and a SST predictor. The first terms on the right hand sides of the equations represent the conditional probabilities. For example, the first right hand term in the first equation represents the probability of AN PR given the occurrence of AN SST. The conditional probabilities are determined from observations (e.g., the R1 dataset in our case). The second terms on the right hand side are the probabilities of the SST categories occurring. For example, the second right hand term in the first equation represents the probability of AN SST occurring. In the standard application of the CAF method (MetEd 2010), the predictor probabilities are forecasted (e.g., forecasts of Nino3.4).

$$P_{AN[PR]} = P^{AN[PR]}_{AN[SST]} x P_{AN[SST]} + P^{AN[PR]}_{NN[SST]} x P_{NN[SST]} + P^{AN[PR]}_{BN[SST]} x P_{BN[SST]}$$
$$P_{NN[PR]} = P^{NN[PR]}_{AN[SST]} x P_{AN[SST]} + P^{NN[PR]}_{NN[SST]} x P_{NN[SST]} + P^{NN[PR]}_{BN[SST]} x P_{BN[SST]}$$
$$P_{BN[PR]} = P^{BN[PR]}_{AN[SST]} x P_{AN[SST]} + P^{BN[PR]}_{NN[SST]} x P_{NN[SST]} + P^{BN[PR]}_{BN[SST]} x P_{BN[SST]}$$

Figure 12. CAF method equations for forecasting the probability of AN, NN, and BN PR (the predictand categories; the terms on the left hand sides of the equations) given: (a); the conditional probabilities of the PR predictand categories given the occurrence of the specified SST predictor categories (the first terms on the right hand sides of the equations); and (b) the probability of SST predictor categories occurring (the second terms on the right hand sides). See main text for more information. The forecast lead time is not specified in these equations. Adapted from MetEd (2010).

The main steps in the CAF methods are:

(1) Select predictand region of interest (e.g., HOA).

(2) Select analysis and forecast periods and lead times (e.g., 1970–2009 dataset for predictand and predictor, Oct–Nov forecast target period, 0-6 month leads).

(3) Select predictor (e.g., SST).

(4) Determine predictand and predictor categories (e.g., terciles).

(5) Determine conditional probabilities based on datasets (e.g., AN PR in Oct–Nov occurred 65% of the time when BN SST conditions occurred near New Zealand in May–Jun).

(6) Conduct risk analysis using hypergeometric distributions to test for statistical significance in predictor-predictand relationship.

(7) Calculate composite analysis forecast for statistically significant relationships at a 90% confidence level. Use alternate LRF method is relationships are not significant.

(8) Verify CAF method with hindcasts.

The strength of the CAF method is that it exploits the same historical observed data used to generate LTMs, yet does so in a way that yields potentially enhanced forecast and decision-making information. The method does however depend on the availability, accuracy and representativeness of the predictor and predictand data. See MetEd (010) for more details on the CAF method. See Hansen (2007), Moss (2007), Crook (2009), and Heidt (2009) for reviews and applications of the CAF method.

In our study (as in Crook 2009 and Heidt 2009), we chose to make the predictors non-forecasted variables (rather than forecasted ones, such as Nino3.4 or DMI). We did this because: (a) our predictors were methodically selected to maximize the predictor-predictand correlations at long lead times; (b) forecasts of our selected were not available; and (c) the selection of leading

predictors meant that once the predictor was observationally determined at the appropriate lead time, there was no need to forecast the predictor. Thus, in our modification of the standard CAF equations (Figure 12), the predictor probability is one for the predictor in the observed tercile and zero for all the other predictor probabilities (Figure 13). The modified CAF equations in Figure 13 represent the equations for a case in which the SST predictor at the forecast lead time is observed to be AN. Thus, for a CAF at this lead time, the SST predictor probability is one for AN SST and zero for NN and BN SST. This means that many of the terms in the standard CAF equations go to zero in the modified CAF equations.

$$P_{AN[PR]} = P^{AN[PR]}_{AN[SST]}$$

$$P_{NN[PR]} = P^{NN[PR]}_{AN[SST]}$$

$$P_{BN[PR]} = P^{BN[PR]}_{AN[SST]}$$

Figure 13. Equations used in our modified CAF process to calculate long-range forecasts of PR based on observed AN SST predictor conditions at the forecast lead time. The lead time is unspecified in these equations. Compare to the standard equations in Figure 12.

A key advantage of our adaptation of the CAF method is that CAFs can be generated for a wide range of customized predictors, rather than just the few predictors that are forecasted at long leads (e.g., Nino3.4). This allows the use of predictors that are well correlated with the predictand but not forecasted. However, for operational use, the predictors must be well observed in real time, so that observed values are available at the appropriate lead times. Thus, for example, well-correlated SST predictors may be good predictors for the adapted

CAF method because SST observations are routinely available in real time. But well correlated near-surface ocean temperatures may not be good predictors, because near-surface ocean temperature observations are generally not available in real time (except for a few special locations (e.g., the equatorial Pacific and other special locations with moored buoy observations of ocean temperature).

e. Optimal Climate Normals (OCN) Approach

LTM climate conditions are the average of conditions observed over a number of years (e.g., 30 years; WMO 2010b). In a stationary climate, LTMs are good estimates of the upcoming expected value for a given variable (e.g., precipitation rate). However, if the climate system varies over periods of several years (e.g., 5–15 years), then taking the average of the most recent years may provide a better estimate of the expected value than would be obtained from a longer period mean (e.g., a better estimate than that obtained from the WMO standard 30 year mean) (van den Dool 2007). The standard way of applying the optimal climate normals (OCN) approach is to calculate a mean value for the predictand from a selected set of consecutive recent years, and then persist that mean to produce a forecast for the year that immediately follows the most recent year of the set (van den Dool 2007). CPC uses OCN for many of its seasonal to interannual forecasts, such as U.S. surface air temperature, precipitation, and North Atlantic hurricane activity (Livezey 2006; van den Dool 2007). CPC uses the average of the most recent 10-15 years when generating operational OCN forecasts.

For this study, we applied the OCN concept by using two approaches to account for recent relationships between the predictor and predictand. In the first, or basic, OCN approach, we used the same predictor that we used when hindcasting all 40 years of our 1970–2009 study period, but we: (a) determined our tercile categories for the predictand and predictor using just the most recent 10- and 15-year periods (2000–2009 and 1995–2009); (b) used

the 10- and 15-year tercile categories in generating hindcasts for those recent years using our four forecast methods; and (c) used the 10- and 15-year tercile categories in verifying the hindcasts. We termed this the basic OCN approach.

In the second, or advanced, OCN approach, we conducted all our analyses (e.g., selection of predictors, composites, correlations, teleconnections) using data from just the most recent 10- or 15-year periods during 1970–2009 (e.g., from just 1995–2009). From this, we identified two new, well correlated, and dynamically plausible predictors that we then used in the four forecast methods described in Sections 5.a-d, above. The resulting hindcasts were then verified against the observed conditions during the most recent 10 to 15 years. This allowed us to determine whether forecast methods that were based on conditions during the most recent 10–15 years could lead to improved forecast skill. We termed this the advanced OCN approach.

In neither OCN approach did we replicate the standard OCN process in which the forecast is based on persisting the mean of the recent 10–15 years (van den Dool 2007). But, both of our approaches apply the basic OCN concept of emphasizing recent conditions when developing forecast methods and generating forecasts. We applied the OCN approach to all four of our forecast methods. Thus, we refer in this report to OCN *approaches*, rather than OCN methods. We distinguished our two OCN approaches and our other approach involving all of our study period years (1970–2009) by referring to them as the *basic OCN approach*, *the advanced OCN approach*, and the *all years approach*, respectively

6. Hindcast and Forecast Verification Methods

All of the predicted PR values from the different forecast methods, with and without applying OCN methods, were binned into AN, NN, and BN terciles to generate categorical PR hindcasts for 1970–2009. These tercile category hindcasts were then compared to the tercile category of the actual PR to assess the skill of the forecast methods. This verification was done using a 3x3

contingency table method to determine the number of hits, misses, false alarms (FA), and correct rejections (CR) (Wilks 2006). The 3x3 table accounts for the three predictor terciles and the three predictand terciles. This contingency table method was applied separately for each predictor, each forecast category (AN, NN, BN), each forecast method, and each lead time. Table 2 shows the assignments that would be made to a 3x3 contingency table for a forecast of AN PR based on BN SST predictor conditions. The four types of assignments are:

1. *Hit:* event forecasted and observed
2. *Miss:* event *not* forecasted but observed
3. *False alarm (FA):* event forecasted and was *not* observed
4. *Correct rejection (CR):* event *not* forecasted and was *not* observed

For the case shown in Table 2: a hit would be assigned when AN PR was forecasted and observed; a miss would be assigned when AN PR was observed but not forecasted; FA would be assigned when AN PR was forecasted but not observed; and CR would be assigned when AN PR was not forecasted and was not observed.

Table 2. Example of contingency table assignments for the verification of forecasts of AN PR when using a categorical SST predictor, for the case in which AN SST leads to a forecast of BN PR.

	Predictand		
Predictor	AN PR	NN PR	BN PR
AN SST	*Miss*	*Correct Rejection*	*Correct Rejection*
NN SST	*Miss*	*Correct Rejection*	*Correct Rejection*
BN SST	*Hit*	*False Alarm*	*False Alarm*

Table 3 shows the hit and miss assignments for AN, NN, and BN PR for a case in which there is a negative correlation between the SST predictor and the PR predictand.

Table 3. Schematic contingency table of hit and miss assignments based on a negative correlation between a SST predictor and a PR predictand.

	Predictand		
Predictor	AN PR	NN PR	BN PR
AN SST	*Miss*	*Miss*	**Hit**
NN SST	*Miss*	**Hit**	*Miss*
BN SST	**Hit**	*Miss*	*Miss*

With the exception of the tercile matching method, each LRF method yields a discrete (non-categorical) forecast of PR or of the probability of a PR category. In order to apply the contingency table method to these discrete and probabilistic forecasts, we: (a) assigned the discrete forecasts to the terciles categories based on the PR terciles determined from the R1 dataset; and (b) in some cases, assigned the probabilistic forecasts to tercile categories based on the highest probability category. This allowed the forecasts from all the forecast methods to be readily compared. Examples of predictand and predictor terciles are shown in Figure 14.

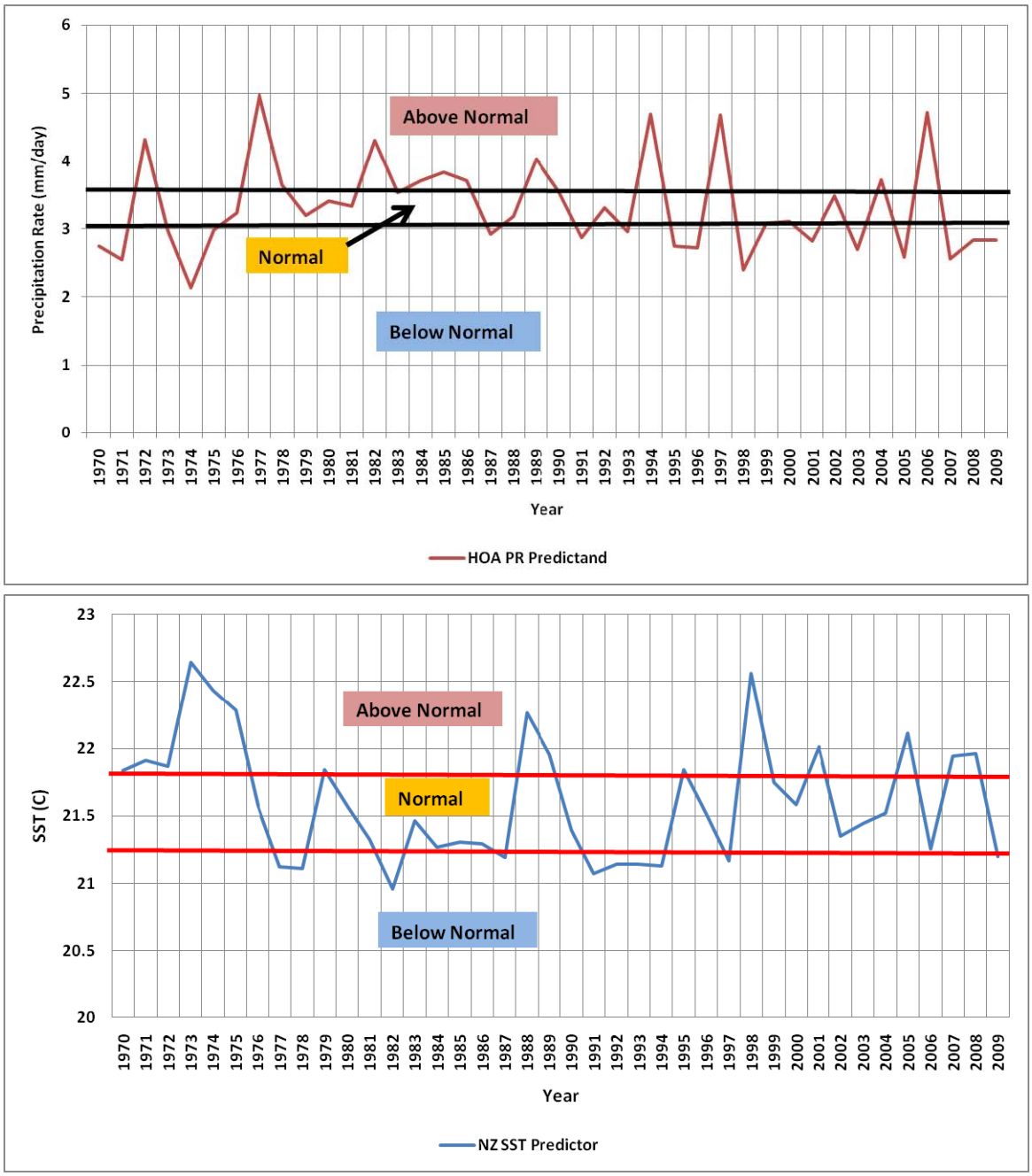

Figure 14. Time series of Oct–Nov HOA PR predictand (top panel) and New Zealand SST predictor (bottom panel) for 1970–2009. of the bold black and red horizontal lines denote the boundaries between the AN, NN, and BN categories for the predictand and predictor, respectively. For example, PR values are categorized as AN when ≥ 3.5 mm/day; NN when < 3.5 mm/day but ≥ 3.1 mm/day, and BN when < than 3.1 mm/day.

The contingency table assignments are used to calculate several forecast verification metrics, including: percent correct (PC) or accuracy rate, FA ratio (FAR), probability of detection (POD), and Heidke skill score (HSS) (Wilks 2006). These metrics were calculated for each predictor, each forecast category (AN, NN, BN), each forecast method, and each lead time. In addition, to see the variation in skill scores among the lead times and predictor events, we calculated: (a) category-average skill scores averaged over all categories (AN, NN, and BN) for each lead time; and (b) total skill scores averaged over all categories and all lead times.

The following equations show how each metric was calculated (Wilks 2006):

1. *PC:* = (hits + CRs) / total
2. *FAR:* = FAs / (hits + FAs)
3. *POD:* = hits / (hits + misses)
4. *HSS:* = (hits + CR – expected correct) / (total – expected correct)

Here, the term *total* refers to the total number of forecasts. The HSS helps answer the question: *"What was the accuracy of the forecast relative to that of random chance?"* where random chance is determined from LTM climatology. HSS is based on a scale from one to minus one—one being the best score and minus one being the worst. Having a HSS of less than zero (zero) means that using the chosen predictor-predictand pair as your forecast method is worse (no better) than using LTM climatology.

The following three metrics thresholds were used to identify forecasts with relatively high skill, especially to determine the viability of each predictor-predictand pair (e.g., their potential viability for use in the CAF method).

(1) PC greater than 50%

(2) POD equal to or greater than FAR

(3) HSS values greater than 0.3

Forecasts and pairs for which all three thresholds were met were identified as especially skillful and viable, respectively. Forecasts and pairs that did not meet these thresholds were rejected from further consideration.

C. SUMMARY OF FORECAST METHODS

Figure 15 summarizes the major data sets and methods we used to produce long-range hindcasts and forecasts.

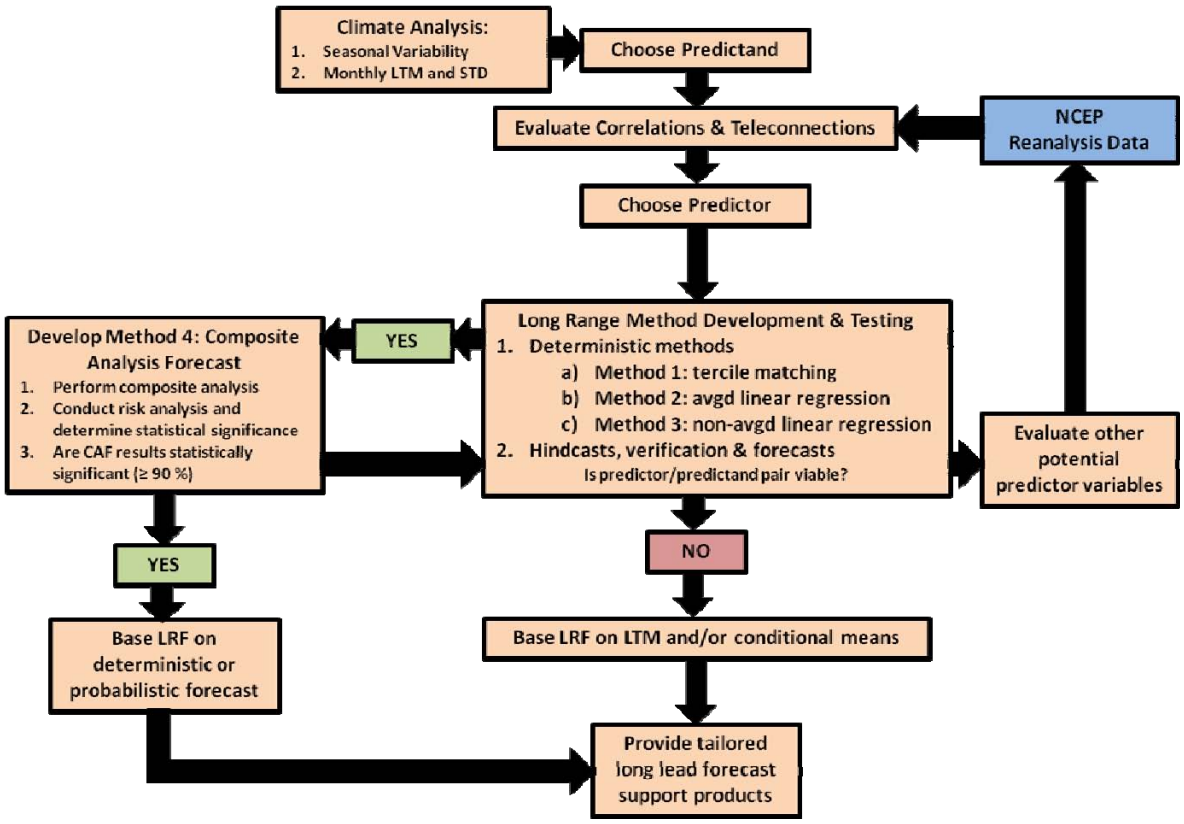

Figure 15. Flow chart showing main datasets and methods used to conduct climate analyses and long-range forecasts in this study.

III. RESULTS

A. CLIMATE ANALYSES

1. Composites Conditioned on Extreme PR in the HOA

We selected our predictand as Oct–Nov HOA PR in the region bounded by 5S-10N, 30-55E. This predictand region is shown by the black box in Figure 16 and includes almost all of the broad HOA region (see Chapter I, Section G.4), with the exception of northern Ethiopia, Eritrea, Djibouti, and most of Sudan. We chose this as our predictand region because of the tendency for similar spatial and temporal patterns of variability in Oct–Nov PR for the points within this region, based on 1970–2009 PR from the R1 dataset (see Chapter II, Section B.1).

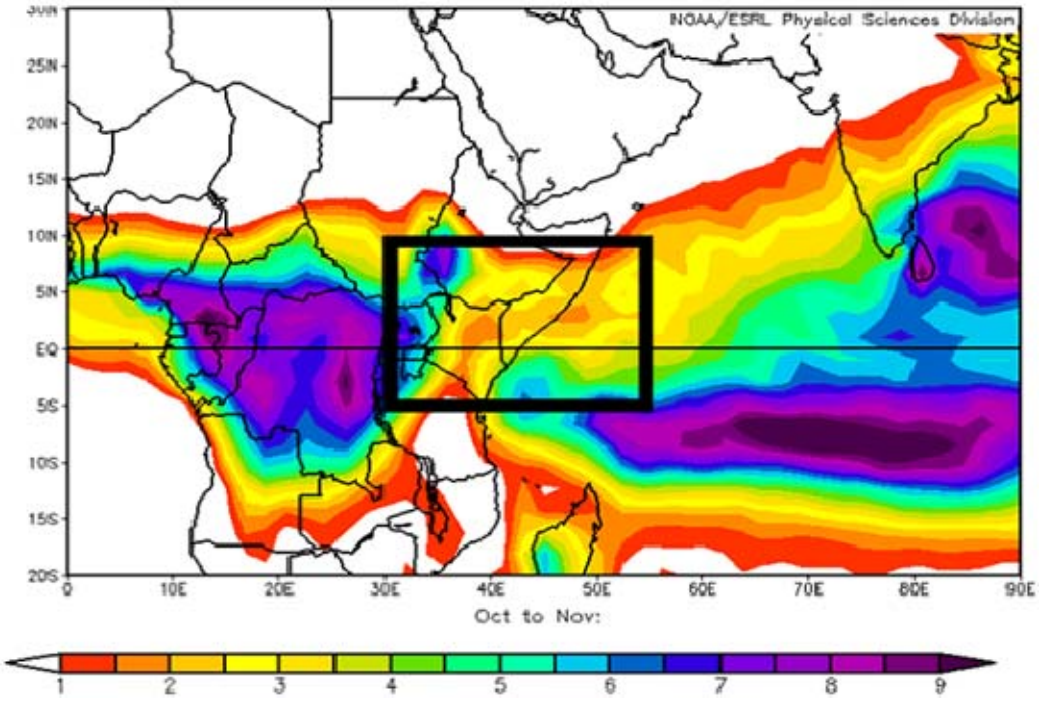

Figure 16. The Oct–Nov HOA PR predictand region for our study (black box) overlaid on the LTM Oct–Nov PR (color shading; mm/day; cf. Figure 10). PR image created using ESRL (2010).

The time series of Oct–Nov PR for 1970–2009 for the predictand region is shown in Figure 17. Note the large interannual variations, especially those exceeding plus or minus one standard deviation. This PR times series was used to: (a) identify the top AN and BN events during 1970–2009 for use in constructing composite anomalies; and (b) to conduct correlation and teleconnection analyses (see Chapter II, Section B.2). Figure 17 also shows the MEI and DMI times series, which reveal a general correspondence between: (a) ENLN and the IOD (Twigg 2007); and (b) the predictand PR and ENLN and the IOD (e.g., Ogallo 1988; Black at al. 2002). Note in particular the general tendency for AN (BN) HOA PR in Oct–Nov during EN (LN) and positive (negative) IOD. These general correspondences suggest that: (a) Oct–Nov HOA PR is teleconnected to global scale climate variations; and (b) ENLN and IOD indices (e.g., the MEI and DMI) may be useful predictors of Oct–Nov HOA PR. However, Figure 17 shows some periods in which one or more of these general correspondences did not hold (e.g., 1980 and a number of years during 1984–1993). In addition, Figure 15 does not show how the ENLN and IOD indices are related to the HOA PR when the indices lead the HOA PR by one or more months. So, it is unclear from Figure 17 alone just how useful these indices would be as long–range predictors of Oct–Nov HOA PR.

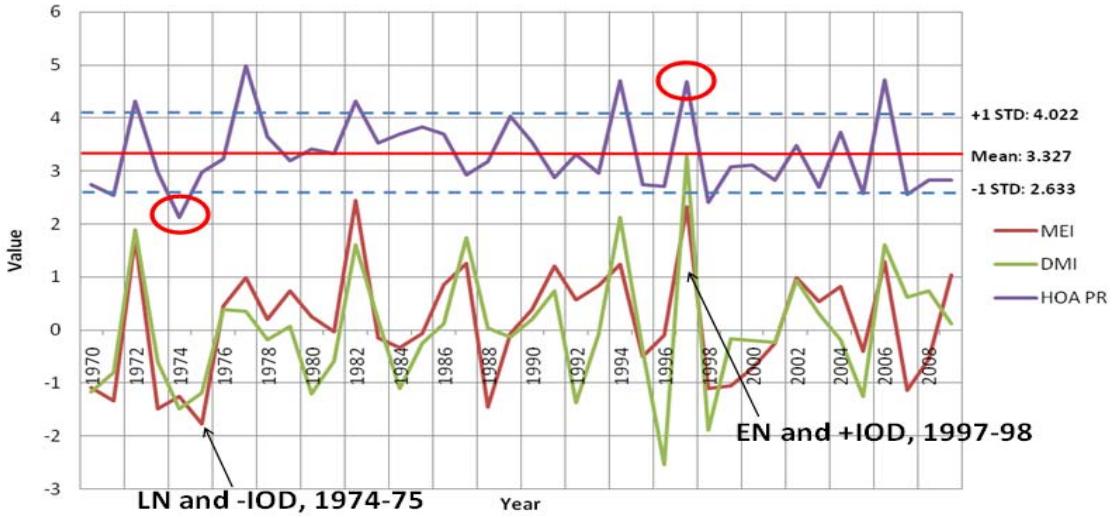

Figure 17. Time series of HOA PR (predictand, purple line, mm/day), and El Nino–La Nina (ENLN) and Indian Ocean Dipole (IOD) indices (MEI, red line, and DMI, green line, respectively) for Oct–Nov 1970–2009. Note the similarities in the interannual variability of the predictand and the two indices. Indications of teleconnections between HOA PR, ENLN, and IOD are highlighted during: (a) a strong LN and negative IOD period in Oct–Nov 1974–75; and (b) a strong EN and positive IOD period in Oct–Nov 1997. Relationships such as these suggest the usefulness of evaluating ENLN and IOD indicators as potential predictors for HOA PR.

To further investigate the regional and global scale patterns and processes associated with HOA PR variations, we constructed conditional composites of the anomalies during the Oct–Nov periods in which our HOA predictand region had the highest and lowest PRs (i.e., the most extreme AN and BN periods). We designated these as the *wet* and *dry* composites, respectively. See Chapter II, Section B.2 for more on what years these were and how they were identified. These and similar composites conditioned on the occurrence of extreme AN and BN PR in our predictand region helped us identify regional and global scale patterns and processes (e.g., teleconnection) that are related to PR extremes in our predictand region.

Figure 18 shows the regional and global wet and dry composites for PR. Note that AN (BN) PR in the HOA is associated with: (a) AN (BN) PR in a large

region that includes the HOA and extends over the western IO; (b) BN (AN) PR over tropical Africa to the west of the HOA; (c) BN (AN) PR over the eastern tropical IO, maritime continent (MC), and South Pacific Convergence Zone (SPCZ); and (d) AN (BN) PR over the central and east tropical Pacific. These patterns are consistent with the results shown in Figure 17 and with prior studies of teleconnections that affect east African and HOA PR (e.g., Ogallo 1988; LaJoie 2006; Vorhees 2006). They are also very useful in identifying: (a) the dynamical processes that cause climate variations in HOA PR; (b) potential predictand regions; and (c) potential predictors of HOA PR.

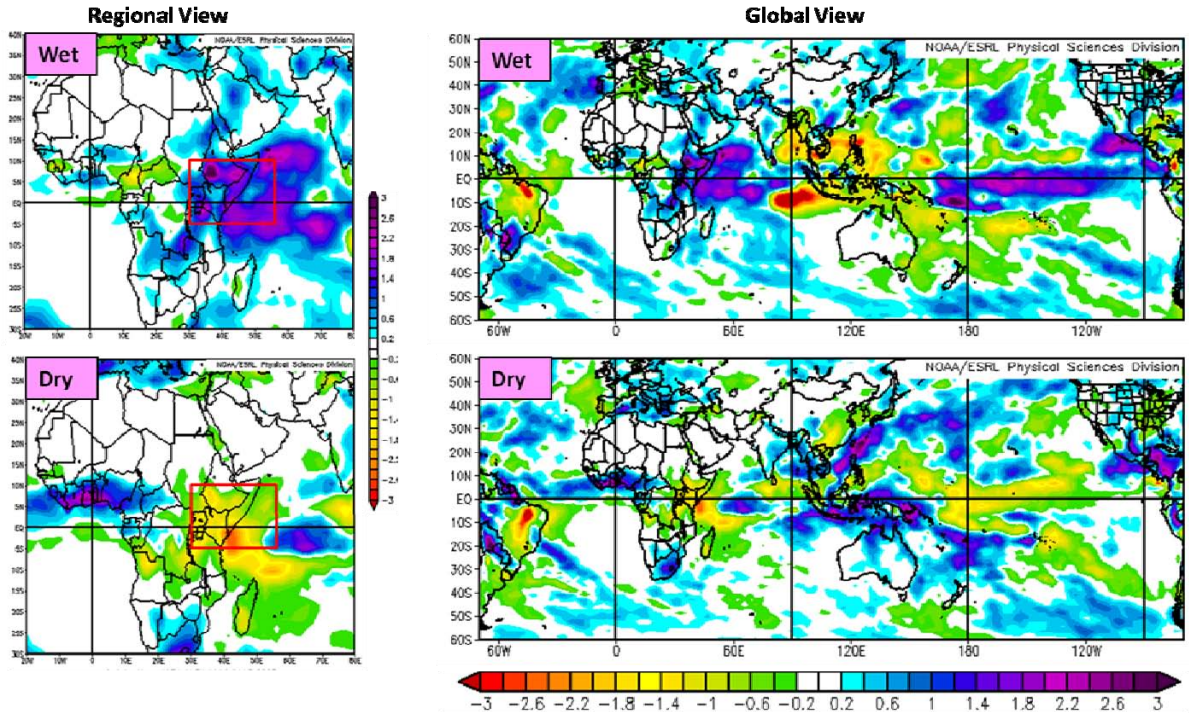

Figure 18. Conditional composite anomalies of Oct–Nov precipitation rate (PR; mm/day) for the five most extreme AN (wet) and BN (dry) events of HOA PR during Oct–Nov for 1970–2009. The left (right) panels show regional (global) scale views. See Chapter II, Section B.2 for the five most extreme AN and BN PR event years. The red box outlines our HOA predictand region. Note the generally opposite patterns in the wet and dry composites, and the correspondence to PR patterns associated with ENLN and the IOD. PR anomaly patterns such as these suggest possible predictors and linkages associated with the climate variations in the HOA. Images created using ESRL (2010).

Figure 19 shows the global scale wet and dry composite SSTAs, with AN (BN) PR in the HOA being associated with SSTAs that are: (a) positive (negative) in the western IO; (b) negative (positive) in the eastern tropical IO, western tropical Pacific, SPCZ–New Zealand region, and in and northeast of the Philippine Sea; and (c) positive (negative) in the central-eastern tropical Pacific and along the west coast of the Americas. These patterns are consistent with the PR anomalies shown in Figure 19, and with the relationships between HOA PR and ENLN and IOD indicated by Figures 18 and 17. The approximately opposite patterns in the wet and dry composites suggest that the global scale dynamical processes associated with interannual variations in HOA PR are predominantly linear.

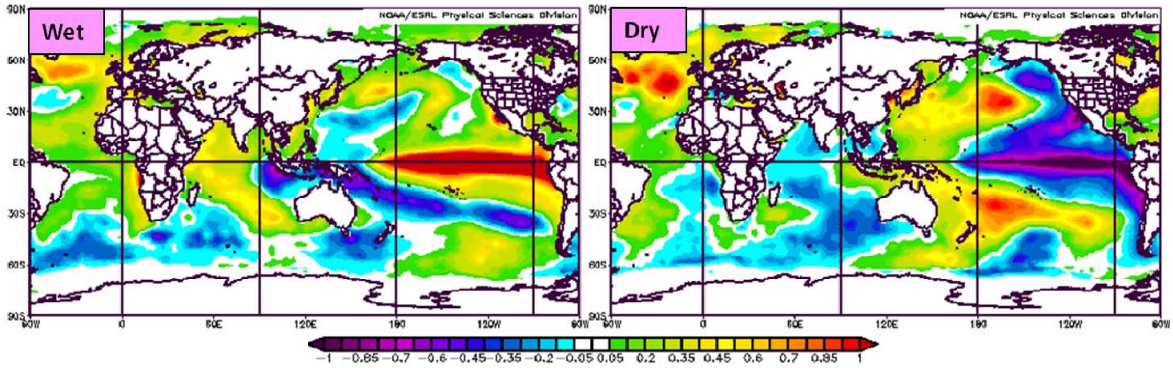

Figure 19. Conditional composite anomalies of sea surface temperature (^{o}C) for five most extreme wet (left panel) and dry (right panel) HOA PR events during Oct–Nov 1970–2009. Note in the wet (dry) composite the positive (negative) SSTAs in the WIO and central-eastern tropical Pacific and the negative (positive) SSTAs in the tropical EIO and western tropical Pacific, consistent with positive (negative) IOD and EN (LN) conditions. Images created using ESRL (2010).

Figure 20 shows the wet and dry composite anomalies for the 200 hPa geopotential height (GPHs). These anomalies are useful in determining the large-scale atmospheric circulation anomalies associated with wet and dry HOA PR periods. The anomalies over the tropics and subtropics show indications of tropical Rossby-Kelvin wave responses to the SST and precipitation anomalies

shown in Figures 18 and 19 (e.g., the paired anticyclones over Africa and the central-eastern tropical Pacific in the wet composite; the negative (positive) GPH anomalies over subtropical Asia and subtropical southern IO in the wet (dry) composite). They are also consistent with prior studies of the Rossby-Kelvin wave response to ENLN and IOD (e.g., LaJoie 2006; Vorhees 2006).

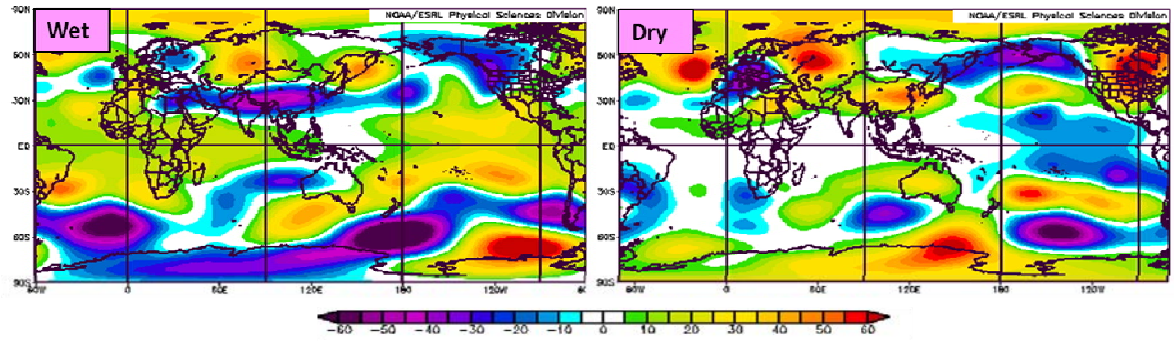

Figure 20. Conditional composite anomalies of 200 hPa GPH (gpm) for five most extreme wet (left panel) and dry (right panel) HOA PR events during Oct–Nov 1970–2009. Note in the wet (dry) composite the positive (negative) GPHAs over Africa and the central-eastern tropical Pacific (central and southern Africa and central-eastern tropical Pacific), consistent with positive (negative) IOD and EN (LN) conditions. These features are indicative of Rossby-Kelvin wave responses to anomalous convection over the WIO, MC and central-eastern tropical Pacific. Images created using ESRL (2010).

In the wet composite, above normal 200 hPa GPHs exist over much of Africa and eastward along the equator in response to enhanced convection over east Africa and the western IO (cf. Figure 18; LaJoie 2006; Vorhees 2006). At about 30 degrees to the north and south of the MC, below normal GPH anomalies occur in response to suppressed convection over the MC. The dry composite GPH anomalies are nearly opposite. This is most visible in the above normal GPH anomalies over southern Asia and Australia extending westward over northern Africa and southern IO, respectively, as a response to the enhanced convection in the MC. In both the wet and dry composites, the 200 hPa GPH anomalies over the equatorial Pacific are consistent with the ENLN related PR and SST anomalies in this region (Figures 18–19). The 200 hPa

GPH anomalies are more pronounced in the wet composite, possibly because the HOA PR, ENLN, and IOD variations in the wet years were more extreme deviations from their LTMs than those in the dry years (cf. Figure 16). The wet and composite shows clear indications of an anomalous wave train extending along an arching path from the maritime continent (MC) sector into the southern hemisphere extratropics, reaching its most poleward latitude at about 90^{o} W, and then extending back into the tropics over the South Atlantic. There is less clear evidence in the dry composite of an oppositely signed anomalous wave train in the southern hemisphere.

The corresponding GPH composite anomalies at 850 hPa (not shown) are, in the tropics and subtropics, nearly opposite to those at 200 HPa (Figure 20). In particular, in the wet (dry) composite, the 850 hPa GPH anomalies are below (above) normal over eastern Africa and the WIO, and above (below) normal over the MC. These GPH anomaly results are consistent with those at 200 hPa and with those associated with ENLN and the IOD (Rassmusson and Carpenter 1982; Saji et al. 1999; LaJoie 2006; Vorhees 2006).

The 850 hPa zonal wind anomalies in the wet composite (Figure 21, left panel) clearly shows anomalous easterlies from the MC converging with anomalous westerlies across central Africa in and near the HOA. The anomalously convergent low level wind flow into the HOA aids precipitation development in the HOA by transporting energy and moisture into the region (and similarly for the central-eastern equatorial Pacific, and oppositely for the MC). The dry composite (Figure 21, right panel) shows opposite low level wind anomaly patterns, with low level convergence centered over the MC and divergence over the HOA and central equatorial Pacific. In addition, in the dry composite, northerly flow from the Caspian Sea region toward the HOA occurs, indicating a tendency for anomalously stable and dry conditions over the HOA. The wet (dry) composite shows anomalous low-level divergence (convergence) in the SPCZ region.

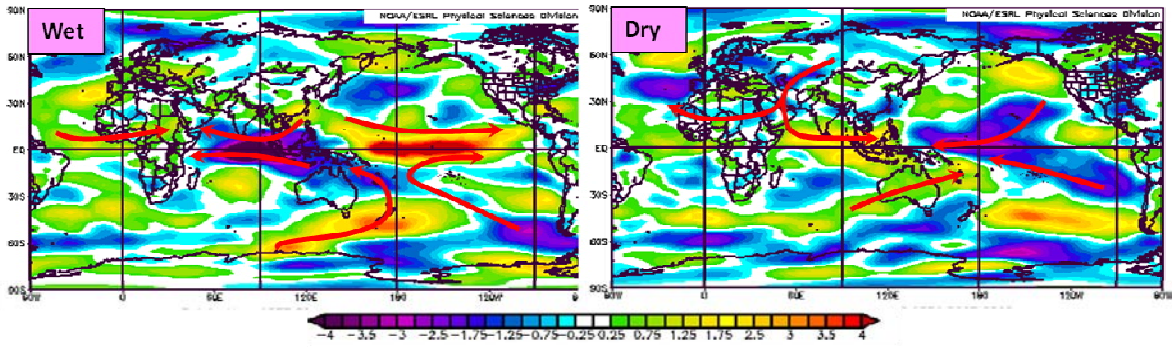

Figure 21. Conditional composite anomalies of 850 hPa zonal wind (m/s) for the five most extreme wet (left panel) and dry (right panel) HOA PR events during Oct–Nov 1970–2009. The red arrows represent the sense of the wind flow anomalies. Note in the wet (dry) composite the anomalous low-level convergence (divergence) over the HOA and divergence (convergence) over the MC, consistent with above normal PR in the HOA and with positive (negative) IOD and EN (LN) conditions. Images created using ESRL (2010).

Figure 22 shows wet and dry composite anomalies for outgoing longwave radiation (OLR). The OLR anomaly (OLRA) patterns are very similar to those for PR and SST (Figures 18–19). This is not surprising, since small changes in SSTs can create large anomalies in the energy and moisture available for atmospheric convection. OLR is a good proxy for convection in the tropics, with positive (negative) OLRAs corresponding to negative (positive) convection anomalies. In the wet composite, the OLRAs are below (above) normal over eastern Africa and western IO and extending northward into southwest Asia, including Afghanistan, and in the central-eastern equatorial Pacific (West Africa, MC, and SPCZ region). The opposite OLRAs occur in the dry composite. We point out the OLR anomalies in southwest Asia because of the ongoing military operations in Afghanistan. This topic has been investigated by Vorhees (2006), but additional research on long-range forecasting of precipitation in southwest Asia using the methods applied in our study should be considered for improving precipitation forecasts for operations in this region.

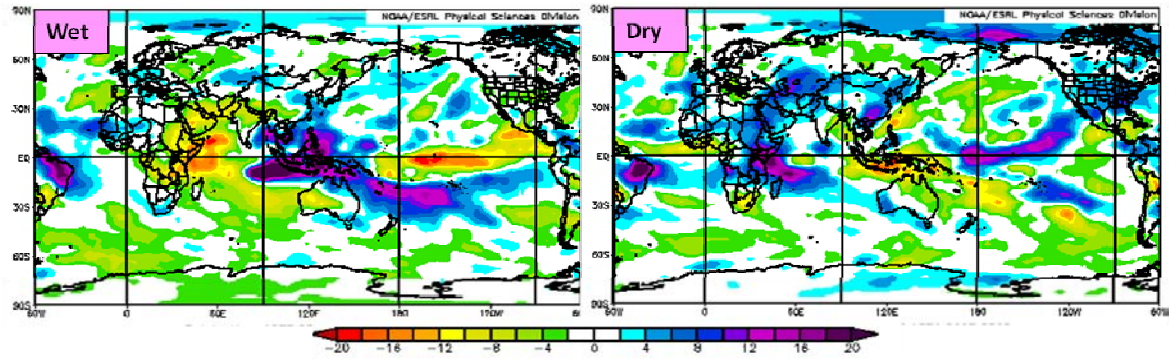

Figure 22. Conditional composite anomalies of OLR (W/m^2) for five most extreme wet (left panel) and dry (right panel) HOA PR events during Oct–Nov 1970–2009. OLR is a good proxy for convection and precipitation in the tropics, with positive (negative) OLRAs indicating negative (positive) convection anomalies. Note in the wet (dry) composite the negative (positive) OLRAs in the HOA, WIO, and central-eastern tropical Pacific, and the positive (negative) OLRAs in the tropical eastern IO and western tropical Pacific, consistent with wet (dry) conditions in the HOA, and positive (negative) IOD and EN (LN) conditions. Images created using ESRL (2010).

2. Correlations

We correlated our Oct–Nov HOA PR predictand time series (Figure 17) with a number of other potential predictors for the period 1970–2009, including: (a) the MEI, DMI, other climate variation indices (e.g., indices of the North Atlantic Oscillation and Arctic Oscillation); and (b) global SST and the other climate variables listed in Table 1. We found that SST and SST based climate variation indices (e.g., MEI, Nino3.4, DMI) in certain regions were: (a) well correlated with the predictand, with the predictor leading the predictand by zero to eight months; and (b) had higher correlations than non-SST related variables at the longer lead times (e.g., four to six months). The correlations with SST in the subtropical southwest Pacific north of New Zealand were especially strong and were statistically significant out to eight months lead. However, we chose to investigate leads only out to six months to focus on the leads at which our LRFs

had the greatest skill. For our optimal climate normals investigations, we conducted additional correlation analyses for the most recent years in the 1970–2009 study period (see Chapter II, Section B.5.e, and Chapter III, Section C).

In the correlation maps shown in this section (e.g., Figure 23), spatial correlation patterns are shown for correlations in which our HOA PR predictand lags the variable of interest (e.g., SST) by zero to six months. Areas of positive (negative) correlations indicate that HOA PR tends to increase (decrease) zero to six months after the variable of interest increases (decreases). The significance levels for the different correlations conducted in our study are described in Chapter II, Section B.2. We generated correlation maps for all the variables listed in Table 1. However, we only show in this report the maps for correlations involving SST and HOA PR, since we determined that SSTs were more viable predictors than the other variables we considered. This was because overall and with respect to the other variables: (a) the correlations with SST were relatively strong, significant, and persistent at all leads, especially at longer leads; (b) the dynamical links between SST and our predictand were relatively straightforward at all leads; and (c) SST is relatively well observed in real time and thus could be a feasible predictor for operational LRFs.

Figure 23 shows the correlations of global SST with the Oct–Nov HOA PR predictand at lead times of one to four months. Note the similarity in the correlation patterns to the wet and dry composite SSTA patterns (Figure 19). This indicates that: (a) the composite SSTAs are representative of the general temporal and spatial patterns associated with wet and dry events; and (b) the correlations provide a good representation of the major dynamical processes associated with extreme wet and dry events. Figure 23 shows an area centered near 30S, 180W (red box north of New Zealand) that has a high negative correlation with the predictand (blue box in panel a), with correlations $\geq$ -0.5 at leads of zero to four months. These correlations indicate that SST in this region tends to decrease (increase) before and when HOA PR increases (decreases). These correlations, significant at the 95% confidence level, may indicate: (a)

potential mechanisms that drive climate variations in HOA PR; and (b) potential predictors for producing skillful long-range forecasts of HOA PR.

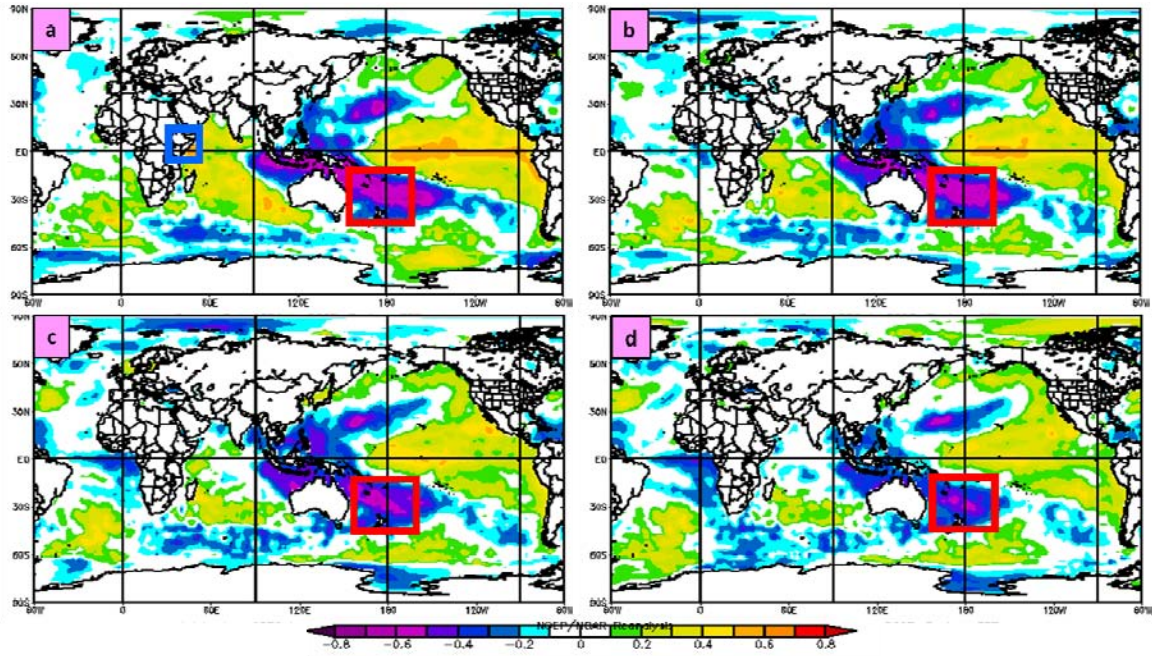

Figure 23. Correlations of HOA PR in Oct–Nov with global SST for 1970–2009 with SST leading by: (a) one month (Sep–Oct), (b) two months (Aug–Sep), (c) three months (Jul–Aug), and (d) four months (Jun–Jul). The blue box represents the Oct–Nov HOA PR predictand region. The red box indicates a region north of New Zealand of persistently strong and significant negative correlation between SST and the predictand. Note the similarities between the correlation patterns in this figure and the SSTA patterns in Figure 18. Images created using ESRL (2010).

Figure 23 shows other areas of significant correlations (e.g., areas of negative correlation centered near 20N, 165E and in the eastern tropical IO; an area of positive correlation in the central-eastern tropical Pacific). But, the area north of NZ has the largest correlations over the largest area at the longest lead times (out to eight months; not shown).

3. Predictor Selection

Based on the correlation results, we investigated further the use of SST north of New Zealand (NZ) as a predictor of Oct–Nov HOA PR. To do so, we began by determining the specific region north of NZ to use as our predictor region, following the same basic process we used to determine our predictand region (see Chapter II, Section B.1). In this process, we evaluated five potential predictor regions within the NZ high correlation region and chose as our NZ predictor region the area bounded by 18-36S, 165E-165W. We chose this region over the other potential NZ regions because the SSTs in this region had: (a) significant correlations at lead times of zero to six months; and (b) the highest mean correlation when averaged over all months of all the potential NZ and global scale climate variation index predictors. We named the SST in this region the NZ SST predictor.

Figure 24 shows the magnitude of the correlations between the predictand and NZ SST, MEI, Nino3.4, and DMI at leads of one to six months. Note that the NZ SST predictor: (a) is significantly correlated at all leads; (b) is better correlated to the predictand than the indices at all leads, especially at longer leads; and (c) is not as well correlated as the indices at a lead of zero months.

Figure 24 shows that the ENLN (MEI and Nino3.4) and IOD (DMI) correlations dropped below the 95% significant level after four and five month lead times, respectively. The lower correlation for Nino3.4 at longer lead times may provide clues as to why the 14 WS LRFs for their HOA region have low skill. Of course, the results in Figure 24 are for our HOA region, not the 14 WS HOA region that extends further to the north than our region, and for a particular forecast valid period (Oct–Nov). Still, these results do suggest that while established climate variation indices that are well correlated with a predictand may be good predictors, they might not be the best possible predictors.

These results indicate the potential value in: (a) doing a methodical search for potential predictors, rather than choosing a pre-established climate variation index as a predictor; and (b) selecting a predictor based on results from multiple lead times, rather than selecting a predictor based mainly on zero lag correlations.

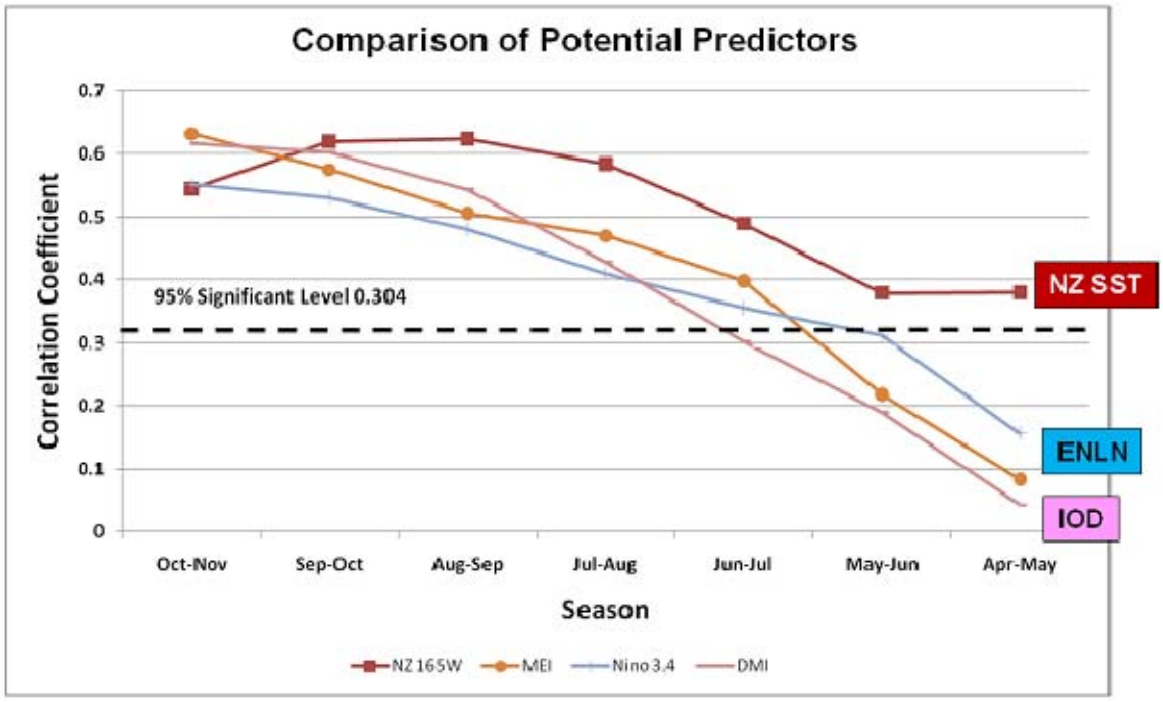

Figure 24. Magnitude of correlations between Oct–Nov HOA PR predictand and four potential predictors of this predictand, with the predictors leading by zero to six months. The four predictors are: NZ SST, MEI, Nino3.4, and DMI. The colored text boxes on the right of the figure describe the climate variations associated with the last three of these potential predictors. Correlations ≥ 0.304 indicate significance at the 95% level (dashed line).

To further test the NZ SST predictor, we visually compared the 1970–2009 predictand time series to the NZ SST predictor time series for all lead times. Figure 25 below shows these comparisons for leads of 0, 3, and 6 months. In general, the three predictor time series are in phase with each other (positively correlated), but with some notable exceptions (e.g., 2006). In general, the three

predictor time series are out of phase with the predictand time series at all lead times (negatively correlated). However, for 1983–1993 the predictor and predictand tended to be in phase (positively correlated). Some prior studies of correlations between IO SST with East African rainfall have found a similar decadal scale correlation pattern reversal (e.g., Clark et al. 2002). The reasons for such reversals need further investigation. The predictor-predictand and predictor-predictand comparisons in Figure 25: (a) help clarify why the predictor-predictand correlation is strong t multiple leads; and (b) indicate the periods for which hindcasts based on the NZ SST predictor may do well and poorly.

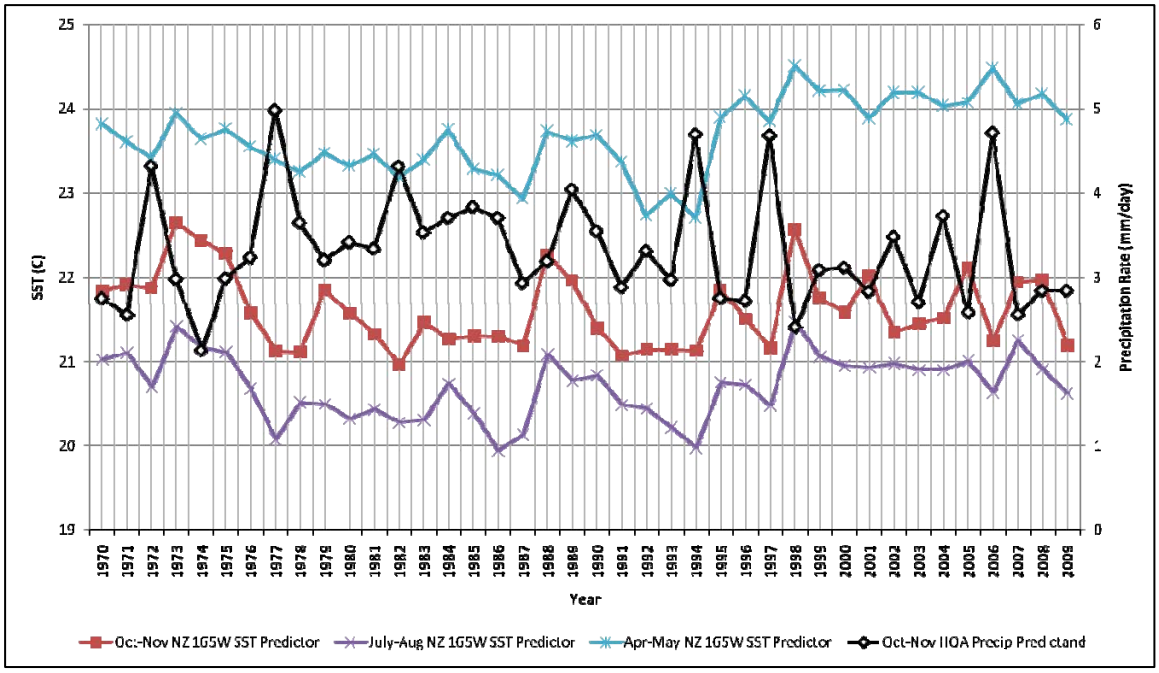

Figure 25. Time series of HOA Oct–Nov PR (mm/day) predictand in Oct–Nov (black line) and NZ SST (^{o}C) predictor in (a) Oct–Nov (red line), (b) Jul–Aug (purple line), and (c) Apr–May (blue line) during 1970–2009. Note the persistence in the SSTs indicated by the similarities in the SST time series. Note also the indications of negative correlations between the predictand and NZ SSTs.

Figure 26 shows the regions for the predictor-predictand pair that we used in our initial LRF model development and hindcasting.

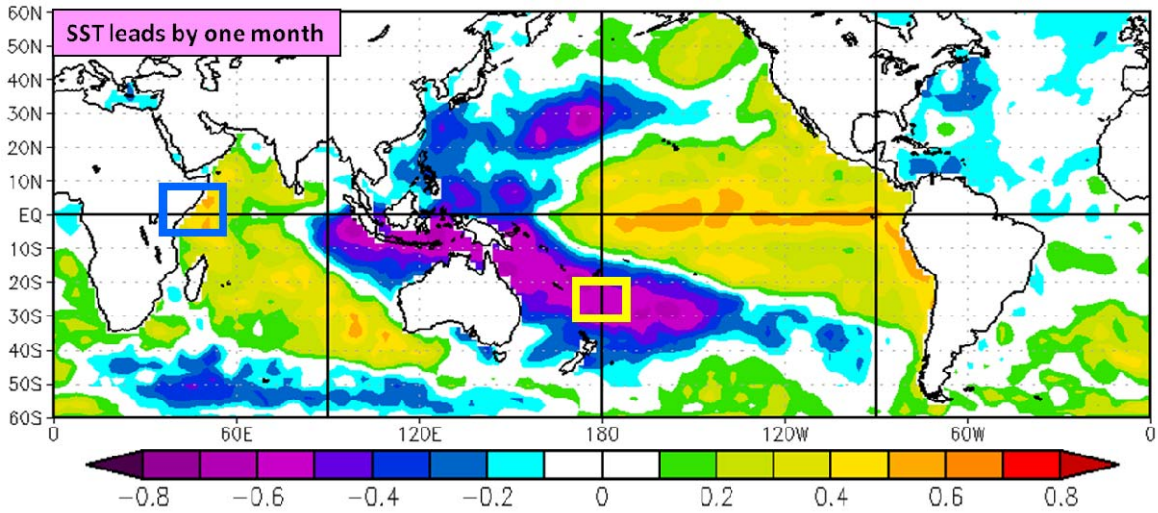

Figure 26. Correlations of HOA PR in Oct–Nov with global SST in Sep–Oct based on data from 1970–2009.. These and related correlations (Figures 23–24) led us to select SST north of New Zealand (red box) as the initial predictor for use in forecasting HOA PR in Oct–Nov (our predictand; blue box) at leads of one to six months. Image created using ESRL (2010).

B. LONG-RANGE HINDCASTS: ALL YEARS APPROACH

1. Tercile Matching Method with NZ SST Predictor

We used the NZ SST predictor to generate hindcasts for 1970–2009 at leads of one to six months using all four forecasting methods (see Chapter II, Section B.5). This resulted in a large number of hindcasts. Representative examples of the results from these hindcasts are presented in this report, along with summaries of the results for all of the hindcasts. These summaries are based mainly on the verification methods described in Chapter II, Section B.6.

Table 4 summarizes the results of the hindcasts made using forecast Method 1 (tercile matching) based on the NZ SST predictor. The overall hindcast performance was very good, especially for the AN and BN categories. For example, HSS for the AN and BN categories is consistently above zero, especially at shorter leads. The lower performance for the NN category is typical

of many LRF systems, due in part to the systems being mainly designed, as ours are, to forecast deviations from the NN category (i.e., deviations from LTM conditions). Overall, our performance criteria (Chapter II, Section B.6) were met (i.e., PC greater than .50, POD greater than FAR, HSS of 0.3 or greater). These results, and similar results from the use of the other forecasting methods, indicate that our NZ SST predictor is: (a) viable when used with forecasting Method 1; and (b) likely to be viable when used in our other forecasting methods.

Table 4. Verification results from hindcasts generated using Method 1 (tercile matching). The hindcasts predicted Oct–Nov HOA PR during 1970–2009 based on the NZ SST predictor, with the predictor leading by zero to six months. Columns A, B, C, and D represent the number of hits, false alarms, misses, and correct rejections, respectively, for predictions of AN, BN, and NN PR. Verification metrics consist of percent correct (% Corr), false alarm rate (FA Rate), probability of detection (POD), and Heidke skill score (HSS). See Chapter II, Section B.6 for more information on our verification methods.

	A	B	C	D	Verification Metrics			
	Hits	FA	Misses	Corr. Rej.	% Corr	FA Rate	POD	HSS
Results for hindcasts at lead times of zero months								
AN PR	8	5	6	21	0.7	0.4	0.6	0.4
BN PR	9	6	4	21	0.8	0.4	0.6	0.5
NN PR	6	6	7	21	0.7	0.5	0.5	0.2
Results for hindcasts at lead time of one month								
AN PR	10	5	4	21	0.8	0.3	0.7	0.5
BN PR	6	4	7	23	0.7	0.4	0.6	0.3
NN PR	6	9	7	18	0.6	0.6	0.4	0.1
Results for hindcasts at lead time of two months								
AN PR	12	12	2	14	0.7	0.5	0.5	0.3
BN PR	1	1	12	26	0.7	0.5	0.5	0.1
NN PR	5	9	8	18	0.6	0.6	0.4	0.1
Results for hindcasts at lead time of three months								
AN PR	7	7	7	19	0.7	0.5	0.5	0.2
BN PR	9	7	4	20	0.7	0.4	0.6	0.4
NN PR	1	9	12	18	0.5	0.9	0.1	-0.3
Results for hindcasts at lead time of four months								
AN PR	6	5	8	21	0.7	0.5	0.5	0.2
BN PR	6	6	7	21	0.7	0.5	0.5	0.2
NN PR	4	13	9	14	0.5	0.8	0.2	-0.2
Results for hindcasts at lead time of five months								
AN PR	8	6	6	20	0.7	0.4	0.6	0.3
BN PR	6	7	7	20	0.7	0.5	0.5	0.2
NN PR	3	10	10	17	0.5	0.8	0.2	-0.1
Results for hindcasts at lead time of six months								
AN PR	8	7	6	19	0.7	0.5	0.5	0.3
BN PR	6	6	7	21	0.7	0.5	0.5	0.2
NN PR	3	10	10	17	0.5	0.8	0.2	-0.1

Figure 27 shows the skill scores averaged over all categories (i.e., AN, NN, and BN) by lead time for the Method 1 hindcasts using the NZ SST predictor (Table 4). These results show that the hindcast performance tends to decrease with increasing lead time, but that there is skill over climatology (LTM based forecasts) even at a six month lead time (e.g., HSS > 0 at all leads).

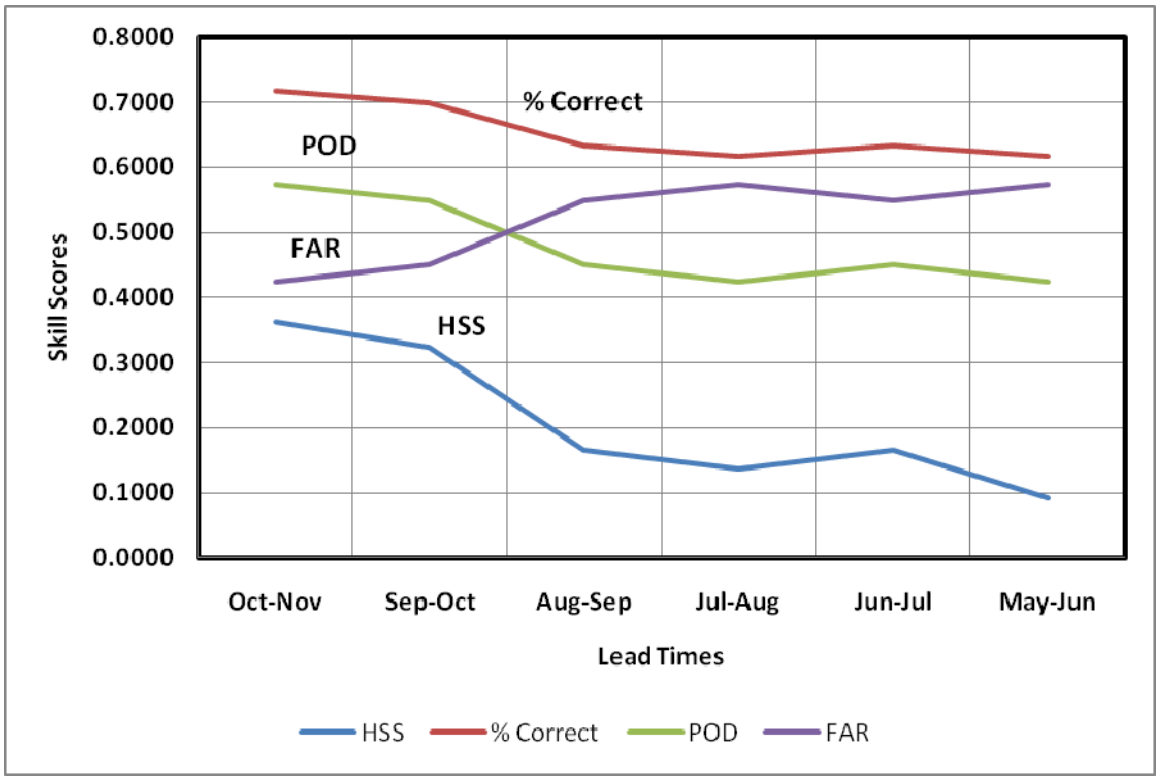

Figure 27. Average verification metrics by forecast lead time for hindcasts of HOA PR in Oct–Nov 1970–2009 using Method 1 (tercile matching) and the NZ SST predictor. Averaging is done over all forecast categories (AN, NN, and BN PR). Verification metrics consist of percent correct (% Corr), false alarm rate (FA Rate), probability of detection (POD), and Heidke Skill Score (HSS). Refer to Chapter II, Section B.6 for more information on the metrics listed in this table. Note the general decline in skill as lead time increases, but that HSS remains positive at all lead times.

2. Composite Analysis Forecasting Method with NZ SST Predictor

Figure 28 shows the hindcast results from applying the composite analysis forecast method and the NZ SST to hindcast HOA PR in Oct–Nov at a lead time of six months (forecast based on NZ SST in Apr–May). Figure 28a shows the historical frequency distributions of PR with respect to NZ SST. The statistically significant results are outlined in black and are: all of the BN PR cases, plus the AN PR and BN SST cases). The existence of these statistically significant results validates the use of the CAF method and indicates that this method should perform better than climatology (i.e., better than forecasts based on LTMs) (MetEd 2010).

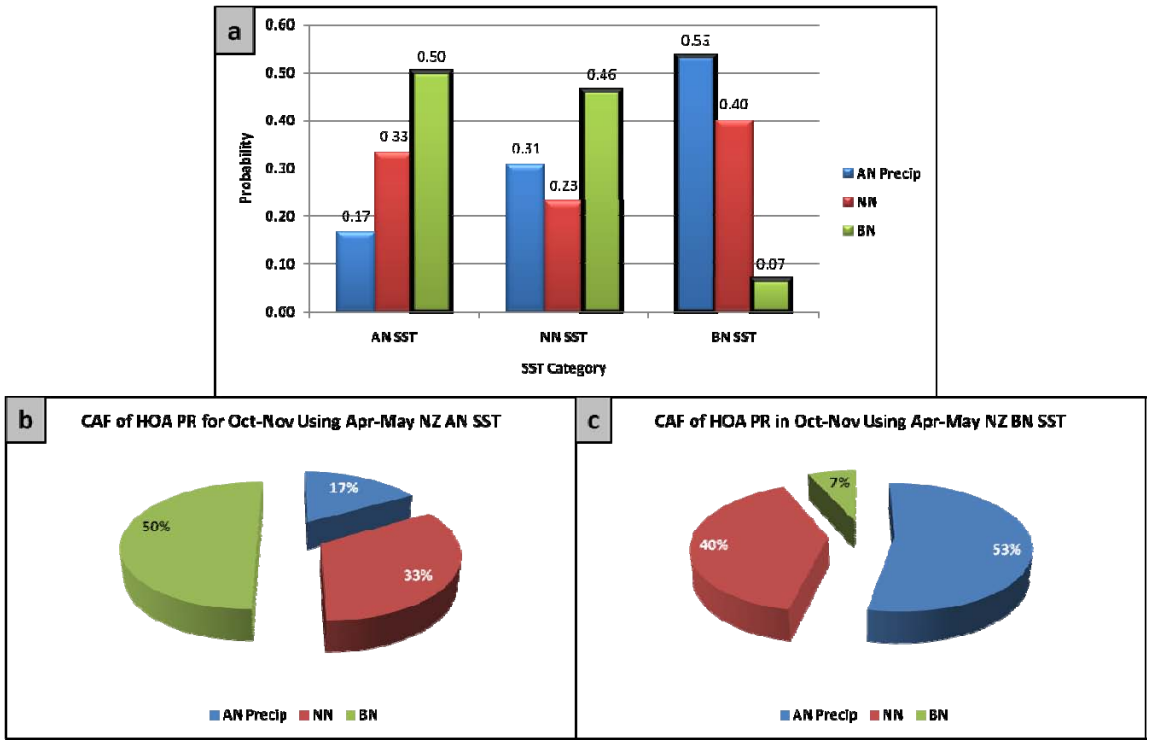

Figure 28. Results from composite analysis forecasts of Oct–Nov HOA PR using the NZ SST predictor at a lead time of six months (i.e., using NZ SST in Apr–May). (a) Historical frequency distribution of HOA PR probabilities given any SST condition at six months lead. Statistically significant results are outlined in black. (b) Corresponding probabilistic long-range hindcast of HOA PR in Oct–Nov based on AN NZ SST in Apr–May. (c) Corresponding probabilistic long-range hindcast of HOA PR in Oct–Nov based on BN NZ SST in Apr–May.

Figure 28 also shows two examples of probabilistic long-range forecasts of HOA PR in Oct–Nov when using the CAF Method and the NZ SST predictor (when based on the frequency distributions shown in Figure 28a). One forecast is based on the occurrence in Apr–May of AN NZ SST (Figure 28b), and the other is based on the occurrence in Apr–May of BN NZ SST (Figure 28c). The CAF prediction of Oct–Nov HOA PR, given AN NZ SST conditions in Apr–May, is: 17% chance of AN PR, 33% chance of NN PR, and 50% chance of BN PR. This example forecast indicates a higher (lower) than normal chance of low

(high) precipitation. In interpreting these types of forecast results, it is important to recall that the normal probability for each of the forecast categories (AN, BN, NN) is 33%. So a forecast of a 17% probability indicates a much lower than normal probability, and a forecast of a 50% probability indicates a much higher than normal probability. A CAF forecast in which one category has a probability of 50% or greater indicates that category is more likely than either of the other two categories.

Figure 28a shows a statistically significant result for BN PR given NN SST. One would not expect this result, since the predictand–predictor correlation is negative, indicating that NN SST would be expected to lead to NN PR. This unexpected result may be due to variations in the predictor category as NZ SSTs evolve through the northern spring and into the northern summer. During this period, the climate system tends to make large adjustments (e.g., onset of Asian summer monsoon, initiation of EN and LN events). NZ SST is closely related to the SPCZ and to ENLN variations (see Figures 18–24, 26), both of which tend to undergo large variations during the northern spring. Thus, unexpected results in Figure 28a may represent the effects on the NZ SST predictor of these variations. This topic is also discussed in later sections of this report that present: (a) results from applying the optimal climate normals approach; and (b) hindcast skill when forecasting through the northern spring predictability barrier (cf. van den Dool 2007).

These unexpected results do not show up in the CAF results for shorter leads. This indicates that forecasters and forecast end users need to pay extra attention to forecast updates to forecasts based on northern spring predictor conditions (e.g., updates issued in Jul to forecasts issued in Apr). For the case shown in Figure 28, our case, updates to the NZ SST predictor and resulting forecasts should be monitored closely as lead time decreases, especially when NN SST conditions were observed in the northern spring.

3. Verification of Hindcasts Based on All Years Approach

Table 5 summarizes the performance of the hindcasts for each of our four forecast methods when using NZ SST as the predictor. In this table, the verification metrics are averages over all forecast categories (AN< BN< NN) and all lead times. All the methods showed skill (e.g., HSS > 0), but Methods 2 and 3 (linear regression methods) had the highest performance, while Method 1 (tercile matching) had the lowest performance. Based on all the verification metrics results, we concluded that NZ SST is a viable predictor for generating deterministic and probabilistic LRFs.

Table 5. Average verification metrics for hindcasts of HOA PR in Oct–Nov 1970–2009 using each of the four forecast methods and the NZ SST Predictor. Averaging done over all forecast categories (AN, BN, NN) and all lead times of zero to six months. Note the HSS values are all positive, indicating forecast skill. See Chapter II, Section B.6 for more information on the metrics listed in this table.

	% Correct	F.A. Rate	POD	HSS
NZ Method 1	0.6	0.5	0.5	0.2
NZ Method 2	0.8	0.3	0.7	0.5
NZ Method 3	0.8	0.3	0.7	0.5
NZ Method 4	0.7	0.5	0.5	0.3

C. LONG-RANGE HINDCASTS: OPTIMAL CLIMATE NORMALS APPROACH

When we examined the time series of the HOA PR predictand and the NZ SST predictor, we found the negative correlation between the two variables was largely due to the relationship between them during the early and later part of the study period, 1970–2009 (Figure 25). When we produced the hindcasts for that period using the tercile matching method and the NZ SST predictor, we found

that the number of hits was higher at the beginning and the end of the period, especially for the last 15 years, 1995–2009. These variable correlation and variable skill results indicated that the relationship between the predictor and predictand changed during the study period. This may have occurred due to changes in the climate system factors that cause variations of the predictor and/or predictand. Whatever, the causes, these changes in the predictor–predictand relationship indicated that we needed to consider optimal climate normals (OCN) approaches to our forecasting (see Chapter II, Section B.5.e). OCN approaches allowed us to explicitly account for the changing relationship by weighting our forecasts toward the relationships that were dominant in the most recent years. The OCN approach is based on the recognition that, in a rapidly changing environment, the predictors and forecast methods previously used may eventually become non-viable. We applied OCN approaches in the basic and advanced forms described in Chapter II, Section B.5.e.

1. Basic OCN Approach

The relationship between the HOA PR predictand the NZ SST predictand was relatively constant during the last 10–15 years of the 1970–2009 period, as indicated by the time series comparisons and the hit rates. Thus, we decided to repeat our forecast development and testing process using just the most recent 15 and the most recent 10 years of data—that is, using data from 1995–2009 and from 2000–2009 (cf. van den Dool 2007).

We first did so by taking a basic OCN approach in which we set the tercile categories for the predictor and predictand using data from just the most recent 10 and the most recent 15 years (s opposed to using all 40 years as we did in the all years approach (see Chapter III, Section B). This led to changes in the AN, BN, and NN categories—for example, the NN HO PR for Oct–Nov category were 2.9–3.5 mm/day for 1970–2009 and 2.7–3.1 mm/day for 1995–2009. We then rehindcasted the most recent 10-year and 15-year periods using the NZ SST predictor and the revised tercile categories.

To help assess the results of the basic OCN approach, we calculated the correlations between the NZ SST predictor and the HOA PR predictand for the most recent 10 and 15 years, with the predictor leading by zero to six months (Figure 29). The significance levels for the different correlations conducted in our study are described in Chapter II, Section B.2. Figure 29 shows that the correlations are negative at leads of zero to three months, zero at leads of four to five months, and positive at leads of five to six months, including a significant positive correlation at a lead of six months. This change in the sign of the correlation with lead time was not found when using all forty years of the study period (Figure 24).

Figure 29 also shows the HSS values for hindcasts of 1995–2009 and 2000–2009 based on tercile matching, and the 10- and 15-year tercile categories (or bins) for the predictor and predictand, at all lead times (denoted by *10-yr bins* and *15-yr bins* in the figure legend). The corresponding HSS values when using the 40-year tercile categories are also shown (*40-yr bins* in the figure legend). The HSS values decrease with lead time and are approximately zero or less than zero (indicating no skill or negative skill) at leads of four to six months.

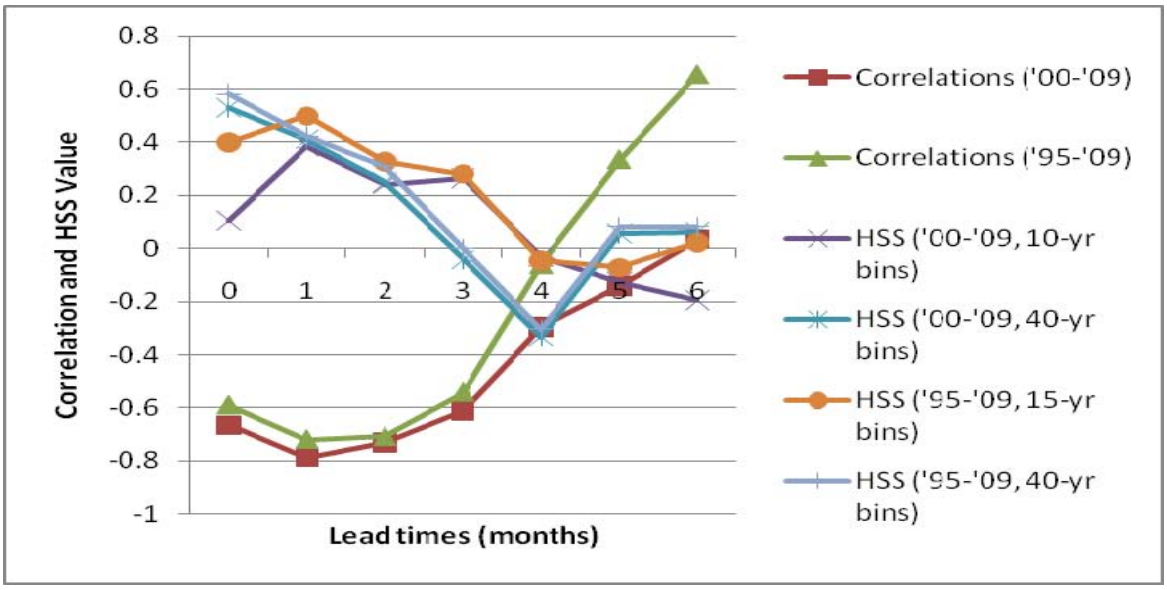

Figure 29. Time series by forecast lead time of: (1) correlations between HOA PR predictand and NZ SST predictor; and (2) HSS values for tercile matching method hindcasts at lead times of zero to six months, and using tercile categories based on the most recent 10, 15, and 40 years. (a) 1995–2009 correlations (green line); (b) 2000–2009 correlations (red line); (c) 1995–2009 hindcast HSS values (orange and light blue lines); and (d) 2000–2009 hindcast HSS values (purple and turquoise lines). The bin periods represent the period used to form the predictor and predictand AN, NN, and BN categories. Note that the correlations shift from negative to positive, and the HSS values decrease, as lead time increases.

The correlations shown in Figure 29 indicate that the NZ SST predictor may not be the optimal predictor for the recent 10 to 15 years. For the 40-year period overall, this predictor performed well. But, changes in the climate system within that 40-year period may make this predictor less suitable for forecasting recent and upcoming years. The correlations in Figure 29 also indicate that predictor selection, and forecasting methods in general, may need to vary according to the forecast period. In particular, the correlations suggest that other variables may be better predictors than NZ SST for the recent 10 and 15 years, and upcoming years.

2. Advanced OCN Approach

The results of the basic OCN approach led us to consider a more advanced OCN approach in which we repeated our composite and correlation analyses using just the most recent 15 years of data. From these analyses, we identified two new predictors of HOA PR in Oct–Nov: (a) SST east of the Philippines (03N–10N, 143E–152E) for leads of zero to three months; and (b) SST west of Namibia (19S–25S, 03W–02E) for leads of four to six months. For each of these predictors, there was a negative correlation with the HOA PR predictand. Figure 30 shows representative correlations between global SST and our HOA PR predictand, with a focus on the correlations used to identify the new predictors. We termed these the multi-region (MR) SST predictors that we used when applying the advanced OCN approach to our four forecasting methods.

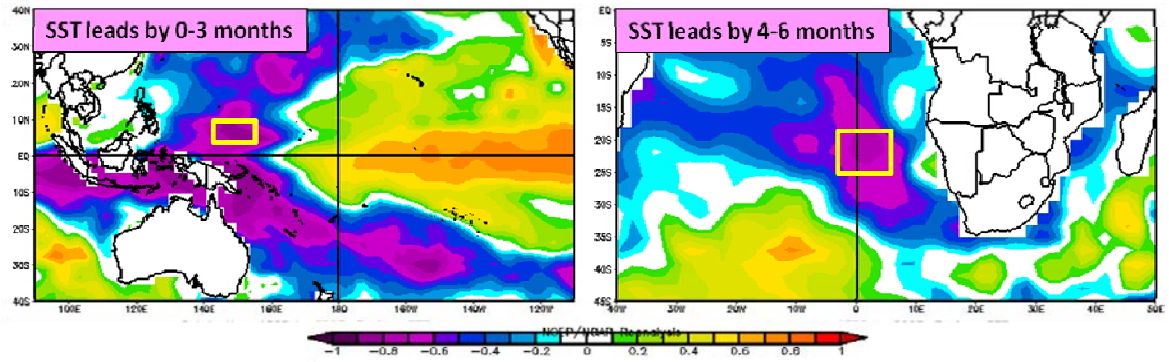

Figure 30. Correlations of HOA PR in Oct–Nov with global SST for 1995–2009 with SST leading by: (left panel) zero months (Oct–Nov) and (right panel) four months (Jun–Jul). The yellow outlined boxes represent the multi-region SST predictor regions identified as having the highest correlations to the HOA PR predictand at specific lead times when using the advanced OCN approach. We used the SST predictor east of the Philippines (left panel) was used for forecasting at leads of zero to three months. We used the SST predictor west of Namibia (right panel) for forecasting at leads of four to six months. Images created using ESRL (2010).

All of our statistical significance results using the MR SST predictors showed at least one statistically significant relationship for each lead time and predictor condition. Thus, we used the advanced OCN approach with each of our four forecasting methods, including the CAF method.

3. Verification of Hindcasts Based on Advanced OCN Approach

Table 6 summarizes the results of the hindcasts made using forecast Method 1 (tercile matching) based on the MR SST predictors. The overall hindcast performance was very good, especially for leads of zero to three months, and for the AN categories. The NN results were, overall, an improvement on those using a non-OCN approach (Table 4). But there were some notable cases in which our performance criteria (Chapter II, Section B.6) were not met (i.e., POD greater than .50, POD greater than FAR, and/or HSS of 0.3 or greater were not met). However, the results from using the advanced OCN approach were better when applied to the other forecasting methods.

Table 6. TVerification results from hindcasts generated using Method 1 (tercile matching). The hindcasts predicted Oct–Nov HOA PR during 1995–2009 based on the multi-region SST predictors (advanced OCN approach; Figure 39), with the predictor leading by zero to six months. Columns A, B, C, and D represent the number of hits, false alarms, misses, and correct rejections, respectively, for predictions of AN, BN, and NN PR. Verification metrics consist of percent correct (% Corr), false alarm rate (FA Rate), probability of detection (POD), and Heidke skill score (HSS). Compare these advanced OCN verification metrics results to those obtained from non-OCN approaches (Table 4).

	A	B	C	D	Verification Metrics			
	Hits	FA	Misses	Corr. Rej.	% Corr	FA Rate	POD	HSS
Results for hindcasts at lead time of zero months								
AN PR	**4**	**2**	**1**	**8**	**0.8**	**0.3**	**0.7**	**0.6**
BN PR	**2**	**2**	**1**	**10**	**0.8**	**0.5**	**0.5**	**0.4**
NN PR	**3**	**2**	**4**	**6**	**0.6**	**0.4**	**0.6**	**0.2**
Results for hindcasts at lead time of one month								
AN PR	**4**	**0**	**1**	**10**	**0.9**	**0.0**	**1.0**	**0.8**
BN PR	**2**	**5**	**1**	**7**	**0.6**	**0.7**	**0.3**	**0.2**
NN PR	**3**	**1**	**4**	**7**	**0.7**	**0.3**	**0.8**	**0.3**
Results for hindcasts at lead time of two months								
AN PR	**4**	**3**	**1**	**7**	**0.7**	**0.4**	**0.6**	**0.5**
BN PR	**2**	**2**	**1**	**10**	**0.8**	**0.5**	**0.5**	**0.4**
NN PR	**3**	**1**	**4**	**7**	**0.7**	**0.3**	**0.8**	**0.3**
Results for hindcasts at lead time of three months								
AN PR	**4**	**1**	**1**	**9**	**0.9**	**0.2**	**0.8**	**0.7**
BN PR	**2**	**2**	**1**	**10**	**0.8**	**0.5**	**0.5**	**0.4**
NN PR	**4**	**2**	**3**	**6**	**0.7**	**0.3**	**0.7**	**0.3**
Results for hindcasts at lead time of four months								
AN PR	**4**	**1**	**1**	**9**	**0.9**	**0.2**	**0.8**	**0.7**
BN PR	**1**	**4**	**2**	**8**	**0.6**	**0.8**	**0.2**	**0.0**
NN PR	**2**	**3**	**5**	**5**	**0.5**	**0.6**	**0.4**	**-0.1**
Results for hindcasts at lead time of five months								
AN PR	**4**	**1**	**1**	**9**	**0.9**	**0.2**	**0.8**	**0.7**
BN PR	**1**	**5**	**2**	**7**	**0.5**	**0.8**	**0.2**	**-0.1**
NN PR	**2**	**2**	**5**	**6**	**0.5**	**0.5**	**0.5**	**0.0**
Results for hindcasts at lead time of months months								
AN PR	**4**	**1**	**1**	**9**	**0.9**	**0.2**	**0.8**	**0.7**
BN PR	**1**	**3**	**2**	**9**	**0.7**	**0.8**	**0.3**	**0.1**
NN PR	**5**	**1**	**2**	**7**	**0.8**	**0.2**	**0.8**	**0.6**

However, the results from using the advanced OCN approach were better when applied to the other forecasting methods. Table 7 shows the skill scores averaged over all categories (AN, BN, NN) and all lead times when the advanced OCN approach was applied to each of our four forecasting methods. The advanced OCN approach yielded higher hindcast verification metrics for each of the four forecast methods than were obtained when using non-OCN approaches (Table 5). This indicates that using recent predictors and forecast categories based on recent years may be improve forecasts of upcoming years.

Table 7. Average verification metrics for hindcasts of HOA PR in Oct–Nov 1995–2009 using each of the four forecast methods and the multi-region SST predictors (advanced OCN approach; Figure 30). Averaging done over all forecast categories (AN, BN, NN) and all lead times of zero to six months. Compare these advanced OCN verification metrics results to those obtained from non-OCN approaches (Table 5).

	% Correct	F.A. Rate	POD	HSS
M-R Method 1	0.7	0.4	0.6	0.4
M-R Method 2	0.9	0.2	0.8	0.7
M-R Method 3	0.9	0.2	0.8	0.7
M-R Method 4	0.7	0.4	0.6	0.4

D. LONG-RANGE HINDCAST CASE STUDIES

In order to further validate our predictive scheme, we tested each LRF method, using the NZ SST and MR SST predictors, for individual years within the 1970–2009 period. We wanted to see how the LRF methods would perform in extreme AN and BN years, and the current year. For this, we chose 1997 and 2006 (AN), 1998 (BN), and 2009 (current year) to use as our hindcast case studies.

Each hindcast was simulated as if we were the forecasters at the regional forecast office, or military installation, asked to predict the coming October–November season's rainfall in the HOA as input for planning an operation. We used as our predictors NZ SST and MR SST. We started by analyzing the Apr–May SSTs in each predictor region (e.g., NZ or SW Atlantic for the MR), applied the analyzed SSTs to the LRF methods, and compared the forecasted PR to the actual PR that occurred in the HOA for the October–November period of the year being forecasted. We repeated the process for each lead time, and switched to the Philippine SST predictor at leads of zero to three months.

1. 2009 Test Case

In 2009, the Apr–May analyzed SSTs in the NZ and SW Atlantic predictor regions were 23.875C and 22.958C, respectively (Figure 31).

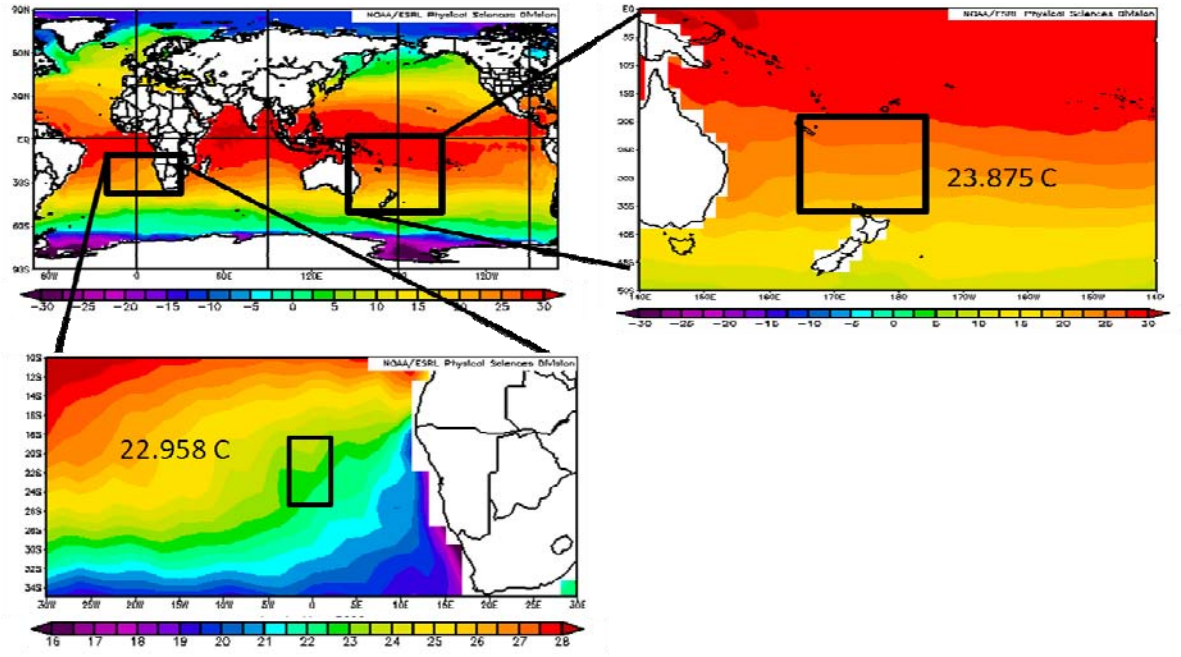

Figure 31. Composite mean SST (^{o}C) in Apr–May 2009 averaged over: (top right) NZ predictor region and (bottom left) MR predictor region. The black (red) box represents the NZ (MR) SST predictor regions used for analyzing the SSTs at lead times of six months. The area averaged SST for Apr–May 2009 was 23.875 (22.958) ^{o}C in the NZ (MR) predictor regions. Images created using ESRL (2010).

The Apr–May NZ and MR SSTs fell into NN SST bins and thus yielded a NN precipitation rate forecast for the HOA in Oct–Nov when applying Method 1 (tercile matching). For Methods 2 and 3, the analyzed SSTs into the formulated regression equations based on data from the appropriate years (1970–2009 for the NZ SST, 1995–2009 for the MR SST), and the resulting PR value was binned into the appropriate tercile category. The NZ predictor region yielded NN precipitation rate values of 3.258 (mm/day) and 3.290 (mm/day), for Method 2 and 3, respectively. The MR SST predictors yielded lower values than the NZ SST predictor, yet within the same tercile category of NN precipitation for Oct–Nov. The CAF method produced forecasted probabilities of 42% BN rainfall and 80% NN rainfall in Oct–Nov for the NZ and MR predictors, respectively, given an analyzed NN SST in Apr–May (see Chapter II, Section 6, for a description of how probabilistic categorical forecasts from the CAF method were verified).

The actual Oct–Nov PR in the HOA for 2009 was 2.836 (mm/day) which is in the NN tercile for the 40-yr tercile bin ranges, and BN for the 15-year tercile bin ranges. Recall that the formulation of the tercile bin ranges is dependent on the number of years in the dataset, which is why there is a difference between the actual PR terciles even though the PR value is the same.

Therefore, by using the NZ predictor we would have forecasted a NN PR for Oct–Nov 2009 given a NN SST in Apr–May, and thus forecasted correctly. Using the MR predictor, we would have forecast a NN PR, yet BN precipitation occurred and thus forecasted incorrectly. Figure 32 shows the actual and anomaly PR reanalysis fields for Oct–Nov 2009.

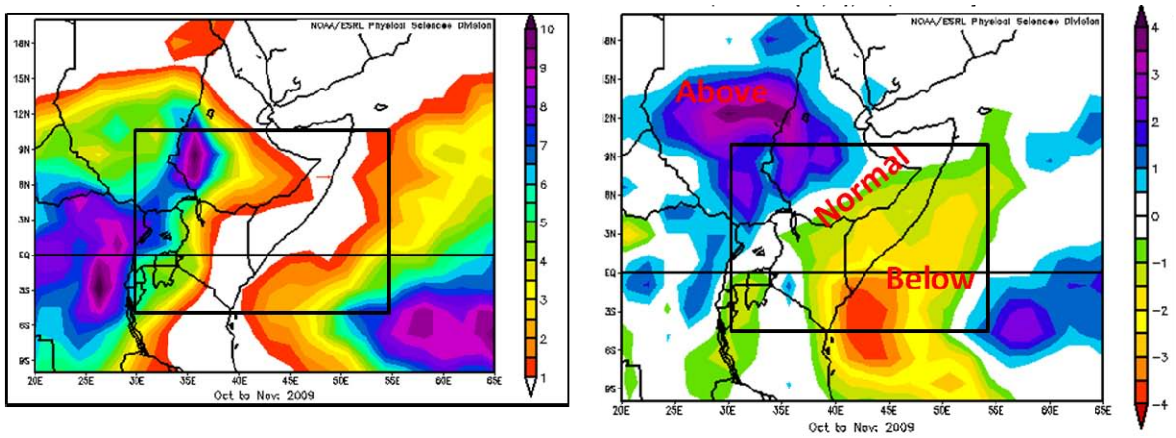

Figure 32. Composite mean (left panel) and anomaly (right panel) PR (mm/day) in Oct–Nov 2009. The black outlined box represents the HOA PR predictand region. Note that AN, NN, and BN PR anomalies occurred within the predictand region (right panel); however the actual area-averaged PR was 2.836 mm/day, or NN. Images created using ESRL (2010).

Note that there were AN, NN, and BN anomalies that occurred within the predictand region, and therefore the forecast may have been accurate or inaccurate, depending on the area within the HOA predictand region. This highlights a limitation of area averaged predictand regions—that they cannot explicitly represent sub-regional variations. This limitation can be mitigated if the region being averaged is small and/or tends to experience spatially homogeneous climate variations. Of course, for LRF users and planning lead times, this limitation may not be critical (e.g., users who do need high spatial resolution for long lead planning).

We also hindcasted the Oct–Nov 2009 PR in the HOA at each lead time to see how the forecasts compared with varying lead time. Table 8 shows the results for the 2009 test case. Accurate forecasts are those for which the forecasted and observed categories match (e.g., NN forecasted (gray) matches NN observed gray, indicating a hit). The categories are color-coded: pink for AN, blue for BN, and gray for NN. So, forecast performance can be quickly determined by comparing the observed color with the forecast color. Note that the gray NN (blue BN) forecasts from the NZ SST (MR SST) predictor tended to

perform well. Forecast consistency form one lead to the next can be determined by comparing the forecast colors along a row (e.g., all one color along a row indicates high consistency).

Table 8 shows that the forecast performance was low at the shorter lead times for all methods, and at most of the lead times using the CAF methods (note the many cells in the table that are colored blue (BN) or pink (AN) instead of gray (NN)). Overall, the consistency in the forecasts from one lead to the next was greater for the NN forecasts, except for the CAF forecasts at the shortest lead times. The NZ SST (non-OCN) predictor forecasted slightly better overall than the MR SST (OCN) predictor.

Note from Table 8 that Methods 1–3 using the NZ SST predictor performed well at most lead times, but that all the methods, with both predictors, did poorly at the shorter leads when they tended to forecast AN PR. This occurred because the 2009 SST predictors switched from mainly NN at the longer leads to BN at the shortest leads (not shown), thus leading to AN PR forecasts at short leads. In summary, the hindcast results for the 2009 case were less than ideal, but better than LTM based forecasts would have been, when viewed over all lead times. This was a challenging case for all the methods, perhaps in part because of the inhomogeneity of the observed HOA PR with the HOA (Figure 32) and the variation of the predictors in the transition from longer leads to shorter leads.

Table 8. Results from hindcasts of HOA PR (mm/day) for Oct–Nov 2009 for each forecast method using each of the four forecast methods, and the NZ SST (non-OCN) and MR SST (OCN) predictors, at lead times of zero to six months. The forecast methods (1–4) are listed at the left. Lead times (top row) decrease from left to right. The SST predictor used (NZ or MR) is listed in the second row from the top. The forecasted PR values are the numerical quantities shown within the columns for each lead time and each predictor. The forecasted tercile categories are shown just below each forecasted PR. The actual Oct–Nov HOA PR value and categories are located at the bottom left (left (right) column shows observed tercile category based on non-OCN (OCN) process). Method 1: tercile matching; Method 2: averaged linear regression; Method 3: non-averaged linear regression; and Method 4: CAF.

	6 months lead		5 months lead		4 months lead		3 months lead		2 months lead		1 month lead		zero months lead	
LRF Method	NZ	M-R	NZ	M-R	NZ	M-R	NZ	M-R	NZ	M-R	NZ	M-R	NZ	M-R
1	NORMAL	NORMAL	NORMAL	NORMAL	NORMAL	BELOW	NORMAL	BELOW	ABOVE	NORMAL	NORMAL	NORMAL	ABOVE	BELOW
2	3.259	3.045	3.323	2.851	3.497	2.735	3.436	2.704	3.327	3.019	3.416	3.31	3.666	3.516
Category	NORMAL	NORMAL	NORMAL	NORMAL	NORMAL	NORMAL	NORMAL	NORMAL	NORMAL	NORMAL	NORMAL	ABOVE	ABOVE	ABOVE
3	3.245	3.062	3.331	2.852	3.525	2.723	3.468	2.717	3.352	3.033	3.443	3.348	3.698	3.589
Category	NORMAL	NORMAL	NORMAL	NORMAL	ABOVE	NORMAL	NORMAL	NORMAL	NORMAL	NORMAL	NORMAL	ABOVE	ABOVE	ABOVE
4	42%	80%	42%	67%	44%	75%	67%	67%	52%	67%	43%	67%	67%	80%
Category	BELOW	NORMAL	BELOW	BELOW	ABOVE	NORMAL	ABOVE	BELOW	ABOVE	NORMAL	NORMAL	NORMAL	ABOVE	ABOVE
ACTUAL PRECIP	2.836	2.836												
	NORMAL	BELOW												

2. 1997, 1998, and 2006 Test Cases

In 1997, the HOA received a considerable amount of rainfall during the short-rains season, along with devastating impacts to the region's livelihoods (ICRC 2004). The HOA PR was well into the AN category. The flooding of 1997 was followed by drought conditions in 1998, and devastating floods again in 2006. We investigated these three cases because of their extreme PRs and because their actual PR anomalies were relatively coherent within the predictand region (Figure 33), unlike the 2009 case.

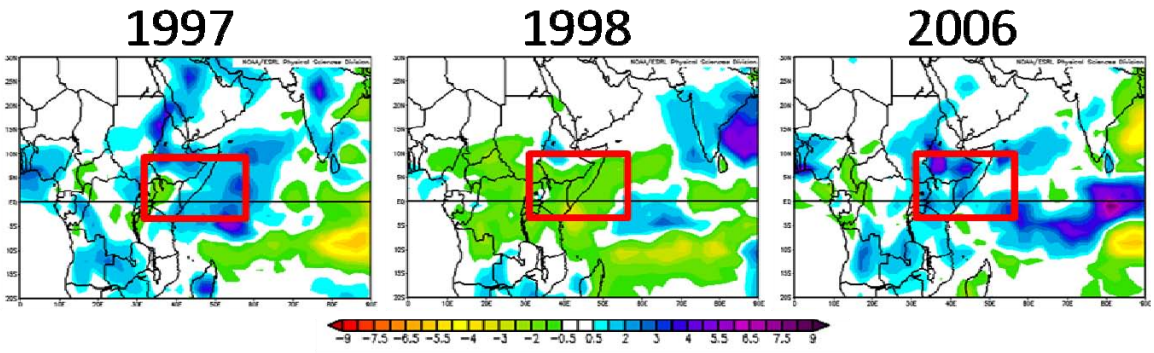

Figure 33. Composite anomalies of PR (mm/day) during Oct–Nov for three different years: (left panel) 1997, (middle panel) 1998, and (right panel) 2006. The red outlined boxes represent the HOA PR predictand region. The HOA experienced extreme AN or BN PR in each of these years: AN in 1997 and 2006, and BN in 1998). These years were chosen to test the four forecast methods using the non-OCN and OCN-based predictor sets. Images created using ESRL (2010).

The hindcast results are shown in Table 9. This table is the same as Table 8 but for three different years. Thus, the instructions for interpreting Table 8 (see above) apply to interpreting Table 9. Each LRF method performed well in each of the three years, with some exceptions (e.g., Methods 1 and 4 at the longest leads). The MR (OCN) SST based forecasts performed better overall. For 1998, each LRF method performed well, with the exception of Method 4 using the MR SST predictors. Using the Method 4 forecast in isolation would give decision makers inaccurate information. But, when combined with the other LRF methods, a forecaster might hedge towards a BN PR forecast, since two out of three of the other methods forecasted BN PR. The 2006 LRFs at longer leads are inconsistent with each other. But, at leads of three to four months and less, the forecasts tend toward AN forecasts, in line with actual conditions.

Table 9. Results from hindcasts of HOA PR (mm/day) for Oct–Nov of three different years using each of the four forecast methods, and the NZ SST (non-OCN) and multi-region (OCN) SST predictors, at lead times of zero to six months The years are: (top table) 1997, (middle table) 1998, and (bottom table) 2006. The forecast methods (1–4) are listed at the left. Lead times (top row) decrease from left to right. The SST predictor used (NZ or MR) is listed in the second row from the top. The forecasted PR values are the numerical quantities shown within the columns for each lead time and each predictor. The forecasted tercile categories are shown just below each forecasted PR. The actual Oct–Nov HOA PR value and categories are located at the bottom left (left (right) column shows observed tercile category based on non-OCN (OCN) process). Method 1: tercile matching; Method 2: averaged linear regression; Method 3: non-averaged linear regression; and Method 4: CAF. Note that all forecast method perform well at lead times of zero to four months, but have lower skill at the longer lead times, possibly indicating the effects of the spring predictability barrier (Chapter III, Section B.2; van den Dool 2007). The OCN approach leads to some improvement in performance, especially at the longer leads.

	6 months lead		5 months lead		4 months lead		3 months lead		2 months lead		1 month lead		zero months lead	
LRF Method	NZ	M-R	NZ	M-R	NZ	M-R	NZ	M-R	NZ	M-R	NZ	M-R	NZ	M-R
1	NORMAL	ABOVE	NORMAL	ABOVE	NORMAL	ABOVE	NORMAL	ABOVE	ABOVE	ABOVE	ABOVE	ABOVE	ABOVE	ABOVE
2	3.265	4.361	3.337	4.481	3.408	4.335	3.5975	4.457	3.847	4.505	3.906	4.227	3.692	4.27
Category	NORMAL	ABOVE	NORMAL	ABOVE	NORMAL	ABOVE	ABOVE	ABOVE	ABOVE	ABOVE	ABOVE	ABOVE	ABOVE	ABOVE
3	3.24	4.092	3.296	4.297	3.378	4.08	3.58	4.338	3.822	4.367	3.878	4.011	3.633	4.106
Category	NORMAL	ABOVE	NORMAL	ABOVE	NORMAL	ABOVE	ABOVE	ABOVE	ABOVE	ABOVE	ABOVE	ABOVE	ABOVE	ABOVE
4	46%	80%	46%	80%	46%	80%	50%	80%	50%	57%	67%	100%	62%	67%
Category	BELOW	ABOVE	BELOW	ABOVE	ABOVE	ABOVE	ABOVE	ABOVE	ABOVE	ABOVE	ABOVE	ABOVE	ABOVE	ABOVE
ACTUAL PRECIP	4.714	4.714												
	ABOVE	ABOVE												

	6 months lead		5 months lead		4 months lead		3 months lead		2 months lead		1 month lead		zero months lead	
LRF Method	NZ	M-R	NZ	M-R	NZ	M-R	NZ	M-R	NZ	M-R	NZ	M-R	NZ	M-R
1	BELOW	NORMAL	BELOW	BELOW	BELOW	BELOW	BELOW	BELOW	BELOW	BELOW	BELOW	BELOW	BELOW	BELOW
2	3.051	2.975	2.844	2.559	2.642	2.272	2.483	2.219	2.547	2.296	2.632	2.329	2.534	2.311
Category	NORMAL	NORMAL	BELOW	BELOW	BELOW	BELOW	BELOW	BELOW	BELOW	BELOW	BELOW	BELOW	BELOW	BELOW
3	3.208	3.021	2.965	2.584	2.658	2.227	2.464	2.172	2.554	2.268	2.637	2.31	2.568	2.288
Category	NORMAL	NORMAL	BELOW	BELOW	BELOW	BELOW	BELOW	BELOW	BELOW	BELOW	BELOW	BELOW	BELOW	BELOW
4	45%	100%	42%	80%	45%	100%	53%	67%	100%	67%	56%	67%	57%	67%
Category	BELOW	NORMAL	BN/NN	NORMAL	BN/NN	NORMAL	BELOW	NORMAL	NORMAL	NORMAL	BELOW	NORMAL	BELOW	NORMAL
ACTUAL PRECIP	2.404	2.404												
	BELOW	BELOW												

	6 months lead		5 months lead		4 months lead		3 months lead		2 months lead		1 month lead		zero months lead	
LRF Method	NZ	M-R	NZ	M-R	NZ	M-R	NZ	M-R	NZ	M-R	NZ	M-R	NZ	M-R
1	BELOW	ABOVE	BELOW	ABOVE	NORMAL	ABOVE	NORMAL	ABOVE	ABOVE	ABOVE	ABOVE	ABOVE	ABOVE	ABOVE
2	3.259	3.568	3.015	3.689	3.167	3.573	3.427	4.074	3.447	3.568	3.553	3.584	3.621	4.211
Category	NORMAL	ABOVE	NORMAL	ABOVE	NORMAL	ABOVE	NORMAL	ABOVE	NORMAL	ABOVE	ABOVE	ABOVE	ABOVE	ABOVE
3	2.731	3.419	2.93	3.526	3.116	3.428	3.407	3.903	3.428	3.435	3.532	3.445	3.568	4.025
Category	BELOW	NORMAL	NORMAL	ABOVE	NORMAL	NORMAL	NORMAL	ABOVE	NORMAL	NORMAL	ABOVE	NORMAL	ABOVE	ABOVE
4	55%	67%	50%	75%	38%	75%	56%	75%	48%	50%	64%	100%	58%	60%
Category	BELOW	NORMAL	BELOW	ABOVE	ABV/BN	ABOVE	ABOVE	ABOVE	ABOVE	ABOVE	ABOVE	ABOVE	ABOVE	ABOVE
ACTUAL PRECIP	4.714	4.714												
	ABOVE	ABOVE												

These three case studies, in which extreme and spatially homogeneous PR occurred in the HOA, provide clear evidence that all four forecast methods, and the non-OCN and OCN SST predictors, are capable of producing consistently accurate LRFs at leads of one to six months. However, the performance is noticeable less at leads of five to six months. The LRFs with these leads are issued during the northern spring, suggesting that the poorer performance the longer lead times may represent the spring predictability barrier (Chapter III, Section B.2; van den Dool 2007). In the NH spring, many climate processes (e.g., Asian Monsoon, ENSO, IOD, etc) are resetting. As a result, predictions that extend through the northern spring tend to have lower skill. Thus, forecasts from the longer lead times should be used with extra caution.

These case study results suggest several conclusions for forecasters based on our forecasting methods that may be applicable to other long-range forecasting methods. First, the forecasts from different forecasting methods, and from non-OCN and OCN processes, might be best used together, rather than separately. Thus, for example, a consensus of all the forecasts might in general be better than any individual forecast. Second, forecast trends should be monitored as lead time decreases, since important changes in the forecasts can occur as leads decrease, and especially as the spring predictability barrier is passed. Third, the proximity of the forecasted PR values to the category thresholds should be monitored and accounted for in issuing and verifying forecasts. For example, account for close-call forecasts, such as a forecasted

PR value of 3.47 mm/day, which is a borderline NN PR forecast, with the AN PR being 3.50 mm/day or above. Fourth, forecasters and forecast users should be familiar with the characteristic climate variations patterns for their region of interest (e.g., familiar with the results of composite analyses and historical frequency distributions associated with ENLN, IOD, etc.).

E. HINDCAST VERIFICATION SUMMARY

Figure 34 shows a summary of the hindcast results for each LRF method and each predictor (NZ SST / non-OCN) and MR SST / OCN), according to the dataset and predictor used. The skill scores are what we termed *total verification metrics*, meaning skill scores averaged over all forecast categories (AN, BN, NN) and all lead times. The total verification metrics for hindcasts that used the NZ SST (MR SST) predictor are shown in the four leftmost (rightmost) columns. Each column is numbered according to the LRF method (see method key in lower right). Each skill metric is represented by a different colored symbol (see key on left). A reference key at the bottom right shows the type of method for each column. For example: the second column from the left (column 2) shows the skill metrics for LRF Method 2 (averaged linear regression applied) using the NZ SST predictor; and the second column from the right (column 7) shows the skill metrics for LRF Method 3 (non-averaged linear regression(using the MR SST predictors. To compare the skill of the hindcasts based on the NZ SST predictor to that of the LRFs based on the MR SST predictors, compare the left and right columns with the same numbers (e.g., left (right) column 3 shows Method 3 metrics for NZ SST (MR SST)).

Figure 34 shows that all of the HSS values are positive, indicating that each predictor-predictand pair has skill. In general, the MR SST (OCN) predictor has higher skill than the NZ SST predictor, although LRFs based on each of the predictors have higher skill than forecasts using the LTM.

Method 2 and 3 (linear regression LRF models) have the highest total skill scores, with the scores from the MR SST based Methods 2 and 3 being higher

than the scores from the NZ SST based Methods 2 and 3. The linear regression methods may have higher scores than the tercile matching and CAF methods because the linear regression methods predict a discrete value from a relatively complex model that can accommodate and exploit *relatively* subtle differences in predictor and predictand values. The tercile matching and CAF methods, on the other hand, are effectively simpler and cruder models that can only resolve predictor and predictand values into one of three broad categories. Thus, the linear regression methods tend to be better at describing the details of predictor–predictand relationships than the tercile matching and CAF methods. Of the two linear regression methods, the non-averaged performed slightly better. This is consistent with the idea that better resolution of the details in predictor-predictand relationships leads to better forecast performance.

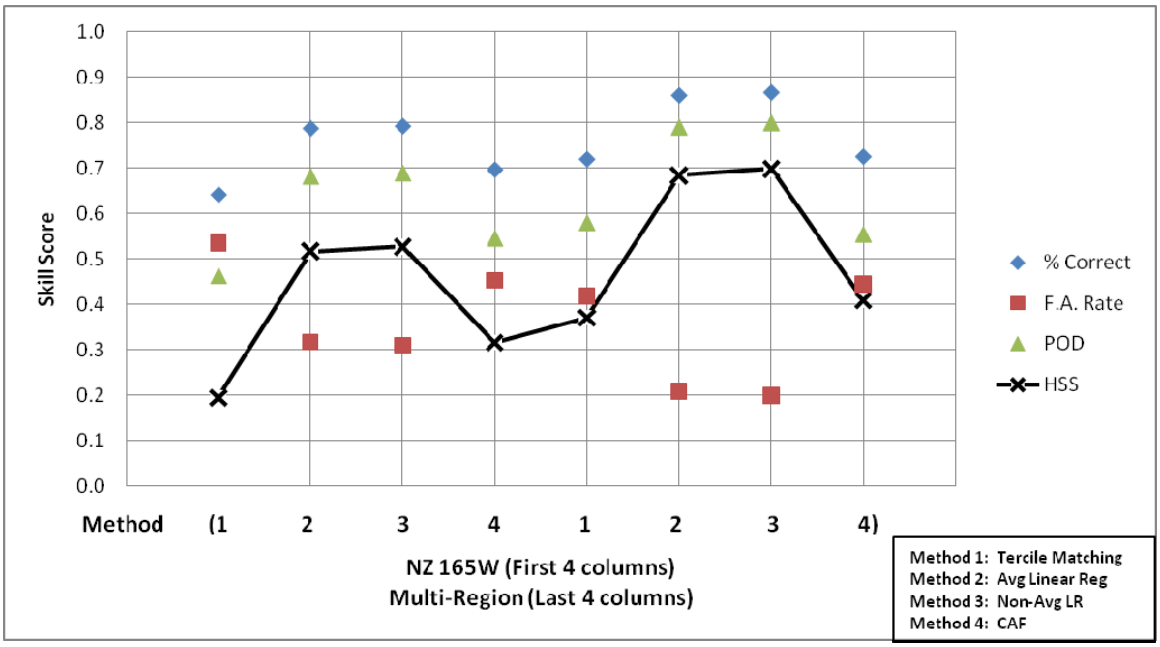

Figure 34. Total verification metrics for hindcasts of HOA PR in Oct–Nov averaged over all forecast categories (AN, BN, NN) and all lead times of zero to six months. Columns 1–4 (5–8) represent verification metrics using the NZ (Multi-Region) SST predictor for 1970–2009 (1995–2009) with each of the forecast methods listed at the bottom right of the figure (e.g., tercile matching, linear regression and CAF). For example, column 5 represents the verification metrics for Method 1 (tercile matching) using the Multi-Region SST predictor. Verification metrics consist of percent correct (% Corr), false alarm rate (FA Rate), probability of detection (POD), and Heidke Skill Score (HSS). Refer to Chapter II, Section B.6 for more information on these metrics. The bold black line highlights the HSSs.

Figures 35–38 compare the time series of hindcasted and observed HOA PR for Oct–Nov of 1970–2009 for different forecast methods, predictors, and lead times. We used these comparisons to help identify the conditions under which the hindcasts did performed well and poorly. For example, Figures 35–36 clearly show that Method 2 and 3 hindcasts based on the NZ SST predictor: (a) had better performance before 1984 and after 1993 than in between; (b) had a low bias, especially at long leads; and (c) were better at short leads than long leads.

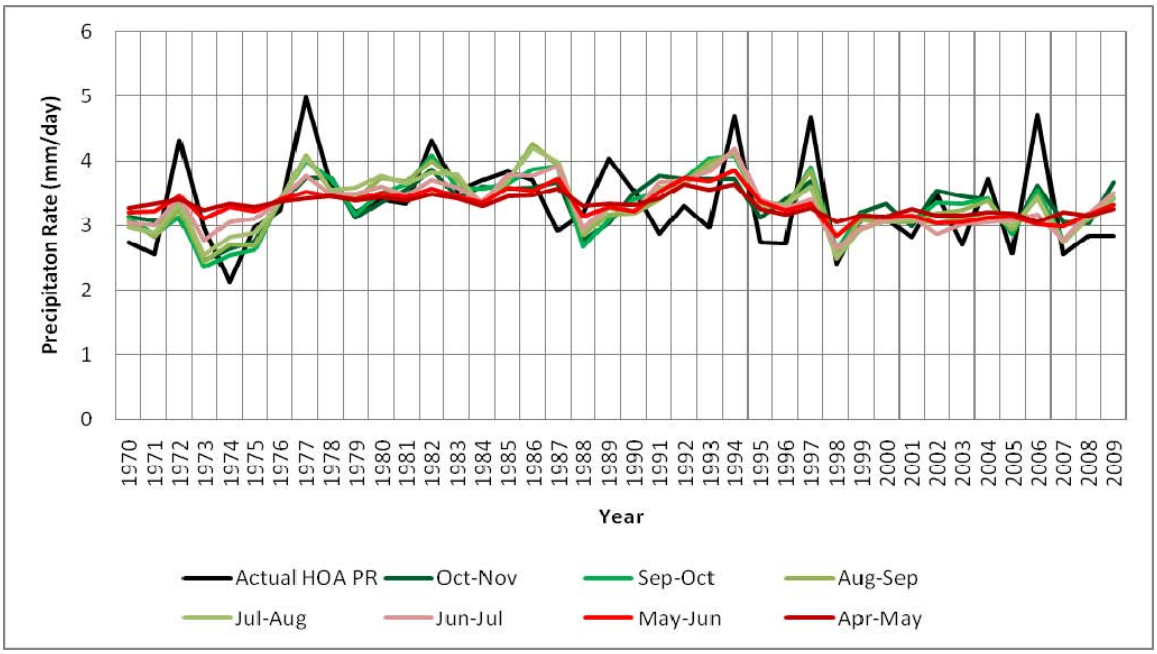

Figure 35. Time series of actual HOA PR (black line) and hindcasted PR values using Method 2 (averaged linear regression) and the NZ SST predictor for Oct–Nov 1970–2009 at lead times of zero to six months. The hindcast PR values are dark red (green) at the longest (shortest) lead times. Note: (a) the periods of relatively good model performance before 1984 and after 1993 (see Chapter III, Section A.3; Figure 24); and (b) the lower variability in the hindcasted PR than the observed PR, especially at longer leads. All PR values in mm/day.

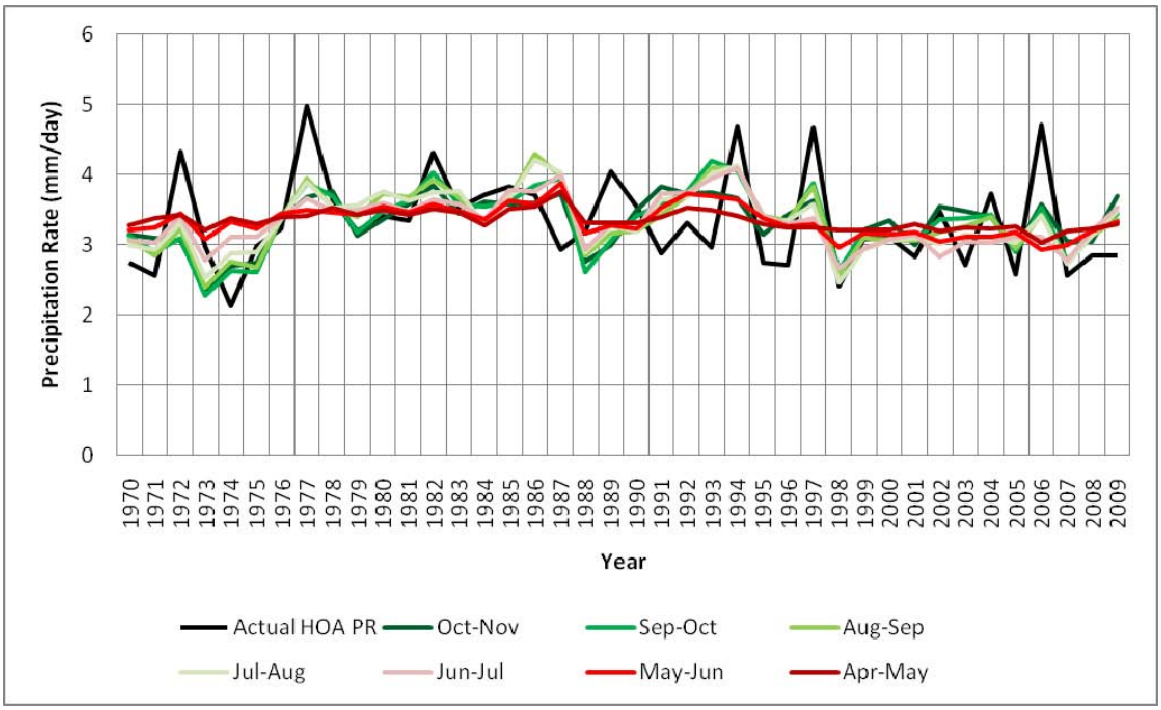

Figure 36. Time series of actual HOA PR (black line) and hindcasted PR values using Method 3 (non-averaged linear regression) and the NZ SST predictor for Oct–Nov 1970–2009 at lead times of zero to six months. The hindcast PR values are dark red (green) at the longest (shortest) lead times. Note: (a) the periods of relatively good model performance before 1984 and after 1993 (see Chapter III, Section A.3; Figure 24); and (b) the lower variability in the hindcasted PR than the observed PR, especially at longer leads. All PR values in mm/day.

Figures 37–38 show overall very good model performance using Methods 2 and 3 and the MR SST predictors, especially at shorter leads. These hindcasts also show relatively realistic variability, especially at shorter leads. The MR SST predictors do better than the NZ SST predictor in hindcasting the amplitudes of the interannual variations than relative to the NZ predictor. However, the MR SST based hindcasts have relatively low skill between 1999–2002 and then again in 2007. The cause for this is not certain, but 1999–2002 was a period of NN PR for the HOA, and the forecast models have lower skill forecasting NN PR

events. Methods 2 and 3 with the MR predictor were especially skillful in hindcasting the extreme events during 1995–2009, especially the AN PR events (e.g., 1997, 2004, and 2006) and at shorter leads (Figures 37–38).

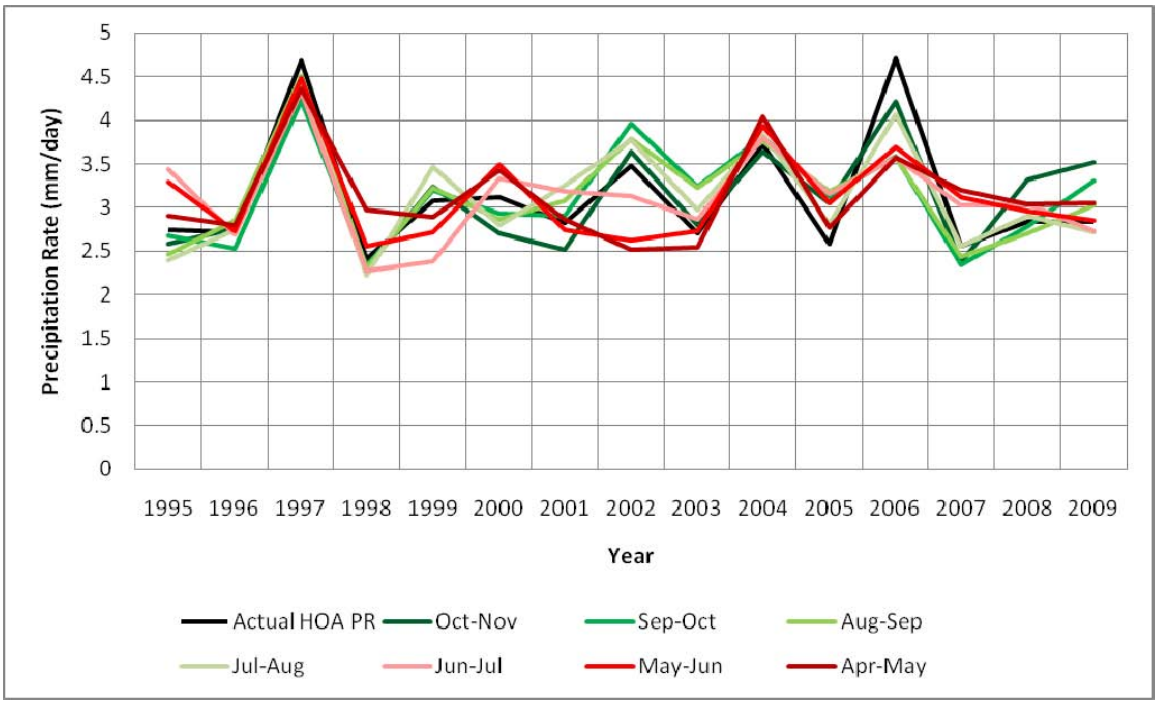

Figure 37. Time series of actual HOA PR (black line) and hindcasted PR values using Method 2 (averaged linear regression) and the MR SST predictors for Oct–Nov 1995–2009 at lead times of zero to six months. The hindcast PR values are dark red (green) at the longest (shortest) lead times. Note: (a) the overall very good model performance, especially at shorter leads; and (b) the relatively realistic variability, especially at shorter leads. All PR values in mm/day.

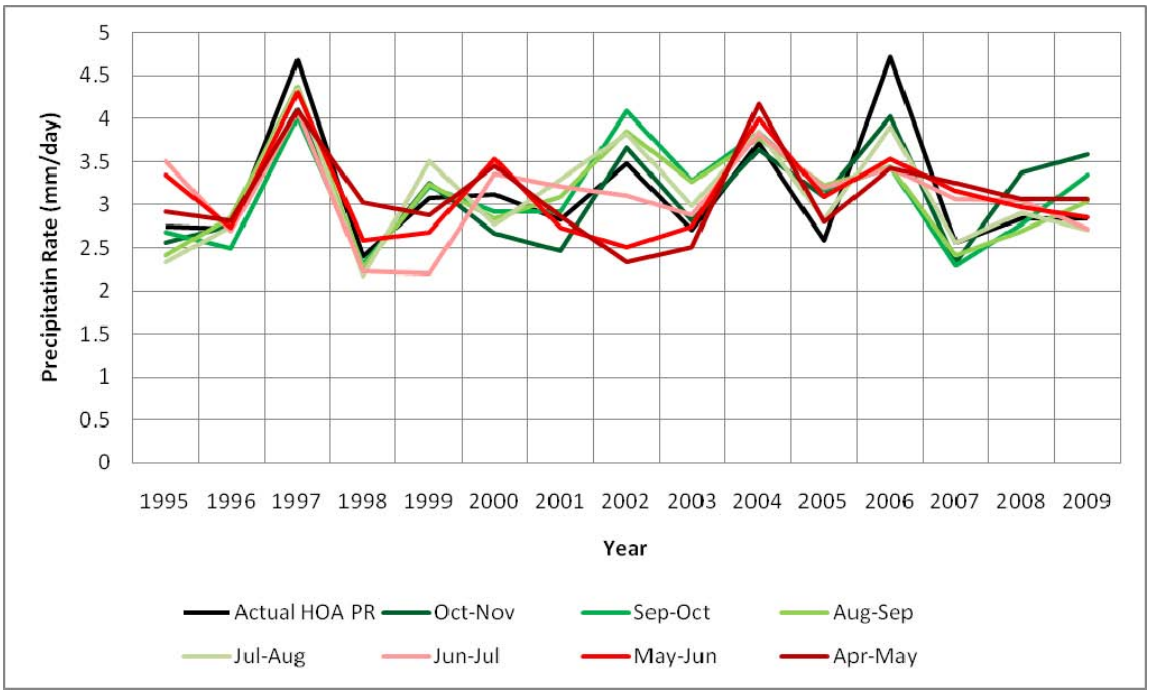

Figure 38. Time series of actual HOA PR (black line) and hindcasted PR values using Method 3 (non-averaged linear regression) and the MR SST predictors for Oct–Nov 1995–2009 at lead times of zero to six months. The hindcast PR values are dark red (green) at the longest (shortest) lead times. Note: (a) the overall very good model performance, especially at shorter leads; and (b) the relatively realistic variability, especially at shorter leads variability in the hindcasted PR than the observed PR, especially at longer leads. All PR values in mm/day.

Figure 39 shows the correlations between the actual Oct–Nov HOA PR and the hindcasted HOA PR values shown in Figures 35–38 by lead time. Note that the highest correlations are for Methods 2 and 3 based on the MR SST predictors, with the Method 2 hindcasts being slightly better correlated than the Method 3 hindcasts. The differences in the correlations between the hindcasts involving the MR SST predictors and those involving the NZ SST predictors is likely due: (a) the smaller number of years represented the hindcasts involving the MR SST predictors; and (b) the exclusion from the hindcasts involving the MR SST predictors of the problematic years in the middle of the study period (1984–1993; Figures 24, 37–38). The correlations involving the NZ SST

predictor are more regular across lead times, perhaps due to the larger number of hindcasts involved in these correlations. The largest correlations occur at leads of two to three months, not at zero months. This may be due to lags between when the predictor starts to change and when the predictand responds to that change (e.g., maximum variation in predictor precedes by two to three months the maximum variation in the predictand). This is plausible, given that the predictors and predictand are widely separated, are in two different components of the climate system (ocean and atmosphere), and are very likely linked via a complex set of low frequency dynamical processes (e.g., ocean temperature advection, tropical Rossby and Kelvin waves associated with ENLN and IOD mechanisms).

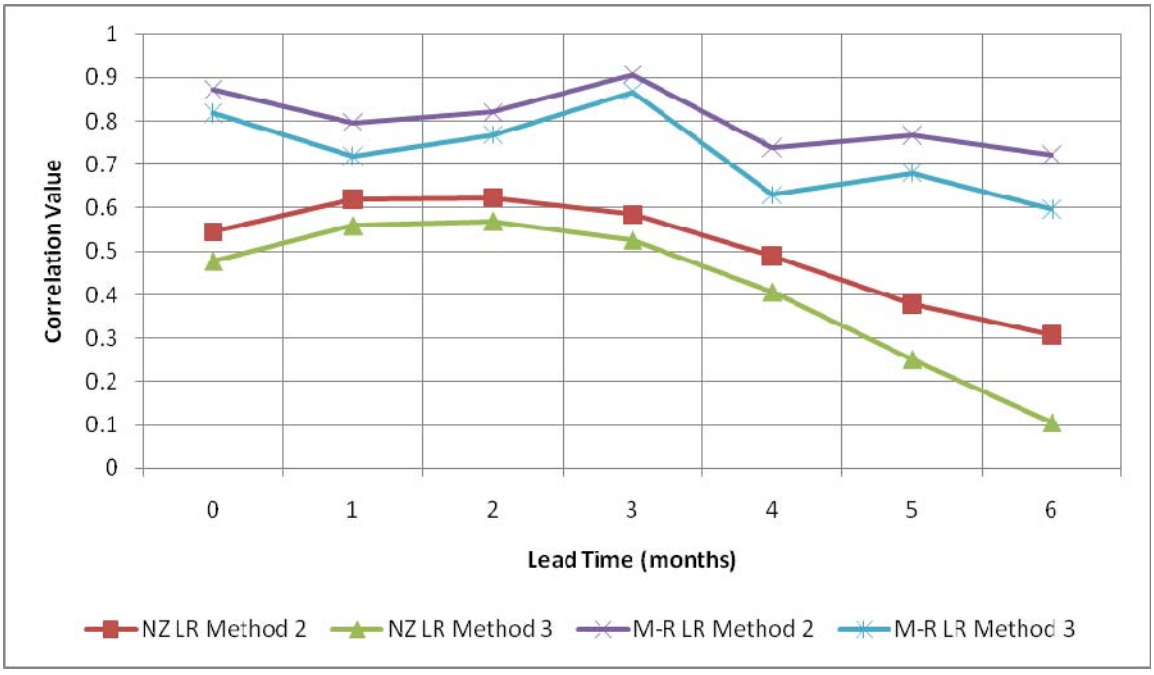

Figure 39. Correlations between the actual Oct–Nov HOA PR and the hindcasted HOA PR values shown in Figures 35–38 by lead time. Forecast method and predictor indicated by colored lines and symbols (see key).

F. FORECAST FOR OCTOBER–NOVEMBER 2010

We produced on 01 June 2010 eight LRFs of HOA PR in October–November 2010 (Table 10). These eight LRFs were based on all four LRF methods, and on the April–May 2010 reanalyzed values for our two SST predictor sets (NZ SST and the MR SST). Thus, our forecasts were six month lead LRFs. The predictor SSTs were all NN in Apr–May 2010, and all but one of the LRFs predicted NN PR in Oct–Nov 2010. This is consistent with the transitioning from EN to LN that was occurring in the tropics during Apr–May 2010. As of the completion of this report, more recent observed predictor values were not available. Since these LRFs were issued during the northern spring transition, these LRFs extend through the spring transition barrier. Thus, they should be used with extra caution and updated LRFs should be monitored by forecast users.

Table 10. Eight long-range forecasts of HOA PR categories for Oct–Nov 2010 that we issued on 01 June 2010 at a six month lead time. The LRF methods and predictors for each LRF are shown in the table. The predictor values were the reanalyzed Apr–May SSTs from the NZ and MR predictor regions. Note that all the LRFs predict NN PR in the HOA for Oct–Nov 2010, except for one (Method 4, CAF, using the NZ SST predictor). Hindcasts generated using these LRF methods and SST predictors have their lowest skill at the longest lead (six months). Thus, these LRFs should be used with caution and updated LRFs at shorter leads should be closely monitored.

Predictor	LRF Method	Forecast PR at 6 months lead
NZ Predictor	1	Normal
SST: 23.76C	2	Normal
	3	Normal
	4	Below Normal
M-R Predictor	1	Normal
SST: 23.03C	2	Normal
	3	Normal
	4	Normal

G. CLIMATE DYNAMICS BASIS FOR LONG-RANGE FORECASTS

We conducted initial analyses of the climate dynamics that underlie the statistical relationships between our HOA precipitation rate predictand and our SST predictors north of New Zealand, east of the Philippines, and west of Namibia. We conducted this investigation to: (a) identify potential additional predictors and predictands; (b) increase our confidence in applying these predictors; (c) improve our understanding of the relevant dynamics; and (d) determine what processes need to be well modeled in order to improve the statistical and dynamical simulation and prediction of HOA precipitation. To develop these dynamical analyses, we constructed composites based on the five most extreme AN and BN events for our three SST predictors, and for EN and LN events. These events are shown in Tables 11 and 12.

Table 11. The years in which the five most extreme AN and BN conditions occurred during Oct–Nov 1970–2009 for each of our three predictors.

	Predictors					
	NZ SST		Philippine SST		Namibia SST	
Categories	AN	BN	AN	BN	AN	BN
Years	1973	1977	1995	1997	1996	1997
	1974	1978	1998	2002	2001	2000
	1975	1982	2000	2004	2002	2004
	1988	1991	2001	2006	2003	2006
	1998	1994	2007	2009	2005	2007

Table 12. The years in which the five most extreme EN and LN conditions occurred during Oct–Nov 1970–2009, as indicated by the MEI.

	EN	LN
Years	1972	1971
	1982	1973
	1987	1974
	1994	1975
	1997	1988

1. NZ SST and HOA Precipitation Teleconnections

Figure 40 shows the composite SSTAs for the five most extreme BN NZ SSTs events during Oct–Nov 1970–2009. Recall that BN NZ SST is associated with AN HOA PR during Oct–Nov. Note, in this figure: (a) the large area of negative SSTAs in the southwestern Pacific centered on our NZ SST predictor region (red box) and underlying the SPCZ; (b) the EN pattern of SSTAs in the tropical Pacific; (c) the IOD pattern of SSTAs in the IO; (d) the negative SSTAs in the tropical Atlantic; and (e) the strong resemblance to the composite SSTAs during AN HOA PR (Figure 19). The corresponding SSTAs for the five most extreme AN NZ SST events shows nearly opposite patterns. These results indicate that our NZ SST predictor is closely related not just to HOA PR but also to SPCZ variations, ENLN, IOD, and SST variations in the Atlantic. These indications provide information about how NZ SSTs are dynamically related to HOA PR.

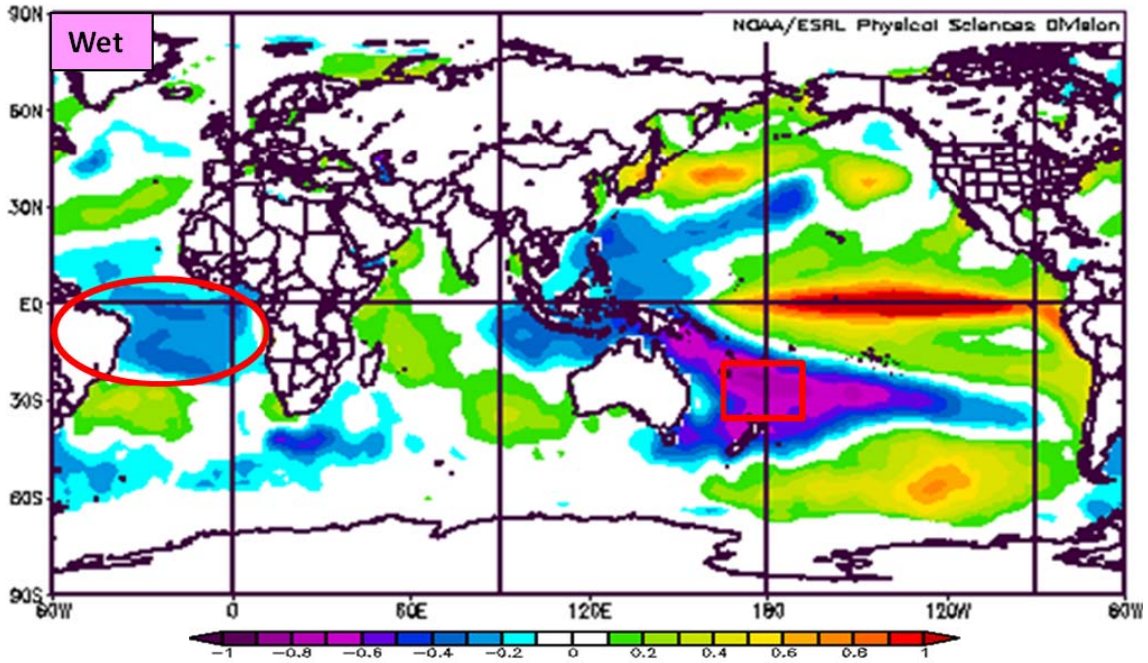

Figure 40. Conditional composite anomalies of sea surface temperature (^{o}C) for the five most extreme BN NZ SST events during Oct–Nov 1970–2009. Recall that BN NZ SST is associated with EN and positive IOD events (Figure 17), and with AN HOA PR during Oct–Nov. Red box indicates NZ SST region. Red oval indicates area of pronounced negative SSTAs in the tropical Atlantic. Image created using ESRL (2010).

Figure 41 shows the composite SSTAs for extreme EN and LN events during Oct–Nov 1970–2009. Note: (a) the strong resemblance to the composite SSTAs during AN and BN HOA PR (Figure 19); and (b) the strong resemblance to the composite SSTAs during BN NZ SST events (Figure 19); and (c) the negative (positive) SSTAs in the tropical Atlantic during EN (LN). These results indicate that our NZ SST predictor is closely related to ENLN variations. However, the SSTAs in the tropical Atlantic may be better represented by the NZ SST predictor than by an ENLN based predictor (e.g., better than by MEI or Nino3.4).

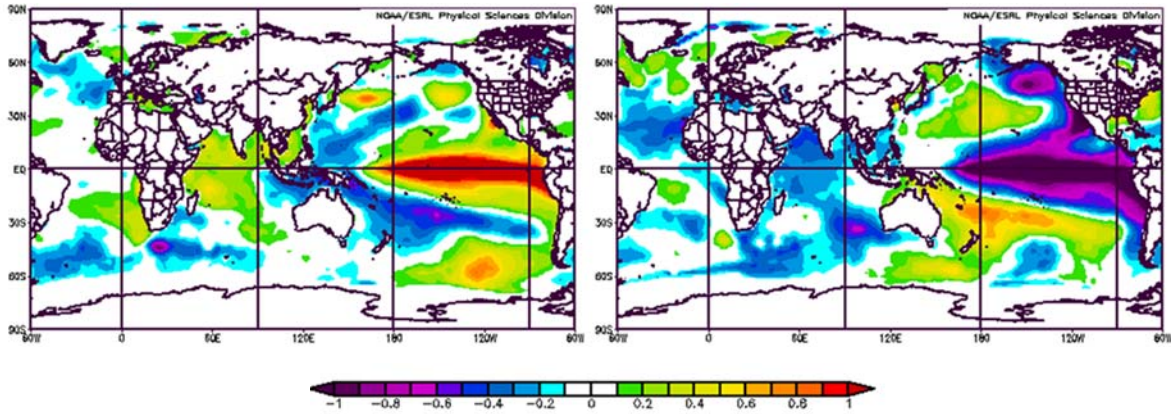

Figure 41. Conditional composite anomalies of sea surface temperature (^{o}C) for the five most extreme EN events (left panel) and LN events (right panel) during Oct–Nov 1970–2009. EN and LN events identified by use of MEI. Image created using ESRL (2010).

Rassmusson and Carpenter (1982), as well as many other ENLN studies, have shown a close relationship between ENLN and shifts in the locations of the SPCZ and ITCZ. In particular, these studies have shown that the SPCZ tends to shift to the east (west) during EN (LN) events, while the ITCZ tends to shift to the south (north) during EN (LN) events. Figure 42 shows the circulation anomalies associated with AN NZ SST, and their overall similarity to the circulation anomalies during LN events. Note in particular the indications of enhanced low level convergence into the SPCZ, consistent with the indications of enhanced low level convergence, convection, and precipitation in the SPCZ during AN NZ SST and BN HOA PR events (Figures 21, 22, and 18, respectively). Recall too that AN NZ SST is associated with LN and negative IOD events (Figure 17), and with BN HOA PR during Oct–Nov. These results confirm that the NZ SST predictor is closely linked to global scale changes in the tropical ocean and atmosphere, extending across the Atlantic, India, and Pacific sectors.

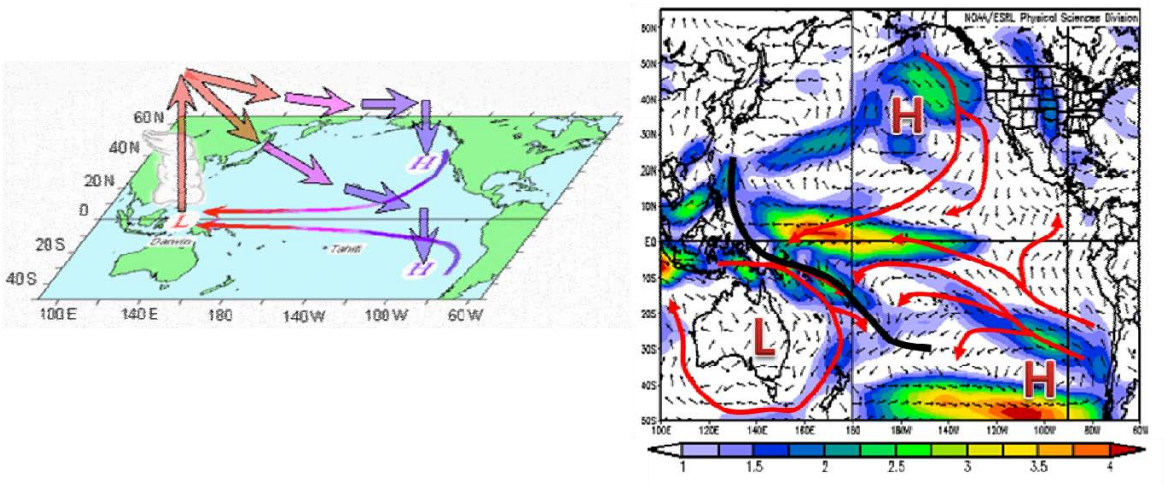

Figure 42. (Left panel) 3-D schematic of the anomalous Hadley-Walker Circulation (HWC) over the Pacific Ocean corresponding to LN events and enhanced convection over the MC. (Right panel) Conditional composite anomalies of 850 hPa vector winds (m/s) for the five most extreme AN NZ SST events during Oct–Nov 1970–2009. Recall that AN NZ SST is associated with LN and negative IOD events (Figure 17), and with BN HOA PR during Oct–Nov. Bold black line indicates SPCZ. H (L) indicates location of anomalous high (low) low-level pressure system. Red arrows schematically show the anomalous low-level flow. Image on left adapted from Murphree (2009a). Image on right created using ESRL (2010).

Figures 43 and 44 show the composite anomalies of 200 hPa geopotential height associated with AN NZ SST and BN NZ SST, respectively. Both figures show pronounced anomalous wave trains extending from the maritime continent (MC) sector into the extratropics and then back into the tropics over Africa. The southern hemisphere anomalous wave train is particularly clear, especially in the BN SST case (the case associated with AN HOA PR; Figure 43). These wave trains are very likely initiated by convection anomalies in the tropics, especially in the eastern IO - MC – western Pacific region, as indicated by: (1) their apparent emanation from that region; (b) their close association with the corresponding convection anomalies (cf. Figures 18, 22); (c) their close association with EN and LN, for which similar wave trains have been identified (e.g., Ford 2000) and for which tropical upper tropospheric height anomalies similar to those in Figures

43–44 are strongly linked (e.g., height anomalies associated with tropical Rossby-Kelvin waves induced by anomalous tropical convection during ENLN [e.g., Ford 2000; Vorhees 2006]); and (d) their resemblance to wave trains initiated by other tropical convection anomalies (Rosencrans 2006).

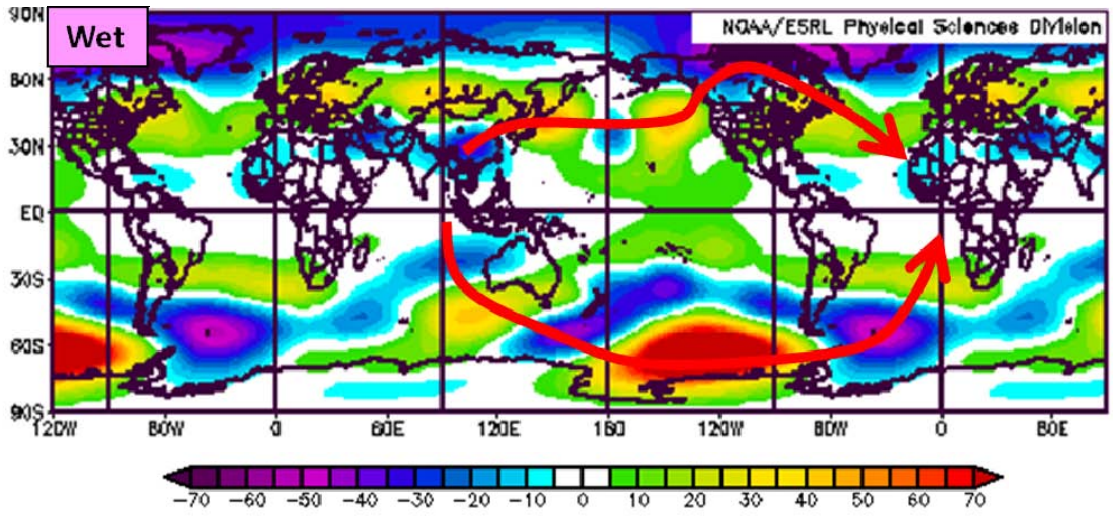

Figure 43. Conditional composite anomalies of 200 hPa GPH (gpm) for the five most extreme BN NZ SST events during Oct–Nov 1970–2009. Recall that BN NZ SST is associated with EN and positive IOD events (Figure 17), and with AN HOA PR during Oct–Nov. The red arrows schematically show anomalous wave trains that emanate from the maritime continent sector, extend into the extratropcial northern and southern hemispheres, and then into the tropics near Africa. The arrow directions indicate schematically the direction of energy propagation in the anomalous wave trains. The *Wet* label in the upper left indicates that these anomalies are associated with above normal precipitation in the HOA. Image created using ESRL (2010).

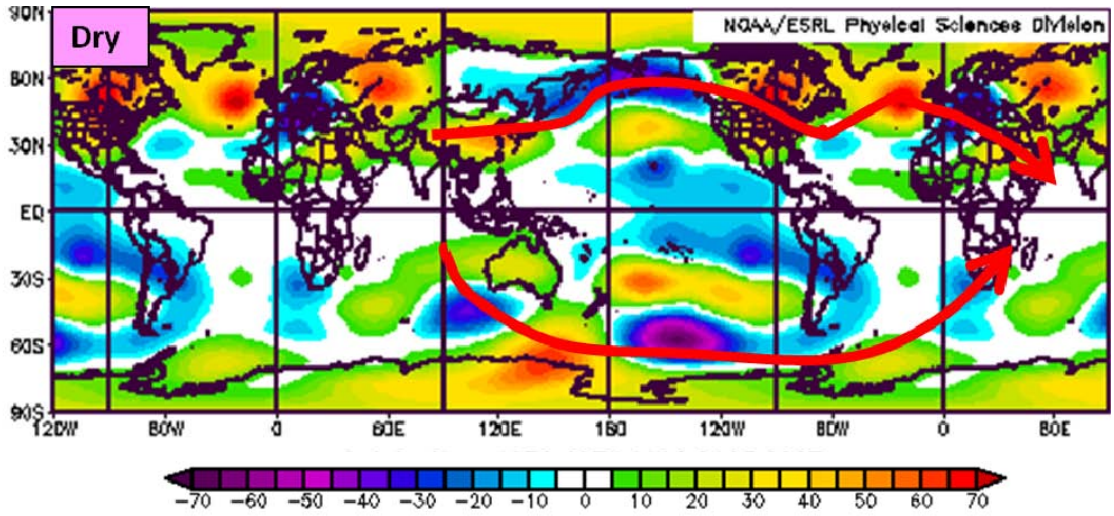

Figure 44. Conditional composite anomalies of 200 hPa GPH (gpm) for the five most extreme AN NZ SST events during Oct–Nov 1970–2009. Recall that AN NZ SST is associated with LN and negative IOD events (Figure 17), and with BN HOA PR during Oct–Nov. The red arrows schematically show anomalous wave trains that emanate from the maritime continent sector, extend into the extratropical northern and southern hemispheres, and then into the tropics near Africa. The arrow directions indicate schematically the direction of energy propagation in the anomalous wave trains. The *Dry* label in the upper left indicates that these anomalies are associated with below normal precipitation in the HOA. Image created using ESRL (2010).

We also investigated the corresponding 200 hPa geopotential height anomalies associated with extreme EN and LN events (not shown). These composites also provide evidence of anomalous wave trains similar in sign and overall pattern to those in Figures 43–44. However, the EN and LN anomalous wave trains tend to: (a) be more zonally oriented in the northern hemisphere; and (b) have energy propagation paths that extend back into the tropics to the east of Africa.

Taken together, these dynamical analysis results indicate that the NZ SST predictor is part of a set of global climate variations that: (a) involve major variations in tropical ocean and atmosphere(e.g., ENLN, IOD); (b) include extensions into and from the extratropics; and (c) link Africa and nearby regions

of the Atlantic and Indian basins to the rest of the tropics and at least parts of the extratropics. They also suggest that the NZ SST predictor may be a better predictor of HOA PR than ENLN or IOD indices because the NZ SST predictor is a better indicator of: (a) anomalies in the strength and location of the SPCZ; and (b) the influence of these SPCZ anomalies on anomalous wave trains that extend through the southern hemisphere and into Africa.

Figure 45 shows the composite anomalies of 850 hPa geopotential height associated with BN NZ SST in the Atlantic– African region. Comparison of the height anomalies in this figure with those in Figure 31 indicate that the Atlantic height anomalies in Figure 45 are part of the anomalous wave trains in the shown in Figure 43, and that the anomalous wave train has equivalent barotropic structure. The associated wind anomalies (red arrows in Figure 45) indicate that the wave trains contribute to anomalous convergence into the HOA, consistent with the association of BN NZ SST with AN HOA PR.

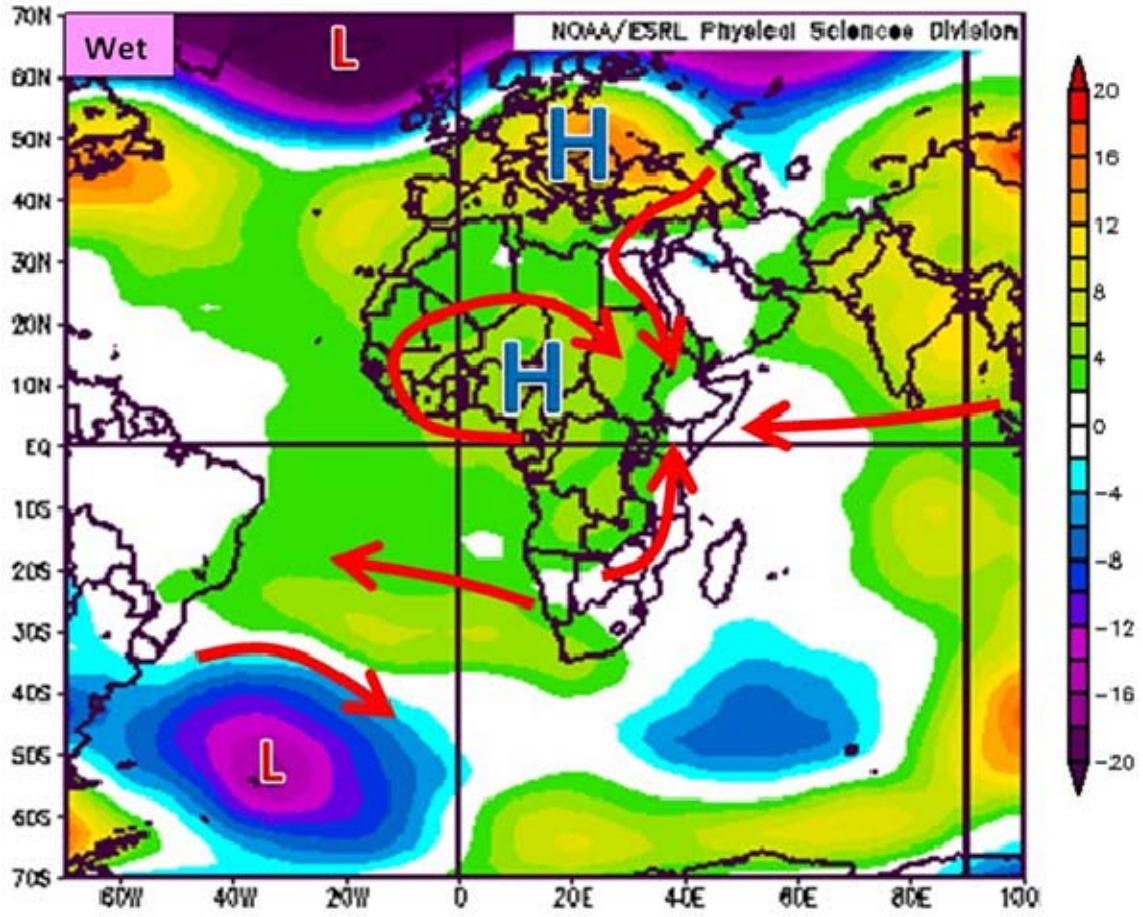

Figure 45. Conditional composite anomalies of 850 hPa GPH (gpm) for the five most extreme BN NZ SST events during Oct–Nov 1970–2009. Recall that BN NZ SST is associated with EN and positive IOD events (Figure 17), and with AN HOA PR during Oct–Nov. H (L) indicates location of anomalous high (low) low level geopotential heights. The red arrows show schematically the anomalous wind directions. Note the anomalous convergence into the HOA region. Image created using ESRL (2010).

Figure 46 shows the composite anomalies of precipitation rate (PR) associated with BN NZ SST in the Atlantic–African region. Note: (a) the positive PR anomalies over the southern Ethiopia, Somalia, and west-central Kenya portion of the HOA, consistent with the corresponding anomalous convergence into that region shown in Figure 45; and (b) the negative PR anomalies to the

east of the HOA, consistent with the corresponding anomalous high pressure over that region shown in Figure 45 and the negative tropical Atlantic SSTs shown in Figure 40.

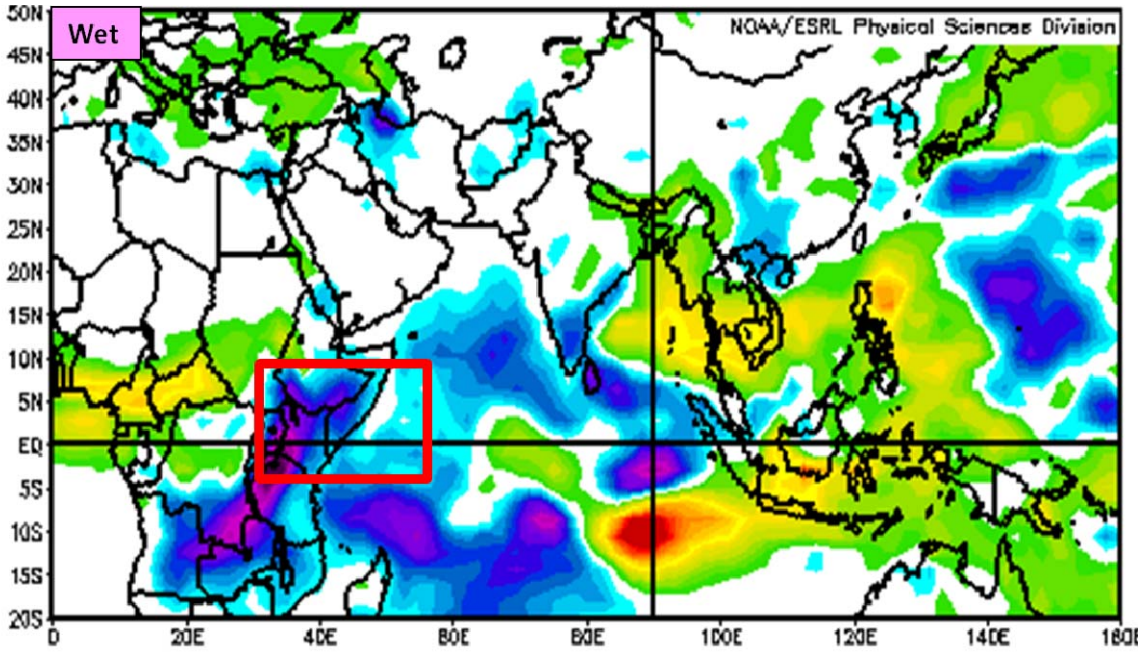

Figure 46. Conditional composite anomalies of precipitation rate (PR; mm/day) for the five most extreme BN NZ SST events during Oct–Nov 1970–2009. Recall that BN NZ SST is associated with EN and positive IOD events (Figure 17), and with AN HOA PR during Oct–Nov. The red box indicates our HOA PR predictand region. Image created using ESRL (2010).

The results in Figures 45–46 indicate that wave trains associated with BN NZ SST contribute to circulation variations over Africa that lead to increased precipitation in the HOA. Similar analyses of conditional composites for extreme AN NZ SST events show approximately opposite patterns.

2. MR SST and HOA Precipitation Teleconnections

The teleconnections between the MR predictors and the HOA are similar to the teleconnections between ENSO and IOD and the HOA, although there are some amplified features that are worth noting.

a. Teleconnections at 4–6 Month Lead Time

At leads of four to six months, we found that SST west of Namibia was a useful predictor of HOA PT in Oct–Nov (Chapter III, Section C.2). In this region a key feature of the climate system is the South Atlantic Subtropical High (SASH). Several prior studies have linked anomalies in the structure and intensity of the SASH have been dynamically linked to changes in east African rainfall (e.g., Nicholson and Entekhabi 1987; Kabanda and Jury 1999; Mutai and Ward 2000; Wang et al. 2009).

The normal low-level circulation pattern around the SASH causes southerly flow along the southwestern coast of Africa and easterly trades along the equator, both of which cause upwelling and LTM SSTs that are relatively cool in those regions. In the center of the SASH, LTM SSTs are relatively warm due to low wind speeds and convergent Ekman transport into that region. Figure 47 shows that four to six months prior to the AN HOA PR in Oct–Nov, the 850 hPa geopotential heights tend to be higher than normal on the southeastern side of the LTM position of the SASH, with corresponding southerly and easterly wind anomalies on the eastern and northern flanks of the SASH that are stronger than normal winds along the coast of southwest Africa and across much of the subtropical South Atlantic (red arrow in Figure 47).

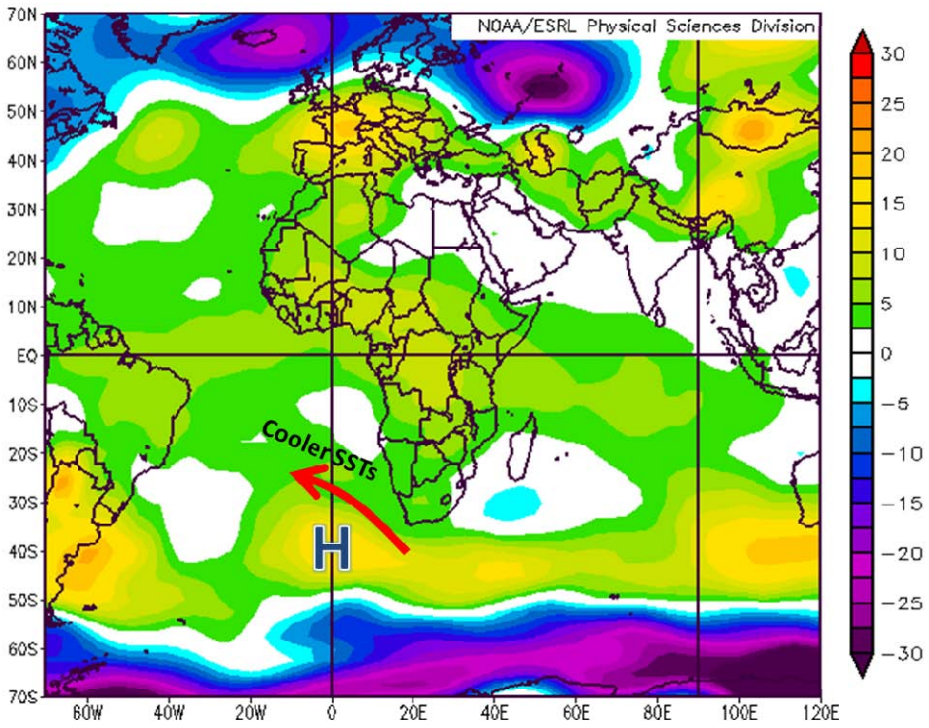

Figure 47. Conditional composite anomalies of 850 hPa GPH (gpm) for the five most extreme BN Namibia SST events during Apr–May 1970–2009. Recall that BN Namibia SST is associated with AN HOA PR during Oct–Nov. The H indicates an anomalous high-pressure region. The direction of the corresponding wind anomalies is shown schematically by the red arrow. The cooler SSTs region is explained in the main text discussion of Figure 40. Image created using ESRL (2010).

Figure 48 shows the SST anomalies corresponding to the height anomalies shown in Figure 47. Note the regions of negative SSTAs occurring under and to the northeast of the southeasterly wind anomalies marked in Figures 47 and 48. The negative SSTA region coincides with our Namibia SST predictor region (Chapter III, Section C.2). These SSTAs are consistent with the wind driven heat flux anomalies and upper ocean Ekman transport anomalies that would be expected from the southeasterly wind anomalies. This suggests that the Namibia SST predictor is associated with anomalies in the SASH. The results shown in Figures 19–20, 22, and 43–45 suggest that the SASH anomalies may be driven by anomalous wave trains that: (a) are initiated by

anomalous SST and convection in the eastern IO—western Pacific region, including anomalies in the SPCZ region; and (b) extend through the southern hemisphere into the South Atlantic.

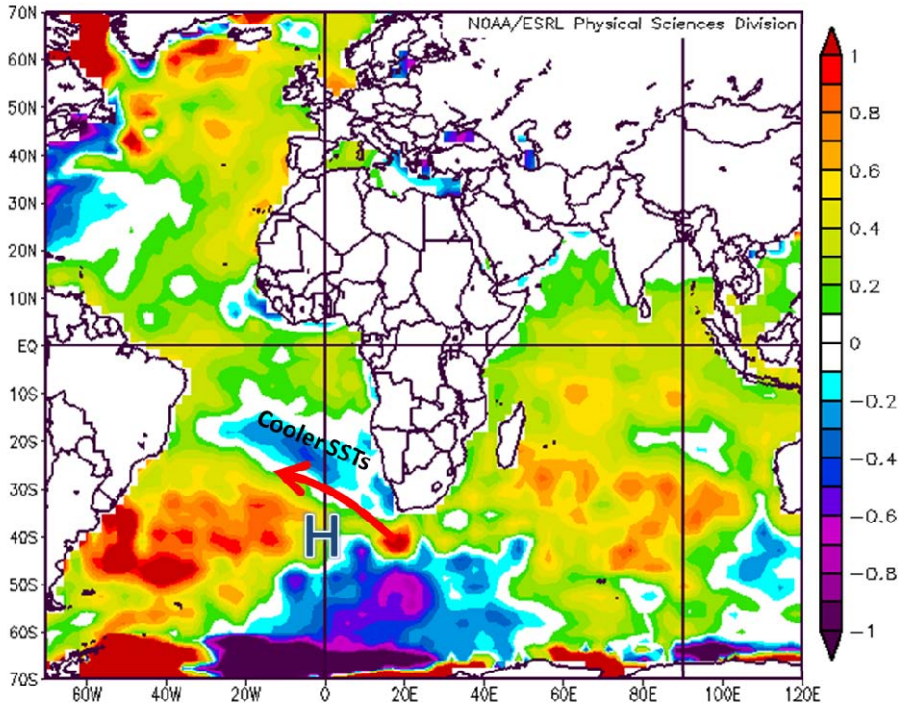

Figure 48. Conditional composite anomalies of SST (°C) for the five most extreme BN Namibia SST events during Apr–May 1970–2009. Recall that BN Namibia SST is associated with AN HOA PR during Oct–Nov. The negative SSTA region west of Namibia corresponds to the Namibia SST predictor region identified as having the highest correlations, at leads of four to six months, to the HOA PR predictand for 1995–2009 (see Chapter III, Section C.2). The H indicates an anomalous lower tropospheric high-pressure region and the black arrow indicates the corresponding wind anomaly (see Figure 47). Image created using ESRL (2010).

b. Teleconnections at 0–3 Month Lead Time

At leads of zero to three months, we found that SST east of the Philippines was a useful predictor of HOA PT in Oct–Nov (Chapter III, Section C.2). Figure 49 shows the correlations between HOA PR in Oct–Nov and global SST in Oct–Nov (zero lead) for our full 40-year study period, 1070–2009, and our

15-year OCN period. The two correlation maps are very similar but the correlations are stronger for the shorter period. In particular, the negative correlations east of the Philippines are much stronger for the shorter period and are the strongest correlations globally for this short period.

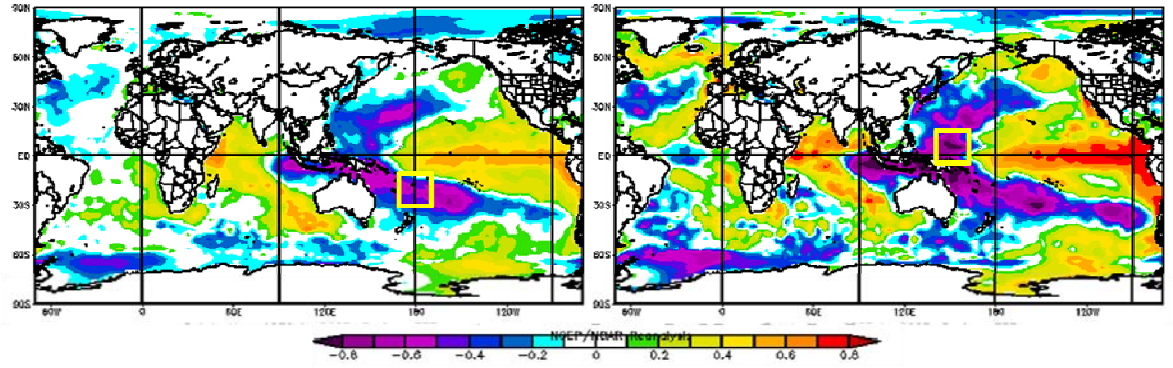

Figure 49. Correlations of HOA PR in Oct–Nov with global SST for 1970–2009 (left panel) and 1995–2009 (right panel), with SSTs leading by zero months (Oct–Nov). The yellow outlined boxes represent NZ predictor region (left panel) and the Philippine SST predictor region (right panel). Note the similar patterns for the two periods, but with stronger correlations for 1995–2009. Images created using ESRL (2010).

The importance of the Philippine SST predictor, and its greater importance in the most recent 15 years, may be related to the long term changes in SST that have occurred in this region and elsewhere. Figure 50 shows the global SSTAs for Oct–Nov of 1970–2009. The LTM base period for the calculation of these anomalies is 1968–1996 (see Chapter II, Section B.2), so these anomalies represent decadal scale changes in SST (e.g., changes associated with global warming). Note in particular that the SSTs in the Philippine SST predictor region and the NZ SST predictor region increased by approximately 0.5^{o} C compared to the LTM values. AN SST in these predictor regions during Apr–Nov is associated with BN HOA PR in Oct–Nov. Thus, the decadal scale SST increases in these two regions might be expected to lead to more BN HOA PR events. The HOA has experienced a higher frequency of

recurring droughts and floods in the last decade relative to the last 40 years (e.g., HOA PR was below its LTM value in nine out of the 15 years during 1995–2009).

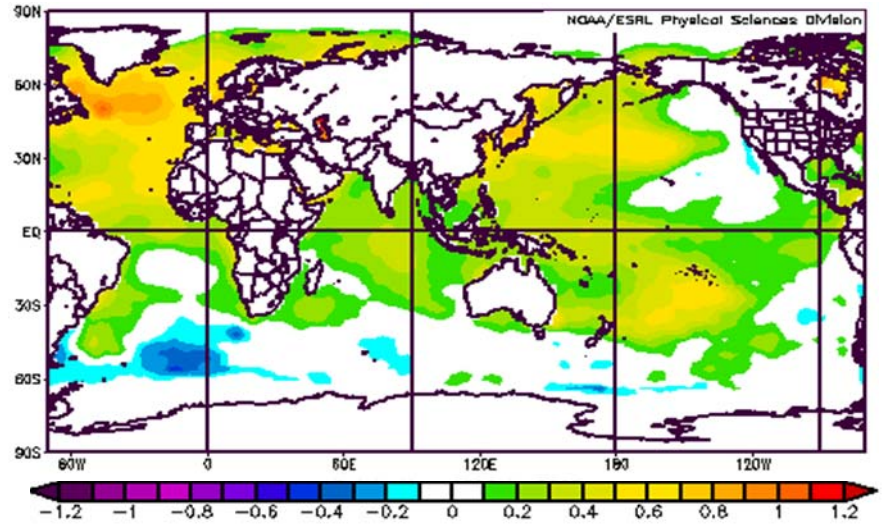

Figure 50. Composite anomalies of SST (^{o}C) for Oct–Nov of 1995–2009. Note the positive SSTAs, especially in the northern hemisphere and in the western North and South Pacific. Image created using ESRL (2010).

3. Summary of Climate Dynamics Analyses

Based on our initial analyses of the climate dynamics, we developed schematic representations of the integrated set of global scale patterns and processes associated with AN and BN PR in the HOA in Oct–Nov (Figures 51–52). These schematic figures describe lower tropospheric and sea surface conditions, but the low level atmospheric circulation features are due in part to anomalous wave trains that extend throughout the troposphere. These schematics primarily describe the conditions associated with AN and BN periods for our NZ SST predictor. However, similar schematics apply to AN and BN periods for our Philippine and Namibia SST predictors.

Figure 51 shows the conditions associated with AN HOA PR *and* BN NZ SST. These are the conditions in the BN NZ SST is likely to perform well in predicting AN PR in our HOA predictand region. Figure 52 shows the conditions

associated with BN HOA PR *and* AN NZ SST. These are the conditions in which the AN NZ SST is likely to perform well in predicting BN PR in our HOA predictand region.

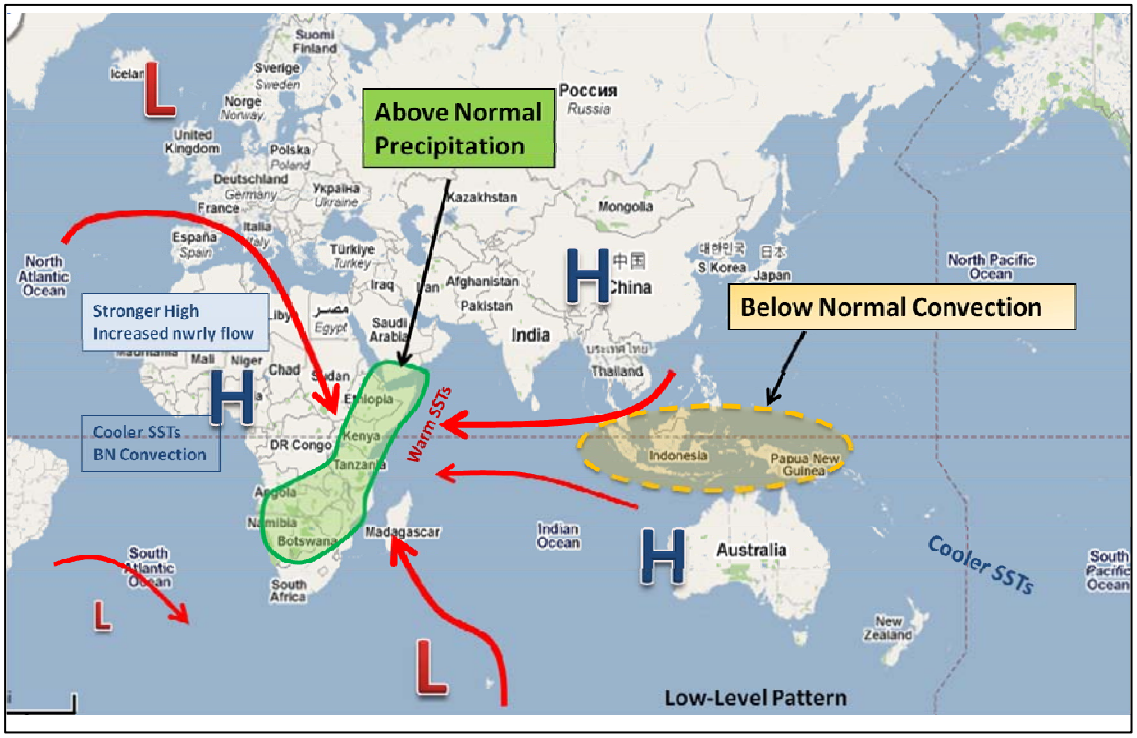

Figure 51. Schematic diagram of lower tropospheric and sea surface conditions that occur in October–November when: (a) precipitation is greater than normal in the HOA (i.e., during AN HOA PR events); *and* (b) when SSTs north of New Zealand are cooler than normal (i.e., during BN NZ SST events) and. Map background from Google Maps (**www.maps.google.com**).

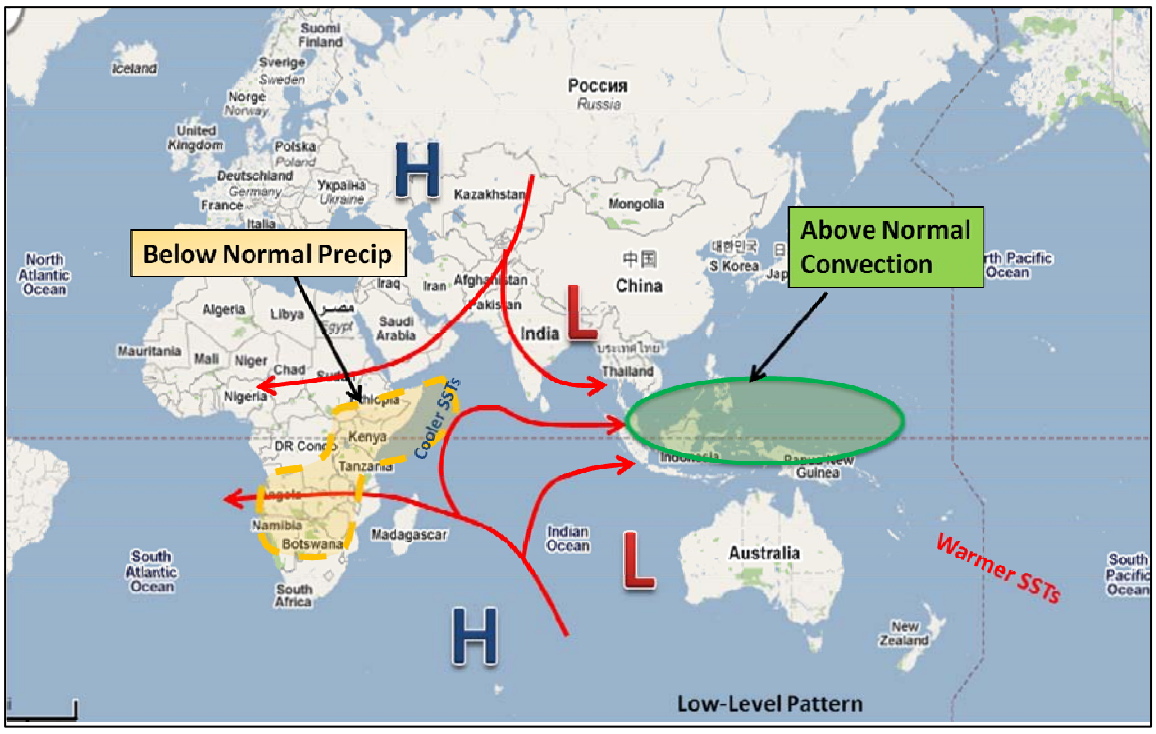

Figure 52. Schematic diagram of lower tropospheric and sea surface conditions that occur in October–November when: (a) precipitation is less than normal in the HOA (i.e., during BN HOA PR events); *and* (b) when SSTs north of New Zealand are warmer than normal (i.e., during AN NZ SST events) and. Map background from Google Maps (**www.maps.google.com**).

Figure 53 shows the conditions associated with above normal precipitation for the greater HOA region. These conditions are very similar to those in Figure 51, but there are some notable differences in the circulation and precipitation patterns over and near Africa. Note that the AN PR region is located further to the north than in Figure 51. The differences between Figures 51 and 53 occur because Figure 51 is focused on conditions associated with BN NZ SST events, and these events are focused on the southern and central portions of the greater HOA region, due to our choice of predictand region (se Chapter II, Section B.1) for which we then identify NZ SST as a good predictor. As discussed in Chapter II, the selection of the predictand is critical in determining the outcomes from the statistical and dynamical analyses, and the selection of predictors, the development of forecast methods, and the results from hindcasts and forecasts.

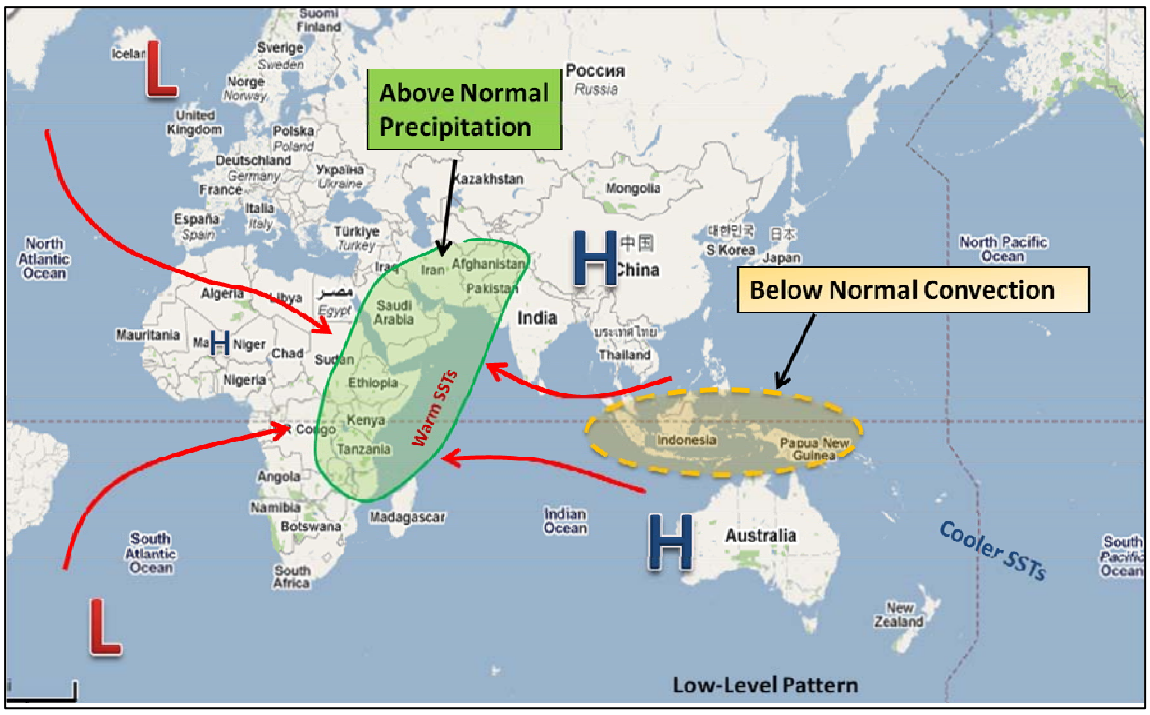

Figure 53. Schematic diagram of lower tropospheric and sea surface conditions that occur in October–November when precipitation is greater than normal in the HOA (i.e., during AN HOA PR events). Map background from Google Maps (**www.maps.google.com**).

In summary, the major patterns associated with anomalously high (low) precipitation in the HOA during Oct–Nov:

1. Anomalously cool (warm) SSTs in the western tropical Pacific, including the regions north of New Zealand and east of the Philippines, the eastern tropical Indian, and the tropical Atlantic basins
2. Anomalously warm (cool) SSTs in the central and eastern tropical Pacific and the western tropical Indian basins
3. Anomalously weak (strong) easterlies over the central and eastern tropical Pacific basin
4. Anomalously strong (weak) easterlies over the western tropical Indian basin

5. Increased (decreased) sea level pressure (SLP) over the maritime continent (MC) and decreased (increased) SLP over eastern Africa
6. Anomalous low level convergence (divergence) into eastern Africa, associated in part with anomalous wave trains emanating from the MC sector and extending through the extratropics and back into the tropics near Africa
7. Anomalies in the Walker circulation that lead to increased (decreased) upward motion and convection over the HOA and decreased (increased) upward motion and convection over the MC

THIS PAGE INTENTIONALLY LEFT BLANK

IV. SUMMARY, CONCLUSION AND RECOMMENDATIONS

A. ANALYSIS OF FORECASTING METHODS AND RESULTS

This study explored the viability of using state-of-the-science climate dataset and methods to develop skillful LRFs of October–November rainfall in the HOA of leads of up to six months. The primary aim of this research was to generate LRF support for military and non-military operations in the HOA. We highlighted that extreme climate events may act as a catalyst for creating or exacerbating the need for operations in the HOA, many of which rely on accurate climate forecasts for their decision making and environmental awareness. We chose to focus our research on the HOA because of its interest to military and non-military operations alike, and because little has been done in regards to developing statistically based precipitation forecasts for the HOA out to six months.

We employed several analysis methods (outlined in Chapter II) using readily available state-of-the-science reanalysis and datasets to conduct analyses of the LTM and climate variations in HOA rainfall. The analyses allowed us to identify global scale interannual patterns and processes related to variations in HOA rainfall, including several climate teleconnections that had not previously been identified and/or investigated for their long-range forecasting potential.

Based on established criteria outlined in Chapter I, we chose a customized predictand region within the HOA for determining the potential for the long-range forecasting of precipitation. After correlating our predictand with several climate variables and indices, we found that SSTs north of New Zealand (NZ) had the highest significant correlations out to six-month lead times. In addition, we applied the optimal climate normals (OCN) concept for long range forecasting, using two different approaches. From our OCN based correlation

analyses, we identified two additional predictors of HOA precipitation in Oct–Nov: (1) SSTs east of the Philippines for leads of zero to three months; and (2) SST west of Namibia for leads of four to six months.

We then used the NZ SST predictor to generate hindcasts of HOA precipitation for Oct–Nov 1970–2009 at leads of zero to six months four different deterministic and probabilistic forecasting methods (e.g., tercile matching, linear regression, composite analysis forecasting). We also applied the same forecasting methods using the Philippine and Namibia SST predictors to hindcast HOA precipitation for Oct–Nov 1995–2009 at leads of zero to six months. We also conducted and analyzed LRFs for five specific cases to: (a) better determine the performance of our predictors and forecast methods; and (b) issue an experimental forecast of precipitation in the HOA for Oct–Nov 2010.

Our results indicate that skillful LRFs of HOA Oct–Nov precipitation are possible out to six month leads for the HOA using our specifically identified SST predictor regions in the Pacific and Atlantic. The skill when using these predictors exceeds that from using more established climate indices as predictors (e.g., ENLN and IOD indices).

We concluded by summarizing the climate dynamics that underlie the predictor-predictand relationships that we used to generate our hindcasts and forecasts.

B. RECOMMENDATIONS

It is clear that climate analyses and long-range forecasts based on the advanced climate datasets and methods used in this study can provide immediate support to the improvement of military and non-military plans and operations in the HOA. The following section highlights some of the key areas of future research that can support these improvements.

1. Our preliminary results were encouraging, but further verification is needed by testing the LRF methods in operational settings and exploring our key

findings in the context of long-range planning for DoD and non DoD operations (e.g., FEWS NET, AFRICOM, 14 WS, etc). Military planners generally fuse climate data products into the planning cycle several months to several years in advance of any possible contingency (Hernandez and Wunder 2004). The LRF processes and methods developed in this study are unique in that they provide planners the ability to adjust their contingency plans for the HOA based on specific climate variations (e.g., EN, positive phase of the IOD, etc.). Using analyses of the regional impacts of extreme climate events, planners can link the effects of each climate variation to the region's socio-economic and political sectors that induce specific military and non-military actions. For example, when LRFs predict AN Oct–Nov rainfall in the HOA, and therefore, likely flooding, military operations may be oriented more towards humanitarian activities such as improving roads and bridges, and hardening shelters for local communities several months before the short rains season. If the LRFs predict a dry short season, the military may help communities prepare by improving water supply systems or by providing peacekeeping and security operations where dry conditions are likely to lead to border conflicts or civil unrest.

2. Expand the type of research we conducted to additional HOA seasons, climate variations, and sub-regions in an effort to fit better with existing forecast products (e.g., products from Kenyan Meteorological Department, 14 WS).

3. Explore inter-decadal and decadal climate variations that may influence PR in the HOA. The decadal scale variations in our correlations in the skill of our hindcasts indicate that more research is needed on the causes of lower frequency variations and their impacts on the HOA. This research will in turn support improvements in long-range forecasting for the HOA.

4. Apply the methods to other operational regions. The readily accessible advanced climate datasets and straightforward methods we used in this study can be adapted to other regions of the world and various operations.

5. Develop a user-friendly online application that produces the deterministic and probabilistic forecasts generated in this study. The data manipulation needed to conduct our analyses and produce our forecasts was relatively complex and lengthy, but it could be automated and made much easier and more accurate if it could be done via a well designed and tested online application.

6. Expand the consideration of partnerships between DoD and civilian organizations, who do advanced climate research and operational climate support (e.g., NOAA), to share ideas on climate research, and climate analyses and forecast products. This could be especially useful in helping DoD leverage existing resources and expertise to rapidly improve support for DoD planning and operations.

LIST OF REFERENCES

14th Weather Squadron (14 WS), cited 2010: Strategic Climate Information Service. [Online at https://notus2.afccc.af.mil/scis/]. Accessed May 2010.

Australian Bureau of Meteorology (BOM), cited 2010. BOM world wide web site. [Online at http://www.bom.gov.au/]. Accessed May 2010.

Baker, P. H., 2010: Forging a U.S. policy toward fragile states. *PRISM,* **1**, no. 2, 69–84.

Behera, S. K., J. Luo, S. Masson, P. Delecluse, S. Gualdi, A. Navarra, and T. Yamagata, 2005: Paramount impact of the Indian Ocean Dipole on the East Africa short rains: A CGCM study. *J. Climate*, **18** (**21**), 4514–4530.

Black E., J. Slingo, and K. Sperber, 2002: An observational study of the relationship between excessively strong short rains in coastal East Africa and Indian Ocean SST. *Mon. Wea. Rev*., **131**, 74–94.

Camberlin, P., S. Janicot, and I. Poccard, 2001: Seasonality and atmospheric dynamics of the teleconnection between African rainfall and tropical sea-surface temperature, Atlantic vs. ENSO: *Int. J. Climatol*, **21**, 973–1005.

Clark, C. O., and J. E. Cole, 2002: Interdecadal variability of the relationship between Indian Ocean Zonal Mode and East African rainfall anomalies. *J. Climate,* **16**, 548–554.

CNN, cited Oct 2009. Flood warning for drought-hit East Africa [Online at http://www.cnn.com/2009/WORLD/africa/10/17/east.africa.flooding/index.html] Accessed March 2010.

Crook, J., 2009: Climate analysis and long-range forecasting of dust storms in Iraq. M.S. thesis, Dept. of Meteorology, Naval Postgraduate School, 85 pp.

Earth Systems Research Laboratory (ESRL), cited 2010. [Accessed online at http://www.cdc.noaa.gov/cgi-bin/PublicData/getpage.pl.] Accessed May 2010.

Failed States Index 2009. cited 2010 [Online at http://www.fundforpeace.org] Accessed May 2010.

Famine Early Warning System Network (FEWS NET), cited 2010. [Online at www.fews.net/] Accessed May 2010.

Farmer, G. 1988: Seasonal forecasting of the Kenya coast short rains, 1901–1984. *J. Climatol*., **8**, 489–497.

Ford, B., 2000: El Nino and La Nina Events, and tropical cyclones: impacts and mechanisms. M.S. thesis, Dept. of Meteorology, Naval Postgraduate School, 120 pp.

Funk, C., 2009. New satellite observations and rainfall forecasts help provide early warning of African drought. *The Earth Observer.,* **21**, no. 1, 23–27.

Google, cited 2010: Google Maps. [Online at http://maps.google.com/maps.] Accessed May 2010.

Hanson, C., 2007: Long-range operational military forecasts for Iraq. M.S. thesis, Dept. of Meteorology, Naval Postgraduate School, 77 pp.

Hastenrath S., Nicklis A., and Greischar L., 1993: Atmospheric–hydrospheric mechanisms of climate anomalies in the western equatorial Indian Ocean. *J. Geophys.* R*es.*: Oceans, **98**, 20219–20235.

——, D. Polzin, and P. Camberlin, 2004: Exploring the predictability of the "short rains" at the coast of East Africa." *Int. J. Climatol*., **24**, 1333–1343.

Heidt, S., 2009: Long-range atmosphere-ocean forecasting in support of USW operations in the western North Pacific. M.S. thesis, Dept. of Meteorology, Naval Postgraduate School, 99 pp.

Hernandez, J., and D. Wunder, 2004: Introduction to the joint planning process – the role of climatology. Advanced Climatology Course, Naval Postgraduate School.

Hunt, Peter. "El Nino Trouble Ahead," *Weekly Times,* June 25, 2009.

Hutchinson P., 1992: The Southern Oscillation and the prediction of 'Der' season rainfall in Somalia. *J. Climate*, **5**, 525–531.

IGAD Climate Prediction and Application Centre (ICPAC), cited 2010: Greater Horn of Africa Climate Outlook Statement 25–March to June rainfall season. [Online at www.icpac.net/forecasts/] Accessed May 2010.

International Committee of the Red Cross (ICRC). 2004: Regional livestock study in the Greater Horn of Africa. [Online at www.icrc.org] Accessed March 2010.

International Research Institute for Climate and Society (IRI), cited 2010: IRI world wide web site [Online from http://iri.columbia.edu]. Accessed March 2010.

Jury, M., 1996: Statistical models for seasonal forecasts of southern Africa summer rainfall. Climate Prediction Center, Bulletin Dec 1996 [Online at http://www.cpc.noaa.gov/products/predictions/experimental/bulletin/Dec96/Dec96_contents.html] Accessed April 2010.

Kabanda, T., and M. R. Jury, 1999: Inter-annual variability of short rains over northern Tanzania. *Climate* R*es.*, **13**, 231–241.

Kalnay, E., and Co-Authors, 1996: The NCEP/NCAR 40-year Reanalysis Project, *Bull Amer. Meteor. Soc.,* **77**, 437–471.

Kenya Meteorological Department seasonal forecast press release, cited 2010 [Online at http://www.meteo.go.ke/] Accessed March 2010.

Kistler, R., and Coauthors, 2001: The NCEP–NCAR 50-Year Reanalysis: Monthly means CD-ROM and documentation. *Bull. Amer. Meteor. Soc.*, **82**, 247–267.

LaJoie, M., 2006: The impact of climate variations on military operations in the Horn of Africa. M.S. thesis, Dept. of Meteorology, Naval Postgraduate School, 153 pp.

Livezey, R. E., 2006: Estimation and extrapolation of climate trends for evaluation and prediction of climate anomalies. *31st Climate Diagnostics and Prediction Workshop*, NOAA.

MetEd, cited 2010: Creating a Local Climate Product Using Composite Analysis. [Online at http://www.meted.ucar.edu/climate/composite/print.htm.] Accessed March 2010.

Montgomery, C., 2008: Climate variations in tropical West African rainfall and the implications for military planners. M.S. thesis, Dept. of Meteorology, Naval Postgraduate School, 111 pp.

Moss, S. M., 2007: Long-range operational military forecasts for Afghanistan. M.S. thesis, Dept. of Meteorology, Naval Postgraduate School, 99 pp.

Murphree, T., 2009a: MR3610 Course Module 2: Review of Circulation Patterns and Processes – Part 2. Department of Meteorology, Naval Postgraduate School, Monterey, California, 21 pp.

——, 2009b: MR3610 Course Module 5: Introduction to Climate Science. Department of Meteorology, Naval Postgraduate School, Monterey, California, 45 pp.

——, 2009c: MR3610 Course Module 6: Smart Climate. Department of Meteorology, Naval Postgraduate School, Monterey, California, 52 pp.

——, 2009d: MR3610 Course Module 14: Kelvin Waves and Climate. Department of Meteorology, Naval Postgraduate School, Monterey, California, 24 pp.

——, 2009e: MR3610 Course Module 15: El Nino, La Nina, and the Southern Oscillation – Part 1. Department of Meteorology, Naval Postgraduate School, Monterey, California, 25 pp.

——, 2009f: MR3610 Course Module 22: Smart Climatology: Concepts and Products. Department of Meteorology, Naval Postgraduate School, Monterey, California, 46 pp.

Mutai, C. C., M. N. Ward, and A. W. Colman, 1998: Towards the prediction to the East Africa short rains based on sea surface temperature-atmosphere coupling. *Int. J. Climatol*., **18**, 975–997.

——, M. N. Ward, 2000: East African rainfall and the tropical circulation/ conveciton on intraseasonal to interannual timescales. *Int. J. Climatol*., **13**, 3915–3939.

Nicholson, S. E., and D. Entekhabi, 1987: Rainfall Variability in Equatorial and Southern Africa – Relationships with Sea Surface Temperature along the Southwestern Coast of Africa. *J. of Climate and Applied Met*., **26**, 5, 561–578.

Ogallo, L. J., 1988: Relationship between seasonal rainfall in East Africa and the Southern Oscillation, *J. Climatol*., **8**, 31–43.

——, cited 2010: Climate Change Activities in the Greater Horn of Africa (GHA) Being Undertaken at DMCN. [Online at http://www.climateadaptation.net/docs/papers/Ogallo%20DMC%20paper.pdf] Accessed May 2010.

Poccard, I., S. Janicot, and P. Camberlin, 2000: Comparison of rainfall structures between NCEP/NCAR reanalyses and observed data over tropical Africa. *Climate Dyn.,* **16**, no. 12. 897–915.

Ramsaur, D.C., 2009: Climate analysis and long-range forecasting of radar performance in the Western North Pacific. M.S. thesis, Dept. of Meteorology, Naval Postgraduate School, 115 pp.

Rasmussen, E. M. and T. H. Carpenter, 1982: Variations in tropical surface temperature and surface wind fields associated with the Southern Oscillation/El Nino. *Monthy Wea. Rev.,* **110**, 354–84.

Rosencrans, M., 2006: Variability in global-scale circulations and their impacts on Atlantic tropical cyclone activity. M.S. thesis, Dept. of Meteorology, Naval Postgraduate School, 99 pp.

Saha, S., and CoAuthors, 2010: The NCEP Climate Forecast System Reanalysis. *Bull. Amer. Meteor. Soc*., accepted.

Saji, N. H., B. N. Goswami, P. N. Vinayachandran, and T. Yamagata, 1999: A dipole mode in the tropical Indian Ocean. *Nature*, **401**, 360–363.

Time, cited November 2009. Floods and Droughts: How Climate Change is Impacting Africa [Online at http://www.time.com/time/specials/packages/article/0,28804,1929071_1929070_1936772,00.html] Accessed March 2010.

Tournay, R., 2008: Long-range forecasting of Korean summer precipitation. M.S. thesis, Dept. of Meteorology, Naval Postgraduate School, Monterey, California, 121 pp.

Trenberth, K. E. 1996 El Niño Definition, Exchanges, Newsletter of the Climate Variability and Predictability Programme (CLIVAR), **1**, no. 3, 6–8.

Trenberth, K. E. 1997. The Definition of El Niño. *Bull. Amer. Meteor. Soc.*, **78**, 2771–2777.

Turek, A., 2008: Smart climatology applications for undersea warfare. M.S. thesis, Dept. of Meteorology, Naval Postgraduate School, Monterey, California, 95 pp.

Twigg, K.L., 2007: A smart climatology of evaporation duct height and surface radar propagation in the Indian Ocean. M.S. thesis, Dept. of Meteorology, Naval Postgraduate School, Monterey, California, 135 pp.

U.S. Army Field Manual 3-07(USAFM), 2008: The Road Map from Conflict to Peace. [Online at http://usacac.army.mil/cac2/Repository/Featured/FM%203-07EXSUM.pdf] Accessed June 2010.

U.S. Africa Command (AFRICOM), cited 2010. [Online at www.africom.mil] Accessed May 2010.

United Nations Environment Programme (UNEP), 2009: From Conflict to Peacebuilding – the Role of Natural Resources and the Environment. [Online at http://unep.org/pdf/pcdmb_policy_01.pdf] Accessed March 2010.

van den Dool, H., 2007: *Empirical Methods in Short-Term Climate Prediction*. Oxford University Press, 215 pp.

Verdin, J., C. Funk., G. Senay, R. Choularton, 2010: Climate science and famine early warning. *Phil. Trans. R. Soc. B 2005,* **360**, 2155–2168.

Vorhees, D., 2006: The impacts of global scale climate variations on Southwest Asia. M.S. thesis, Dept. of Meteorology, Naval Postgraduate School, 175 pp.

Wang, C., Kucharski, F., Barimalala, R., and Bracco, A., 2009: Teleconnections of the tropical Atlantic to the tropical Indian and Pacific Oceans – A review of recent findings. *Met. Zeitschrift,* **18**, no. 4, 445–454.

Wilks, D., 2006: *Statistical Methods in the Atmospheric Science*, Academic Press, 627 pp.

Wolter, K., and M. S. Timlin, 1993: Monitoring ENSO in COADS with a seasonally adjusted principal component index. *Proc. of the 17th Climate Diagnostics Workshop*, Norman, OK, NOAA/N MC/CAC, NSSL, Oklahoma Clim. Survey, CIMMS and the School of Meteor., Univ. of Oklahoma, 52–57.

——, and M. S. Timlin, 1998: Measuring the strength of ENSO - how does 1997/98 rank? *Weather*, **53**, 315–324.

World Meteorological Organization (WMO). cited 2010a: Drought Monitoring and Early Warning: concepts, progress, and future challenges. [Online at http://www.wamis.org/agm/pubs/brochures/WMO1006e.pdf] Accessed May 2010.

——, cited 2010b: Frequently asked questions. [Online at http://www.wmo.int/pages/themes/faq/index_en.html] Accessed May 2010.

INITIAL DISTRIBUTION LIST

1. Defense Technical Information Center
   Ft. Belvoir, Virginia

2. Dudley Knox Library
   Naval Postgraduate School
   Monterey, California

3. Prof. Tom Murphree
   Naval Postgraduate School
   Monterey, California

4. Mr. David Meyer
   Naval Postgraduate School
   Monterey, California

5. Air Force Weather Technical Library
   Asheville, North Carolina